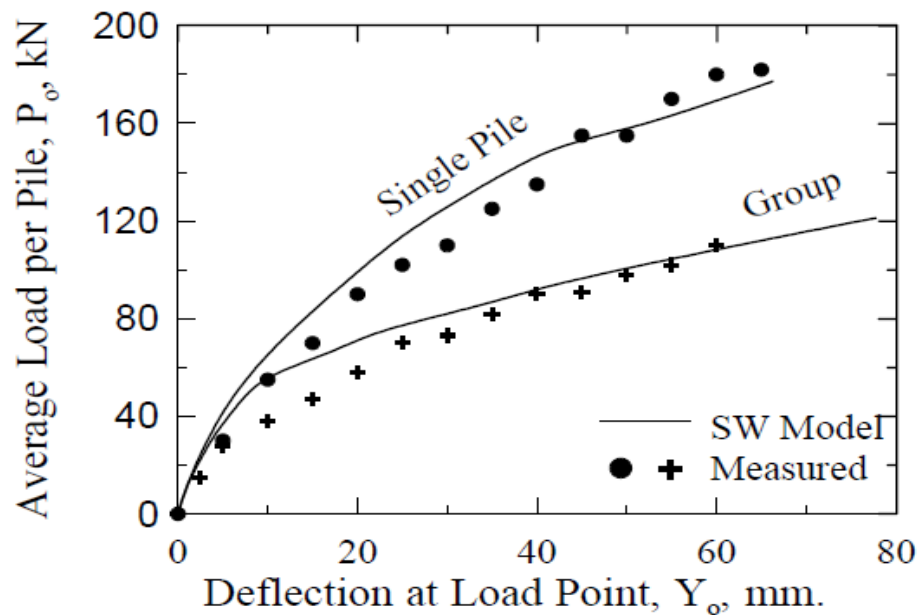
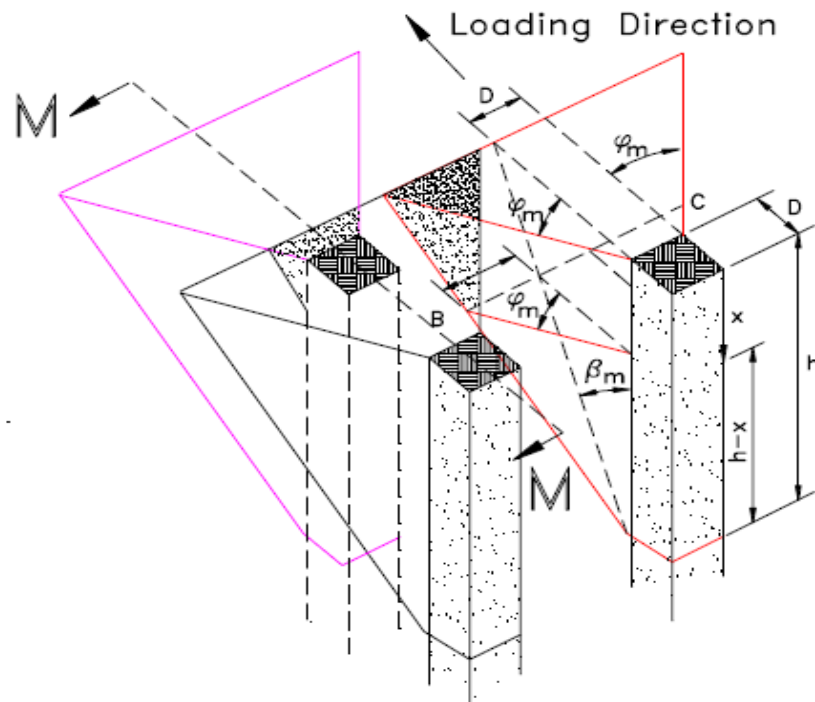


Pile Group Program for Full Material Modeling and Progressive Failure

Final Report



Pile Group Program for Full Material Modeling and Progressive Failure

Final Report

Report No. CA02-0076

December 2008

Prepared By:

Department of Civil and Environmental Engineering
University of Nevada, Reno
Reno, NV 89557

Prepared For:

California Department of Transportation
Engineering Services Center
1801 30th Street
Sacramento, CA 95816

California Department of Transportation
Division of Research and Innovation, MS-83
1227 O Street
Sacramento, CA 95814

DISCLAIMER STATEMENT

This document is disseminated in the interest of information exchange. The contents of this report reflect the views of the authors who are responsible for the facts and accuracy of the data presented herein. The contents do not necessarily reflect the official views or policies of the State of California or the Federal Highway Administration. This publication does not constitute a standard, specification or regulation. This report does not constitute an endorsement by the Department of any product described herein.

STATE OF CALIFORNIA DEPARTMENT OF TRANSPORTATION
TECHNICAL REPORT DOCUMENTATION PAGE
 TR0003 (REV. 10/98)

1. REPORT NUMBER CA02-0076		2. GOVERNMENT ASSOCIATION NUMBER		3. RECIPIENT'S CATALOG NUMBER	
4. TITLE AND SUBTITLE Pile Group Program for Full Material Modeling and Progressive Failure				5. REPORT DATE December, 2008	
				6. PERFORMING ORGANIZATION CODE	
7. AUTHOR(S) Mohamed Ashour, Gary Norris				8. PERFORMING ORGANIZATION REPORT NO. UNR / CCEER 01-02	
9. PERFORMING ORGANIZATION NAME AND ADDRESS Department of Civil & Environmental Engineering University of Nevada Reno, NV 89557-0152				10. WORK UNIT NUMBER	
				11. CONTRACT OR GRANT NUMBER DRI Research Task No. 0076 Contract No. 59A0160	
12. SPONSORING AGENCY AND ADDRESS California Department of Transportation Engineering Services Center 1801 30 th Street Sacramento, CA 95816 California Department of Transportation Division of Research and Innovation, MS-83 1227 O Street Sacramento, CA 95814				13. TYPE OF REPORT AND PERIOD COVERED Final Report	
				14. SPONSORING AGENCY CODE 913	
15. SUPPLEMENTAL NOTES					
16. ABSTRACT <p>Strain wedge (SW) model formulation has been used, in previous work, to evaluate the response of a single pile or a group of piles (including its pile cap) in layered soils to lateral loading. The SW model approach provides appropriate prediction for the behavior of an isolated pile and pile group under lateral static loading in layered soil (sand and/or clay). The SW model analysis covers the entire range of soil strain or pile deflection that may be encountered in practice. The method allows development of p-y curves for the single pile based on soil-pile interaction by considering the effect of both soil and pile properties (i.e. pile size, shape, bending stiffness, and pile head fixity condition) on the nature of the p-y curve.</p> <p>This study has extended the capability of the SW model in order to predict the response of a laterally loaded isolated pile and pile group considering the nonlinear behavior of pile material (steel and/or concrete) and its effect on the soil pile-interaction. The incorporation of the nonlinear behavior of pile material has a significant influence on the lateral response of the pile/shaft and its ultimate capacity. The reduction in pile lateral resistance due to degradation in the pile bending stiffness affects the nature of the accompanying p-y curves, and the distribution of lateral deflections and bending moment along the pile. Contrary to the traditional Matlock-Reese p-y curve that does not account to the variations in the pile bending stiffness, the modulus of subgrade reaction (i.e. the p-y curve) assessed based on the SW model is a function of the pile bending stiffness. In addition, the ultimate value of soil-pile reaction on the p-y curve is governed by either the flow around failure of soil or the plastic hinge formation in the pile.</p> <p>The SW model analysis for a pile group has been modified in this study to assess the p-y curves for an individual pile in a pile group. The technique presented is more realistic and evaluates the variations in the stress and strain (i.e. Young's modulus) in the soil around the pile in question due to the interference with the neighboring piles in a pile group in a mobilized fashion. The nonlinear behavior of pile material is also incorporated in the SW model analysis for a pile group.</p>					
17. KEY WORDS Laterally Loaded Deep Foundations, Pile Groups, Strain Wedge Model, Layered Soils, Nonlinear Behavior of Shaft Material			18. DISTRIBUTION STATEMENT No restrictions. This document is available to the public through the National Technical Information Service, Springfield, VA 22161		
19. SECURITY CLASSIFICATION (of this report) Unclassified		20. NUMBER OF PAGES 166 Pages		21. PRICE	

PILE GROUP PROGRAM FOR FULL MATERIAL MODELING
AND
PROGRESSIVE FAILURE

CCEER 01-02

Prepared by:

Mohamed Ashour
Research Assistant Professor

and

Gary Norris
Professor of Civil Engineering

University of Nevada, Reno
Department of Civil Engineering

Prepared for:

State of California
Department of Transportation

Contract No. 59A0160

July 2001

ACKNOWLEDGMENTS

The authors would like to thank Caltrans for its financial support of this project. The authors would also like to acknowledge Mr. Anoosh Shamsabadi, Dr. Saad El-Azazy, Mr. Steve McBride, Mr. Bob Tanaka and Mr. Tom Schatz for their support and guidance as the Caltrans monitors for this project.

DISCLAIMER

The contents of this report reflect the views of the authors who are responsible for the facts and accuracy of the data presented herein. The contents do not necessarily reflect the official views or policies of the State of California or the Federal Highway Administration. This report does not constitute standard specifications, or regulations.

ABSTRACT

Strain wedge (SW) model formulation has been used, in previous work, to evaluate the response of a single pile or a group of piles (including its pile cap) in layered soils to lateral loading. The SW model approach provides appropriate prediction for the behavior of an isolated pile and pile group under lateral static loading in layered soil (sand and/or clay). The SW model analysis covers a wide range over the entire strain or deflection range that may be encountered in practice. The method allows development of p-y curves for the single pile based on soil-pile interaction by considering the effect of both soil and pile properties (i.e. pile size, shape, bending stiffness, and pile head fixity condition) on the nature of the p-y curve.

This study has extended the capability of the SW model in order to predict the response of a laterally loaded isolated pile and pile group considering the nonlinear behavior of pile material (steel and/or concrete) and its effect on the soil pile-interaction. The incorporation of the nonlinear behavior of pile material has a significant influence on the lateral response of the pile/shaft and its ultimate capacity. The reduction in pile lateral resistance due to degradation in the pile bending stiffness affects the nature of the accompanying p-y curves, and the distribution of lateral deflections and bending moment along the pile. Contrary to the traditional Matlock-Reese p-y curve that does not account to the variations in the pile bending stiffness, the modulus of subgrade reaction (i.e. the p-y curve) assessed based on the SW model is a function of the pile bending stiffness. In addition, the ultimate value of soil-pile reaction on the p-y curve is governed by either the flow around failure of soil or the plastic hinge formation in the pile.

The SW model analysis for a pile group has been modified in this study to assess the p-y curves for an individual pile in a pile group. The technique presented is more realistic and evaluates the variations in the stress and strain (i.e. Young's modulus) in the soil around the pile in question due to the interference with the neighboring piles in a pile group in a mobilized fashion. The nonlinear behavior of pile material is also incorporated in the SW model analysis for a pile group.

TABLE OF CONTENTS

CHAPTER 1	1
INTRODUCTION.....	1
CHAPTER 2	4
LATERAL LOADING OF A PILE IN LAYERED SOIL USING THE STRAIN WEDGE MODEL	
2.1 INTRODUCTION.....	4
2.2 THE THEORETICAL BASIS OF STRAIN WEDGE MODEL CHARACTERIZATION	4
2.3 SOIL PASSIVE WEDGE CONFIGURATION IN UNIFORM SOIL	5
2.4 STRAIN WEDGE MODEL IN LAYERED SOIL	6
2.5 SOIL STRESS-STRAIN RELATIONSHIP.....	8
2.5.1 Horizontal Stress Level (SL).....	10
2.6 SHEAR STRESS ALONG THE PILE SIDES (SL_t)	12
2.6.1 Pile Side Shear in Sand.....	12
2.6.2 Pile Side Shear Stress in Clay	12
2.7 SOIL PROPERTY CHARACTERIZATION IN THE STRAIN WEDGE MODEL	14
2.7.1 Properties Employed for Sand Soil	14
2.7.2 The Properties Employed for Normally Consolidated Clay	15
2.8 SOIL-PILE INTERACTION IN THE STRAIN WEDGE MODEL	17
2.9 PILE HEAD DEFLECTION	20
2.10 ULTIMATE RESISTANCE CRITERIA IN STRAIN	

WEDGE MODEL	21
2.10.1 Ultimate Resistance Criterion in Sand Soil	21
2.10.2 Ultimate Resistance Criterion in Clay Soil.....	22
2.11 STABILITY ANALYSIS IN THE STRAIN WEDGE MODEL	22
2.11.1 Local Stability of a Soil Sublayer in the Strain Wedge Model	23
2.11.2 Global Stability in the Strain Wedge Model	23
2.12 APPROACH VERIFICATION.....	24
2.12.1 Mustang Island Full-Scale Load Test on a Pile in Submerged Dense Sand.....	25
2.12.2 Pyramid Building at Memphis, Tennessee, Full-Scale Load Test on a Pile in Layered Clay Soil.....	26
2.12.3 Sabine River Full-Scale Load Tests on a Pile in Soft Clay.....	28
2.13 SUMMARY	31
FIGURES.....	32
 CHAPTER 3	 46
PILE GROUPS IN LAYERED SOILS	
3.1 INTRODUCTION.....	46
3.2 CHARACTRIZATION OF PILE GROUP INTERFERENCE	47
3.3 EVALUATION OF YOUN’S MODULUS, E_g.....	51
3.4 EVALUATION OF MODULUS OF SUBGRADE REACTION, E_{Eg}	52
3.5 CASE STUDIES.....	54
3.5.1 Full Scale Load Test on a Pile Group in Layered Clay	54
3.5.2 Full Scale Load Test on a Pile Group in Sand	54
3.5.3 Full Scale Load Test on a Pile Group in Layered Clay	55
3.5.4 Full Scale Load Test on a Pile Group with a Pile Cap in Layered Soil	56
3.5.5 Model Scale Load Test on a Pile Group in Loose and	

	Medium Dense Sand	57
3.6	SUMMARY	57

	FIGURES.....	39
--	--------------	----

CHAPTER 4

	NUMERICAL MATERIAL MODELING.....	70
4.1	INTRODUCTION.....	70
4.2	THE COMBINATION OF MATERIAL MODELING WITH THE SW MODEL	72
	4.2.1 Material Modeling for Concrete Strength and Failure Criteria	73
	4.2.2 Material Modeling of Steel Strength	76
4.3	MOMENT CURAVATURE RELATIONSHIP.....	78
4.4	SOLUTION PROCEDURE	79
	4.4.1 Steel Pile.....	79
	4.4.2 Reinforced Concrete Pile and Drilled Shaft	84
	4.4.3 Steel Pipe Pile Filled with Concrete (Cast in Steel Shell, CISS)	88
	4.4.4 Steel Pipe Pile Filled with Reinforced Concrete (Cast in Steel Shell, CISS)	89
4.5	ILLUSTRATIVE EXAMPLES	90
	4.5.1 Example Problem, a Fixed-Head Steel Pile Supporting a Bridge Abutment.....	90
	4.5.2 Example Problem, a Free-Head Drilled Shaft Supporting a Bridge Abutment	91
	4.5.3 Example Problem, a Fixed-Head Drilled Shaft Supporting a Bridge Abutment	93
4.6	SUMMARY	93

FIGURES.....	95
---------------------	-----------

CHAPTER 5

EFFECT OF NONLINEAR BEHAVIOR OF PILE MATERIAL ON PILE AND PILE GROUP LATERAL RESPONSE	108
5.1 INTRODUCTION.....	108
5.2 EFFECT OF PILE MATERIAL NONLINEAR RESPONSE ON THE P-Y CURVE	109
5.2.1 Steps of Constructing the p-y Curve in the SW Model Analysis.....	111
5.2.2 Effect of Material Modeling on the p-y Curve Ultimate	113
5.3 CASE STUDIES.....	115
5.3.1 Pyramid Building at Memphis, Tennessee, Dull-Scale Load Test on a Pile in Layered Clay Soil	115
5.3.2 Houston Full-Scale Load Test on a Reinforced Concrete Shaft in Stiff Clay.....	118
5.3.3 Las Vegas Test on Drilled Shafts and Shaft Group in a Caliche Layer	121
5.3.4 Southern California Full-Scale Load Test in Stiff Clay	122
5.3.5 Islamorada Full-Scale load Test on a Pile Driven in Rock.....	123
5.3.6 University of California at Los Angeles Full-Scale Load Test on a Pile Driven in Stiff Clay	125
5.4 SUMMARY	126
5.5 FIGURES.....	127

CHAPTER 1

INTRODUCTION

This report presents a summary of strain wedge (SW) model assessment of the behavior of piles and pile groups subjected to lateral loading in layered soil considering the nonlinear behavior of pile material. A computer code attached to this report has been developed to assess the response of a single pile and pile group in layered soils (sand, clay and/or rock) and the associated p-y curves for various soil and pile conditions. The main goal of this report is to address the influence of the nonlinear behavior of pile/shaft material on the lateral response of isolated piles/shafts and pile groups. The significance of accounting for the variations in strength of pile/shaft is to identify the actual behavior and the ultimate capacity of such piles/shafts. In addition, the associated p-y curves will experience different effects due to the degradation in pile materials.

The California Department of Transportation (CALTRANS) sponsored a significant part of the SW model research through different phases of research project (Ashour et al. 1996, Ashour and Norris 1998, and Ashour and Norris 2000). The SW model relates one-dimensional beam on elastic foundation analysis to the three-dimensional soil pile interaction response. It relates the deflection of a pile versus depth (or its rotation) to the relative soil strain that exists in the growing passive wedge that develops in front of a pile under horizontal load. The SW model assumes that the deflection of a pile under increasing horizontal load is due solely to the deformation of the soil within the mobilized passive wedge, that plane stress change conditions exist within the wedge, and that soil strain is constant with depth in the current wedge.

The passive wedge will exhibit a height that corresponds to the pivot point as determined by a linear approximation of the pile deflection. If the soil strain is known, an equivalent linear Young's modulus value, associated with the soil within the wedge at any depth, can be determined. Assuming plane stress change conditions exist, the increase in horizontal

stress can then be determined. In addition, the beam-on-elastic-foundation line load reaction at any depth along the pile face is equivalent to the increase in horizontal stress times the wedge width at that depth plus the mobilized side shear resistance that develops at that depth along the pile faces parallel to the direction of movement. Since the geometry of the developing wedge is based on known soil properties and the current value of soil strain, the wedge width can be determined at any depth within the wedge. An equivalent face stress from beam on elastic foundation (BEF) analysis can therefore be related to the horizontal stress change in the soil.

The SW model relates one-dimensional BEF analysis (p-y response) to a three-dimensional soil pile interaction response. Because of this relation, the strain wedge model is also capable of determining the maximum moment and developing p-y curves for a pile under consideration since the pile load and deflection at any depth along the pile can be determined. A detailed summary of the theory incorporated into the strain wedge model is presented in Chapter 2.

The problem associated with analyzing a pile group is that loading one pile in the group can dramatically affect the response of other piles in the group. Since the SW model determines the geometry of the developing passive wedge, it allows any overlap between passive wedges within the group to be quantified. By knowing the amount of passive wedge overlap, the effective strain associated with the pile under consideration can be determined which ultimately reduces the lateral load capacity of the pile for a given level of deflection. Despite Ashour and Norris (2000) discussed the assessment of the lateral response of a pile group, a new treatment for the problem of a laterally loaded pile group is presented in this report to upgrade the capability of the SW model technique.

This report illustrates the links between the single pile and the pile group analysis. This is different from the current procedure in common use that employs a p-y multiplier technique. Such multiplier technique is based on reducing the stiffness of the traditional (Matlock-Reese) p-y curve using a multiplier that reduces the stiffness of the p-y curve of the single pile to yield a softer response for an individual pile in the group. A detailed

summary of the theory in which the SW model analyzes pile group behavior is presented in Chapter 3.

A methodology to assess the response of an isolated pile and pile group in layered soil considering the nonlinear behavior of pile material and how the accompanying modulus of subgrade reaction is affected is presented in Chapters 4 and 5. The effect of pile properties, such as the pile bending stiffness, on the pile lateral response has been presented by Ashour et al. (1996). Such a study emphasized the need to study the influence of the variation in pile bending stiffness during the loading process on the soil-pile interaction and therefore lateral response of the isolated pile and pile group. The effect of pile nonlinear behavior of pile material has been studied by other researches (Reese 1994, and Reese and Wang 1991). However, the incorporation of the nonlinear behavior of pile material has not affected the shape of the p-y curve or the soil-pile interaction. In other words, the p-y curve has not accounted for the variation in the pile bending stiffness.

Several case studies are presented in this study to show the capability of the SW model and how the modeling of pile material (steel and/or concrete) is employed in the SW model analysis. A numerical model for confined concrete is employed with the SW model. Such a model accounts for the enhancement of the concrete strength due to the confinement of the transverse reinforcement.

CHAPTER 2

LATERAL LOADING OF A PILE IN LAYERED SOIL USING THE STRAIN WEDGE MODEL

2.1 INTRODUCTION

The strain wedge (SW) model is an approach that has been developed to predict the response of a flexible pile under lateral loading (Norris 1986, Ashour et al. 1996 and Ashour et al. 1998). The main concept associated with the SW model is that traditional one-dimensional Beam on Elastic Foundation (BEF) pile response parameters can be characterized in terms of three-dimensional soil-pile interaction behavior. The strain wedge model was initially established to analyze a free-head pile embedded in one type of uniform soil (sand or clay). However, the SW model has been improved and modified through additional research to accommodate a laterally loaded pile embedded in multiple soil layers (sand and clay). The strain wedge model has been further modified to include the effect of pile head conditions on soil-pile behavior. The main objective behind the development of the SW model is to solve the BEF problem of a laterally loaded pile based on the envisioned soil-pile interaction and its dependence on both soil and pile properties.

The problem of a laterally loaded pile in layered soil has been solved by Reese (1977) as a BEF based on modeling the soil response by p-y curves. However, as mentioned by Reese (1983), the p-y curve employed does not account for soil continuity and pile properties such as pile stiffness, pile cross-section shape and pile head conditions.

2.2 THE THEORETICAL BASIS OF STRAIN WEDGE MODEL CHARACTERIZATION

The SW model parameters are related to an envisioned three-dimensional passive wedge of soil developing in front of the pile. The basic purpose of the SW model is to relate stress-strain-strength behavior of the soil in the wedge to one-dimensional BEF parameters. The SW model is, therefore, able to provide a

theoretical link between the more complex three-dimensional soil-pile interaction and the simpler one-dimensional BEF characterization. The previously noted correlation between the SW model response and BEF characterization reflects the following interdependence:

- the horizontal soil strain (ε) in the developing passive wedge in front of the pile to the deflection pattern (y versus depth, x) of the pile;
- the horizontal soil stress change ($\Delta\sigma_h$) in the developing passive wedge to the soil-pile reaction (p) associated with BEF; and
- the nonlinear variation in the Young's modulus ($E = \Delta\sigma_h/\varepsilon$) of the soil to the nonlinear variation in the modulus of soil subgrade reaction ($E_s = p/y$) associated with BEF characterization.

The analytical relations presented above reflect soil-pile interaction response characterized by the SW model that will be illustrated later. The reason for linking the SW model to BEF analysis is to allow the appropriate selection of BEF parameters to solve the following fourth-order ordinary differential equation to proceed.

$$EI \left(\frac{d^4 y}{d^4 x} \right) + E_s(x) y + P_x \left(\frac{d^2 y}{d^2 x} \right) = 0 \quad (2.1)$$

The closed form solution of the above equation has been obtained by Matlock and Reese (1961) for the case of uniform soil. In order to appreciate the SW model's enhancement of BEF analysis, one should first consider the governing analytical formulations related to the passive wedge in front of the pile, the soil's stress-strain relationship, and the related soil-pile interaction.

2.3 SOIL PASSIVE WEDGE CONFIGURATION IN UNIFORM SOIL

The SW model represents the mobilized passive wedge in front of the pile which is characterized by base angles, Θ_m and β_m , the current passive wedge depth h , and the spread of the wedge fan angle, ϕ_m (the mobilized friction angle). The horizontal stress change at the passive wedge face, $\Delta\sigma_h$, and side shear, τ , act as shown in Fig. 2.1. One of the main assumptions associated with the SW model is that the deflection

pattern of the pile is taken to be linear over the controlling depth of the soil near the pile top resulting in a linearized deflection angle, δ , as seen in Fig. 2.2. The relationship between the actual (closed form solution) and linearized deflection patterns has been established by Norris (1986). This assumption allows uniform horizontal and vertical soil strains to be assessed (as seen later in a Fig. 2.6). Changes in the shape and depth of the passive wedge, along with changes in the state of loading and pile deflection, occur with change in the uniform strain in the developing passive wedge. The configuration of the wedge at any instant of load and, therefore, mobilized friction angle, ϕ_m , and wedge depth, h , is given by the following equation:

$$\Theta_m = 45 - \frac{j_m}{2} \quad (2.2)$$

or its complement

$$b_m = 45 + \frac{j_m}{2} \quad (2.3)$$

The width, \overline{BC} , of the wedge face at any depth is

$$\overline{BC} = D + (h - x) 2 \tan b_m \tan j_m \quad (2.4)$$

where x denotes the depth below the top of the studied passive wedge, and D symbolizes the width of the pile cross-section (see Fig. 2.1). It should be noted that the SW model is based upon an effective stress analysis of both sand and clay soils. As a result, the mobilized fanning angle, ϕ_m , is not zero in clay soil as assumed by Reese (1958, 1983).

2.4 STRAIN WEDGE MODEL IN LAYERED SOIL

The SW model can handle the problem of multiple soil layers of different types. The approach employed, which is called the multi-sublayer technique, is based upon dividing the soil profile and the loaded pile into sublayers and segments of constant thickness, respectively, as shown in Fig. 2.3. Each sublayer of soil is considered to behave as a uniform soil and have its own properties according to the sublayer location and soil type. In addition, the multi-sublayer technique depends on the deflection pattern of the embedded pile

being continuous regardless of the variation of soil types. However, the depth, h , of the deflected portion of the pile is controlled by the stability analysis of the pile under the conditions of soil-pile interaction. The effects of the soil and pile properties are associated with the soil reaction along the pile by the Young's modulus of the soil, the stress level in the soil, the pile deflection, and the modulus of subgrade reaction between the pile segment and each soil sublayer. To account for the interaction between the soil and the pile, the deflected part of the pile is considered to respond as a continuous beam loaded with different short segments of uniform load and supported by nonlinear elastic supports along soil sublayers, as shown in Fig. 2.4. At the same time, the point of zero deflection (X_0 in Fig. 2.4a) for a pile in a particular layered soil varies according to the applied load and the soil strain level.

The SW model in layered soil provides a means for distinguishing layers of different soil types as well as sublayers within each layer where conditions (ε_{50} , SL, φ_m) vary even though the soil and its properties ($\bar{\gamma}$, e or D_r , φ , etc.) remain the same. As shown in Fig. 2.5, there may be different soil layers and a transition in wedge shape from one layer to the next, with all components of the compound wedge having in common the same depth h . In fact, there may be a continuous change over a given sublayer; but the values of stress level (SL) and mobilized friction angle (φ_m) at the middle of each sublayer of height, H_i , are treated as the values for the entire sublayer.

As shown in Fig. 2.5, the geometry of the compound passive wedge depends on the properties and the number of soil types in the soil profile, and the global equilibrium between the soil layers and the loaded pile. An iterative process is performed to satisfy the equilibrium between the mobilized geometry of the passive wedge of the layered soil and the deflected pattern of the pile for any level of loading.

While the shape of the wedge in any soil layer depends upon the properties of that layer and, therefore, satisfies the nature of a Winkler foundation of independent "soil" springs in BEF analysis, realize that there is forced interdependence given that all components of the compound wedge have the same depth (h) in common. Therefore, the mobilized depth (h) of the compound wedge at any time is a function of the various soils (and their stress levels), the bending stiffness (EI), and head fixity conditions (fixed, free, or other) of

the pile. In fact, the developing depth of the compound wedge can be thought of as a retaining wall of changing height, h . Therefore, the resultant “soil” reaction, p , from any soil layer is really a “soil-pile” reaction that depends upon the neighboring soil layers and the pile properties as they, in turn, influence the current depth, h . In other words, the p - y response of a given soil layer is not unique. The governing equations of the mobilized passive wedge shape are applied within each one- or two-foot sublayer i (of a given soil layer I) and can be written as follows:

$$(\Theta_m)_i = 45 - \frac{(\mathbf{j}_m)_i}{2} \quad (2.5)$$

$$(\mathbf{b}_m)_i = 45 + \frac{(\mathbf{j}_m)_i}{2} \quad (2.6)$$

$$(\overline{BC})_i = D + (h - x_i) 2 (\tan \mathbf{b}_m)_i (\tan \mathbf{j}_m)_i \quad (2.7)$$

where h symbolizes the entire depth of the compound passive wedge in front of the pile and x_i represents the depth from the top of the pile or compound passive wedge to the middle of the sublayer under consideration. The equations above are applied at the middle of each sublayer.

2.5 SOIL STRESS-STRAIN RELATIONSHIP

The horizontal strain (ϵ) in the soil in the passive wedge in front of the pile is the predominant parameter in the SW model; hence, the name “strain wedge”. Consequently, the horizontal stress change ($\Delta\sigma_h$) is constant across the width of the rectangle BCLM (of face width \overline{BC} of the passive wedge), as shown in Fig. 2.1. The stress-strain relationship is defined based on the results of the isotropically consolidated drained (sand) or undrained (clay) triaxial test. These properties are summarized as follows:

- The major principle stress change ($\Delta\sigma_h$) in the wedge is in the direction of pile movement, and it

is equivalent to the deviatoric stress in the triaxial test as shown in Fig. 2.2 (assuming that the horizontal direction in the field is taken as the axial direction in the triaxial test).

- The vertical stress change ($\Delta\sigma_v$) and the perpendicular horizontal stress change ($\Delta\sigma_{ph}$) equal zero, corresponding to the standard triaxial compression test where deviatoric stress is increased while confining pressure remains constant.
- The initial horizontal effective stress is taken as

$$\bar{s}_{ho} = K \bar{s}_{vo} = \bar{s}_{vo}$$

where $K=1$ due to pile installation effects. Therefore, the isotropic confining pressure in the triaxial test is taken as the vertical effective stress ($\bar{\sigma}_{vo}$) at the associated depth.

- The horizontal stress change in the direction of pile movement is related to the current level of horizontal strain (ϵ) and the associated Young's modulus in the soil as are the deviatoric stress and the axial strain to the secant Young's modulus ($E = \Delta\sigma_h/\epsilon$) in the triaxial test.
- Both the vertical strain (ϵ_v) and the horizontal strain perpendicular to pile movement (ϵ_{ph}) are equal and are given as

$$\epsilon_v = \epsilon_{ph} = -\nu \epsilon$$

where ν is the Poisson's ratio of the soil.

It can be demonstrated from a Mohr's circle of soil strain, as shown in Fig. 2.6, that shear strain, γ , is defined as

$$\frac{\mathbf{g}}{2} = \frac{1}{2} (\mathbf{e} - \mathbf{e}_v) \sin 2\Theta_m = \frac{1}{2} \mathbf{e} (1 + \mathbf{n}) \sin 2\Theta_m \quad (2.8)$$

The corresponding stress level (SL) in sand (see Fig. 2.7) is

$$SL = \frac{\Delta \mathbf{s}_h}{\Delta \mathbf{s}_{hf}} = \frac{\tan^2(45 + \mathbf{j}_m) - 1}{\tan^2(45 + \mathbf{j}) - 1} \quad (2.9)$$

where the horizontal stress change at failure (or the deviatoric stress at failure in the triaxial test) is

$$\Delta \mathbf{s}_{hf} = \bar{\mathbf{s}}_{vo} \left[\tan^2 \left(45 + \frac{\mathbf{j}}{2} \right) - 1 \right] \quad (2.10)$$

In clay,

$$SL = \frac{\Delta \mathbf{s}_h}{\Delta \mathbf{s}_{hf}} ; \quad \Delta \mathbf{s}_{hf} = 2 S_u \quad (2.11)$$

where S_u represents the undrained shear strength which may vary with depth. Determination of the values of SL and φ_m in clay requires the involvement of an effective stress analysis which is presented later in this chapter.

The relationships above show clearly that the passive wedge response and configuration change with the change of the mobilized friction angle (φ_m) or stress level (SL) in the soil. Such behavior provides the flexibility and the accuracy for the strain wedge model to accommodate both small and large strain cases.

A power function stress-strain relationship is employed in SW model analysis for both sand and clay soils. It reflects the nonlinear variation in stress level (SL) with axial strain (ϵ) for the condition of constant confining pressure. To be applicable over the entire range of soil strain, it takes on a form that varies in stages as shown in Fig. 2.8. The advantage of this technique is that it allows the three stages of horizontal stress, described in the next section, to occur simultaneously in different sublayers within the passive wedge.

2.5.1 Horizontal Stress Level (SL)

Stage I ($\epsilon \leq \epsilon_{50\%}$)

The relationship between stress level and strain at each sublayer (i) in the first stage is assessed using the following equation,

$$SL_i = \frac{I_i e}{(e_{50})_i} \exp(-3.707 SL_i) \quad (2.12)$$

where 3.707 and λ ($\lambda = 3.19$) represent the fitting parameters of the power function relationship, and ε_{50} symbolizes the soil strain at 50 percent stress level.

Stage II ($e_{50\%}$ to $e_{80\%}$)

In the second stage of the stress-strain relationship, Eqn. 2.12 is still applicable. However, the value of the fitting parameter λ is taken to vary in a linear manner from 3.19 at the 50 percent stress level to 2.14 at the 80 percent stress level as shown in Fig. 2.8b.

Stage III ($e_{80\%}$ to $e_{100\%}$)

This stage represents the final loading zone which extends from 80 percent to 100 percent stress level. The following Equation is used to assess the stress-strain relationship in this range,

$$SL_i = \exp \left[\ln 0.2 + \frac{100 e_i}{(m e_i + q_i)} \right] ; SL_i \geq 0.80 \quad (2.13)$$

where $m=59.0$ and $q=95.4$ ε_{50} are the required values of the fitting parameters.

The three stages mentioned above are developed based on unpublished experimental results (Norris 1977).

In addition, the continuity of the stress-strain relationship is maintained along the SL- ε curve at the merging points between the mentioned stages.

As shown in Fig. 2.9, if ε_{50} of the soil is constant with depth (x), then, for a given horizontal strain (ε), SL from Eqns. 2.12 or 2.13 will be constant with x . On the other hand, since strength, $\Delta\sigma_{hf}$ varies with depth (e.g., see Eqns. 2.10 and 2.11), $\Delta\sigma_h (= SL \Delta\sigma_{hf})$ will vary in a like fashion. However, ε_{50} is affected by confining pressure ($\bar{\sigma}_v$) in sand and S_u in clay. Therefore, SL for a given ε will vary somewhat with depth.

The Young's modulus of the soil from both the shear loading phase of the triaxial test and the strain wedge model is

$$E_i = \frac{(\Delta \mathbf{s}_h)_i}{\mathbf{e}} = \frac{SL_i (\Delta \mathbf{s}_{hf})_i}{\mathbf{e}} \quad (2.14)$$

It can be seen from the previous equations that stress level, strain and Young's modulus at each sublayer (i) depend on each other, which results in the need for an iterative solution technique to satisfy the equilibrium between the three variables.

2.6 SHEAR STRESS ALONG THE PILE SIDES (SL_t)

Shear stress (τ) along the pile sides in the SW model (see Fig. 2.1) is defined according to the soil type (sand or clay).

2.6.1 Pile Side Shear in Sand

In the case of sand, the shear stress along the pile sides depends on the effective stress (σ_{vo}) at the depth in question and the mobilized angle of friction between the sand and the pile (φ_s). The mobilized side shear depends on the stress level and is given by the following equation,

$$t_i = (\bar{\mathbf{s}}_{vo})_i \tan(\mathbf{j}_s)_i; \quad \text{where} \quad \tan(\mathbf{j}_s)_i = 2 \tan(\mathbf{j}_m)_i$$

In Eqn. 2.15, note that mobilized side shear angle, $\tan\varphi_s$, is taken to develop at twice the rate of the mobilized friction angle ($\tan\varphi_m$) in the mobilized wedge. Of course, φ_s is limited to the fully developed friction angle (φ) of the soil.

2.6.2 Pile Side Shear Stress in Clay

The shear stress along the pile sides in clay depends on the clay's undrained shear strength. The stress level of shear along the pile sides (SL_t) differs from that in the wedge in front of the pile. The side shear stress level is function of the shear movement, equal to the pile deflection (y) at depth x from the ground surface.

This implies a connection between the stress level (SL) in the wedge and the pile side shear stress level (SL_t). Using the Coyle-Reese (1966) "t-z" shear stress transfer curves (Fig. 2.10), values for SL_t can be determined. The shear stress transfer curves represent the relationship between the shear stress level experienced by a one-foot diameter pile embedded in clay with a peak undrained strength, S_u , and side resistance, τ_{ult} (equal to ζ times the adhesional strength αS_u), for shear movement, y . The shear stress load transfer curves of Coyle-Reese can be normalized by dividing curve A ($0 < x < 3$ m) by $\zeta = 0.53$, curve B ($3 < x < 6$ m) by $\zeta = 0.85$, and curve C ($x > 6$ m) by $\zeta = 1.0$. These three values of normalization (0.53, 0.85, 1.0) represent the peaks of the curves A, B, and C, respectively, in Fig. 2.10a. Figure 2.10b shows the resultant normalized curves. Knowing pile deflection (y), one can assess the value of the mobilized pile side shear stress (τ) as

$$\mathbf{t}_i = (SL_t)_i (\mathbf{t}_{ult})_i \quad (2.16)$$

where

$$(\mathbf{t}_{ult})_i = \mathbf{z}(\alpha S_u)_i \quad (2.17)$$

and α indicates the adhesion value after Tomlinson (1957).

The normalized shear stress load transfer curves can be represented by the following equations.

For the normalized curves A ($x < 3$ m) and B ($3 < x < 6$ m),

$$SL_t = 12.9 y D - 40.5 y^2 D^2 \quad (2.18)$$

For the normalized curve C ($x > 6$ m)

$$SL_t = 32.3 y D - 255 y^2 D^2 \quad (2.19)$$

where y is in cm and D in m.

From the discussion above, it is obvious that SL_t varies nonlinearly with the pile deflection, y , at a given soil depth, x . Also, SL_t changes nonlinearly with soil depth for a given value of soil strain (see Fig. 2.11). These concepts are employed in each sublayer of clay.

2.7 SOIL PROPERTY CHARACTERIZATION IN THE STRAIN WEDGE MODEL

One of the main advantages of the SW model approach is the simplicity of the required soil properties necessary to analyze the problem of a laterally loaded pile. The properties required represent the basic and the most common properties of soil, such as the effective unit weight and the angle of internal friction or undrained strength.

The soil profile is divided into one or two foot sublayers, and each sublayer is treated as an independent entity with its own properties. In this fashion, the variation in soil properties or response (such as ϵ_{50} and ϕ in the case of sand, or S_u and $\bar{\phi}$ in the case of clay) at each sublayer of soil can be explored. It is obvious that soil properties should not be averaged at the midheight of the passive wedge in front of the pile for a uniform soil profile (as in the earlier work of Norris 1986), or averaged for all sublayers of a single uniform soil layer of a multiple layer soil profile.

2.7.1 Properties Employed for Sand Soil

- Effective unit weight (total above water table, buoyant below), $\bar{\gamma}$
- Void ratio, e , or relative density, D_r
- Angle of internal friction, ϕ
- Soil strain at 50% stress level, ϵ_{50}

While standard subsurface exploration techniques and available correlations may be used to evaluate or estimate $\bar{\gamma}$, e or D_r , and ϕ , some guidance may be required to assess ϵ_{50} .

The ε_{50} represents the axial strain (ε_1) at a stress level equal to 50 percent in the ε_1 -SL relationship that would result from a standard drained (CD) triaxial test. The confining (consolidation) pressure for such tests should reflect the effective overburden pressure ($\bar{\sigma}_{vo}$) at the depth (x) of interest. The ε_{50} changes from one sand to another and also changes with density state. In order to obtain ε_{50} for a particular sand, one can use the group of curves shown in Fig. 2.12 (Norris 1986) which show a variation based upon the uniformity coefficient, C_u , and void ratio, e . These curves have been assessed from sand samples tested with “frictionless” ends in CD tests at a confining pressure equal to 42.5 kPa (Norris 1977). Since the confining pressure changes with soil depth, ε_{50} , as obtained from Fig. 2.12, should be modified to match the existing pressure as follows:

$$(e_{50})_i = (e_{50})_{42.5} \left(\frac{(\bar{\sigma}_{vo})_i}{42.5} \right)^{0.2} \quad (2.20)$$

$$(\Delta s_{hf})_i = (\bar{\sigma}_{vo})_i \left[\tan^2 \left(45 + \frac{J_i}{2} \right) - 1 \right] \quad (2.21)$$

where $\bar{\sigma}_{vo}$ should be in kPa.

2.7.2 The Properties Employed for Normally Consolidated Clay

- Effective unit weight $\bar{\gamma}$
- Plasticity index, PI
- Effective angle of friction, $\bar{\phi}$
- Undrained shear strength, S_u
- Soil strain at 50% stress level, ε_{50}

Plasticity index, PI, and undrained shear strength, S_u , are considered the governing properties because the effective angle of internal friction, $\bar{\phi}$, can be estimated from the PI based on Fig. 2.13. The ε_{50} from an undrained triaxial test (UU at depth x or CU with $\sigma_3 = \bar{\sigma}_{vo}$) can be estimated based on S_u as indicated in Fig. 2.14.

An effective stress (ES) analysis is employed with clay soil as well as with sand soil. The reason behind using the ES analysis with clay, which includes the development of excess porewater pressure with undrained loading, is to define the three-dimensional strain wedge geometry based upon the more appropriate effective stress friction angle, $\bar{\phi}$. The relationship between the normally consolidated clay undrained shear strength, S_u , and $\bar{\sigma}_{vo}$ is taken as

$$S_u = 0.33 \bar{\sigma}_{vo} \quad (2.22)$$

assuming that S_u is the equivalent standard triaxial test strength. The effective stress analysis relies upon the evaluation of the developing excess porewater pressure based upon Skempton's equation (1954), i.e.

$$\Delta u = B \left[\Delta \sigma_3 + A_u (\Delta \sigma_1 - \Delta \sigma_3) \right] \quad (2.23)$$

where B equals 1 for saturated soil. Accordingly,

$$\Delta u = \Delta \sigma_3 + A_u (\Delta \sigma_1 - \Delta \sigma_3) \quad (2.24)$$

Note that $\Delta \sigma_3 = 0$ both in the shear phase of the triaxial test and in the strain wedge. Therefore, the mobilized excess porewater pressure is

$$\Delta u = A_u \Delta \sigma_1 \quad (2.25)$$

$$\Delta u = A_u \Delta \sigma_h \quad (2.26)$$

where $\Delta \sigma_1$ represents the deviatoric stress change in the triaxial test and $\Delta \sigma_h$ in the field, i.e.

$$(\Delta u)_i = (A_u)_i SL_i (\Delta \sigma_{hf})_i = (A_u)_i SL_i 2 (S_u)_i \quad (2.27)$$

Therefore, using the previous relationships, the Skempton equation can be rewritten for any sublayer (i) as follows:

The initial value of parameter A_u is 0.333 and occurs at very small strain for elastic soil response. In

$$(A_{uf})_i = \frac{1}{2} \left(1 + \frac{1}{\frac{(S_u)_i}{(\bar{\sigma}_{vo})_i}} - \frac{1}{\sin \bar{j}_i} \right) \quad (2.28)$$

addition, the value of parameter A_{uf} that occurs at failure at any sublayer (i) is given by the following relationship

after Wu (1966) as indicated in Fig. 2.15.

In Eqn. 2.28, $\bar{\phi}$ symbolizes the effective stress angle of internal friction; and, based on Eqn. 2.22, $S_u / \bar{\sigma}_{vo}$ equals 0.33. However, A_u is taken to change with stress level in a linear fashion as

$$(A_u)_i = 0.333 + SL_i [(A_{uf})_i - 0.333] \quad (2.29)$$

By evaluating the value of A_u , one can effectively calculate the excess porewater pressure, and then can determine the value of the effective horizontal stress, $(\bar{\sigma}_{vo} + \Delta\sigma_h - \Delta u)$, and the effective confining pressure, $(\bar{\sigma}_{vo} - \Delta u)$ at each sublayer, as shown in Fig. 2.15. Note that the mobilized effective stress friction angle, $\bar{\phi}_m$, can be obtained from the following relationship.

$$\tan^2 \left(45 + \frac{(\bar{j}_m)_i}{2} \right) = \frac{(\bar{s}_{vo} + \Delta s_h - \Delta u)_i}{(\bar{s}_{vo} - \Delta u)_i} \quad (2.30)$$

The targeted values of $\bar{\phi}_{mi}$ and SL_i in a clay sublayer and at a particular level of strain (ϵ) can be obtained by using an iterative solution that includes Eqns 2.11 through 2.13, and 2.27 through 2.30.

2.8 SOIL-PILE INTERACTION IN THE STRAIN WEDGE MODEL

The strain wedge model relies on calculating the modulus of subgrade reaction, E_s , which reflects the soil-pile interaction at any level of soil strain during pile loading. E_s also represents the secant slope at any point on the p-y curve, i.e.

$$E_s = \frac{p}{y} \quad (2.31)$$

Note that p represents the force per unit length of the pile or the BEF soil-pile reaction, and y symbolizes the pile deflection at that soil depth. In the SW model, E_s is related to the soil's Young's modulus, E , by two linking parameters, A and Ψ_s . It should be mentioned here that the SW model establishes its own E_s from the Young's modulus of the strained soil, and therefore, one can assess the p - y curve using the strain wedge model analysis. Therefore, E_s should first be calculated using the strain wedge model analysis to identify the p and y values.

Corresponding to the horizontal slice (a soil sublayer) of the passive wedge at depth x (see Fig. 2.1), the horizontal equilibrium of horizontal and shear stresses is expressed as

$$p_i = (\Delta \sigma_h)_i \overline{BC}_i S_1 + 2 \tau_i D S_2 \quad (2.32)$$

where S_1 and S_2 equal to 0.75 and 0.5, respectively, for a circular pile cross section, and equal to 1.0 for a square pile (Briaud et al. 1984). Alternatively, one can write the above equation as follows:

$$A_i = \frac{p_i / D}{(\Delta \sigma_h)_i} = \frac{\overline{BC}_i S_1}{D} + \frac{2 \tau_i S_2}{(\Delta \sigma_h)_i} \quad (2.33)$$

where A symbolizes the ratio between the equivalent pile face stress, p/D , and the horizontal stress change, $\Delta \sigma_h$, in the soil. (In essence, it is the multiplier that, when taken times the horizontal stress change, gives the equivalent face stress.) From a different perspective, it represents a normalized width (that includes side shear and shape effects) that, when multiplied by $\Delta \sigma_h$ yields p/D . By combining the equations of the passive wedge geometry and the stress level with the above relationship, one finds that

$$A_i = S_1 \left(1 + \frac{(h - x_i) 2 (\tan \mathbf{b}_m \tan \mathbf{j}_m)_i}{D} \right)^{\frac{1}{2}} + \frac{2 S_2 (\overline{\sigma}_{vo})_i (\tan \mathbf{f}_s)_i}{(\Delta \sigma_h)_i} \quad \text{in sand} \quad (2.34)$$

$$A_i = S_l \left(1 + \frac{(h - x_i) 2 (\tan \mathbf{b}_m \tan \bar{\mathbf{j}}_m)_i}{D} \right) \frac{S_2 (SL_t)_i}{SL_i} \quad \text{in clay} \quad (2.35)$$

Here the parameter A is a function of pile and wedge dimensions, applied stresses, and soil properties.

However, given that $\Delta \sigma_h = E \varepsilon$ in Eqn. 2.33,

$$p_i = A_i D (\Delta \mathbf{s}_h)_i = A_i D E_i \mathbf{e} \quad (2.36)$$

The second linking parameter, Ψ_s , relates the soil strain in the SW model to the linearized pile deflection angle, δ . Referring to the normalized pile deflection shape shown in Figs. 2.2 and 2.6

$$\mathbf{d} = \frac{\mathbf{g}}{2} \quad (2.37)$$

$$\frac{\mathbf{g}}{2} = \frac{\mathbf{g}_{\max}}{2} \sin 2 \Theta_m \quad (2.38)$$

and

$$\frac{\mathbf{g}_{\max}}{2} = \frac{\mathbf{e} - \mathbf{e}_v}{2} = \frac{(1 + \mathbf{n}) \mathbf{e}}{2} \quad (2.39)$$

where γ denotes the shear strain in the developing passive wedge. Using Eqns. 2.38 and 2.39, Eqn. 2.37 can be rewritten as

$$\mathbf{d} = \frac{\mathbf{e}(1 + \mathbf{n}) \sin 2 \Theta_m}{2} \quad (2.40)$$

Based on Eqn. 2.40, the relationship between ε and δ can be expressed as

$$\Psi = \frac{\mathbf{e}}{\mathbf{d}} \quad (2.41)$$

or

$$\Psi = \frac{2}{(1 + \mathbf{n}) \sin 2 \Theta_m} \quad (2.42)$$

The parameter Ψ varies with the Poisson's ratio of the soil and the soil's mobilized angle of internal friction (φ_m) and the mobilized passive wedge angle (Θ_m).

Poisson's ratio for sand can vary from 0.1 at a very small strain to 0.5 or larger (due to dilatancy) at failure, while the base angle, Θ_m , can vary between 45° (for $\varphi_m = 0$ at $\varepsilon = 0$) and 25° (for, say, $\varphi_m = 40^\circ$ at failure), respectively. For this range in variation for ν and φ_m , the parameter Ψ for sand varies between 1.81 and 1.74 with an average value of 1.77. In clay soil, Poisson's ratio is assumed to be 0.5 (undrained behavior) and the value of the passive wedge base angle, Θ_m , can vary between 45° (for $\varphi_m = 0$ at $\varepsilon = 0$) and 32.5° (for, say, $\varphi_m = 25^\circ$ at failure). Therefore, the value of the parameter Ψ will vary from 1.47 to 1.33, with an average value of 1.4.

It is clear from the equations above that employing the multi-sublayer technique greatly influences the values of soil-pile interaction as characterized by the parameter, A_i , which is affected by the changing effective stress and soil strength from one sublayer to another. The final form of the modulus of subgrade reaction

can be expressed as

$$(E_s)_i = \frac{p_i}{y_i} = \frac{A_i D e E_i}{d(h - x_i)} = \frac{A_i}{(h - x_i)} D \Psi E_i \quad (2.43)$$

It should be mentioned that the SW model develops its own set of non-unique p-y curves which are function of both soil and pile properties, and are affected by soil continuity (layering) as presented by Ashour et al. (1996).

2.9 PILE HEAD DEFLECTION

As mentioned previously, the deflection pattern of the pile in the SW model is continuous and linear. Based on this concept, pile deflection can be assessed using a simplified technique which provides an estimation for the linearized pile deflection, especially y_o at the pile head. By using the multi-sublayer technique, the deflection of the pile can be calculated starting with the base of the mobilized passive wedge and moving upward along the pile, accumulating the deflection values at each sublayer as shown in the following relationships and Fig. 2.16.

$$y_i = H_i d_i = H_i \frac{e}{\Psi} \quad (2.44)$$

$$y_o = \sum y_i \quad i = 1 \text{ to } n \quad (2.45)$$

where the Ψ_s value changes according to the soil type (sand or clay), and H_i indicates the thickness of sublayer i and n symbolizes the current number of sublayers in the mobilized passive wedge.

The main point of interest is the pile head deflection which is a function of not only the soil strain but also of the depth of the compound passive wedge that varies with soil and pile properties and the level of soil strain.

2.10 ULTIMATE RESISTANCE CRITERIA IN STRAIN WEDGE MODEL

The mobilized passive wedge in front of a laterally loaded pile is limited by certain constraint criteria in the

SW model analysis. Those criteria differ from one soil to another and are applied to each sublayer. Ultimate resistance criteria govern the shape and the load capacity of the wedge in any sublayer in SW model analysis. The progressive development of the ultimate resistance with depth is difficult to implement without employing the multi-sublayer technique.

2.10.1 Ultimate Resistance Criterion of Sand Soil

The mobilization of the passive wedge in sand soil depends on the horizontal stress level, SL , and the pile side shear resistance, τ . The side shear stress is a function of the mobilized side shear friction angle, φ_s , as mentioned previously, and reaches its ultimate value ($\varphi_s = \varphi$) earlier than the mobilized friction angle, φ_m , in the wedge (i.e. $SL_t \geq SL$). This causes a decrease in the rate of growth of sand resistance and the fanning of the passive wedge as characterized by the second term in Eqns 2.32 and 2.34, respectively.

Once the stress level in the soil of a sublayer of the wedge reaches unity ($SL_i = 1$), the stress change and wedge fan angle in that sublayer cease to grow. However, the width BC the face of the wedge can continue to increase as long as ε (and, therefore, h in Eqn. 2.7) increases. Consequently, soil-pile resistance, p , will continue to grow more slowly until a condition of initial soil failure ($SL_i = 1$) develops in that sublayer. At this instance, $p = p_{ult}$ where p_{ult} in sand, given as

$$(p_{ult})_i = (\Delta s_{hf})_i \overline{BC}_i S_1 + 2(t_f)_i D S_2 \quad (2.46)$$

p_{ult} is a temporary ultimate condition, i.e. the fanning angle of the sublayer is fixed and equal to φ_i , but the depth of the passive wedge and, hence, BC continue to grow. The formulation above reflects that the near-surface “failure” wedge does not stop growing when all such sublayers reach their ultimate resistance at $SL = 1$ because the value of h at this time is not limited. Additional load applied at the pile head will merely cause the point at zero deflection and, therefore, h to move down the pile. More soil at full strength ($SL = 1$) will be mobilized to the deepening wedge as BC , therefore, p_{ult} will increase until either flow around failure or a plastic hinge occurs.

Recognize that flow around failure occurs in any sublayer when it is easier for the sand at that depth to flow around the pile in a local bearing capacity failure than for additional sand to be brought to failure and added to the already developed wedge. However, the value at which flow failure occurs [$A_i = (A_{ult})_i$, $(p_{ult})_i = (\Delta\sigma_{hf})_i (A_{ult})_i D$] in sand is so large that it is not discussed here. Alternatively, a plastic hinge can develop in the pile when the pile material reaches its ultimate resistance at a time when $SL_i \leq 1$ and $A_i < (A_{ult})_i$. In this case, h becomes fixed, and BC_i and p_i will be limited when SL_i becomes equal to 1.

2.10.2 Ultimate Resistance Criterion of Clay Soil

The situation in clay soil differs from that in sand and is given by Gowda (1991) as a function of the undrained strength $(S_u)_i$ of the clay sublayer.

$$(p_{ult})_i = 10(S_u)_i D S_1 + 2(S_u)_i D S_2 \quad (2.47)$$

Consequently,

$$(A_{ult})_i = \frac{(p_{ult})_i}{(\Delta\sigma_{hf})_i} = \frac{(p_{ult})_i}{D 2(S_u)_i} = 5 S_1 + S_2 \quad (2.48)$$

A_{ult} indicates the limited development of the sublayer wedge geometry for eventual development of flow around failure ($SL_i = 1$) and, consequently, the maximum fanning angle in that sublayer becomes fixed, possibly at a value $\phi_m \leq \bar{\phi}$. If a plastic hinge develops in the pile at SL_i less than 1, then h will be limited, but BC , and p_i will continue to grow until A_i is equal to A_{ult} or p_i is equal to $(p_{ult})_i$.

2.11 STABILITY ANALYSIS IN THE STRAIN WEDGE MODEL

The objective of the SW model is to establish the soil response as well as model the soil-pile interaction through the modulus of subgrade reaction, E_s . The shape and the dimensions of the passive wedge in front of the pile basically depend on two types of stability which are the local stability of the soil sublayer and the global stability of the pile and the passive wedge. However, the global stability of the passive wedge

depends, in turn, on the local stability of the soil sublayers.

2.11.1 Local Stability of a Soil Sublayer in the Strain Wedge Model

The local stability analysis in the strain wedge model satisfies equilibrium and compatibility among the pile segment deflection, soil strain, and soil resistance for the soil sublayer under consideration. Such analysis allows the correct development of the actual horizontal stress change, $\Delta\sigma_h$, pile side shear stress, τ , and soil-pile reaction, p , associated with that soil sublayer (see Fig. 2.1). It is obvious that the key parameters of local stability analysis are soil strain, soil properties, and pile properties.

2.11.2 Global Stability in the Strain Wedge Model

The global stability, as analyzed by the strain wedge model, satisfies the general compatibility among soil reaction, pile deformations, and pile stiffness along the entire depth of the developing passive wedge in front of the pile. Therefore, the depth of the passive wedge depends on the global equilibrium between the loaded pile and the developed passive wedge. This requires a solution for Eqn. 2.1.

The global stability is an iterative beam on elastic foundation (BEF) problem that determines the correct dimensions of the passive wedge, the corresponding straining actions (deflection, slope, moment, and shear) in the pile, and the external loads on the pile. Satisfying global stability conditions is the purpose of linking the three-dimensional strain wedge model to the BEF approach. The major parameters in the pile global stability problem are pile stiffness, EI , and the modulus of subgrade reaction profile, E_s , as determined from local stability in the strain wedge analysis. Since these parameters are determined for the applied soil strain, the stability problem is no longer a soil interaction problem but a one-dimensional BEF problem. Any available numerical technique, such as the finite element or the finite difference method, can be employed to solve the global stability problem. The modeled problem, shown in Fig. 2.4c, is a BEF and can be solved to identify the depth, X_o , of zero pile deflection.

2.12 VERIFICATION OF APPROACH

Based on the SW model concepts presented in this chapter and Ashour et al. (1996), a computer program

(SWSG) has been developed to solve the problem of a laterally loaded isolated pile and a pile group in layered soil (Ashour et al. 1996). Any verification of the methodology and algorithms employed should incorporate comparisons to field and laboratory tests for single piles and pile groups. The results presented below demonstrate the capability of the SW model approach and SWM program (Ashour et al 1997 and 1998) in solving problems of laterally loaded piles relative to different soil and pile properties. It should be noted that pile and soil properties employed with the SW model analyses for the following field tests are the same properties mentioned in the references below.

2.12.1 Mustang Island Full-Scale Load Test on a Pile in Submerged Dense Sand (Reese et al. 1974 and Cox et al. 1974)

As reported by Reese et al (1974), a series of full-scale lateral load tests was performed on two single piles in sand at Mustang Island near Corpus Christi, Texas in 1966. The results obtained from those tests were used to develop criteria for the design of laterally loaded piles in sand and to establish a family of p-y curves at different depths in the sand soil. In addition, the field results were used to characterize the pile-head load-deflection curve at the ground surface.

Pile Configuration and Material Properties

Tests were performed on two 0.61 m outside diameter (O.D.) steel pipe piles (A-53) with a wall thickness of 9.5 mm. The two piles were driven to a penetration of 21 m below the ground surface.

The two closed end piles were instrumented along their lengths for the measurement of bending moment.

Each pile tested consisted of a 11.6-m uninstrumented section, a 9.75-m instrumented section, and a 3-m uninstrumented section. The piles maintained an approximate stiffness, EI, of 167168 kN-m².

Connecting flanges of 91.5 x 51 x 3.81 cm were welded to the instrumented section and to the 3-m

section. Small holes were cut in the pile wall just below the diaphragm to allow water and air to escape from the bottom of the 11.65-m section during driving. More details about the lateral load testing can be obtained by referring to Cox et al (1974).

Table 1. Pile Properties Employed in the SWM Program

Pile Type	Shape	Length	Diam.	Wall thick.	Stiffness, EI	Head Fixity
Steel Pipe	Round	21 m	0.61 m	9.5 mm	167168 KN-m ²	Free-head

Foundation Material Characterization

Two soil borings were taken at the test site which were at the Shell Oil Company battery of tanks on the Mustang Island near Port Arkansas, Texas. As mentioned in Cox et al (1974), a comparison of the logs of borings 1 and 2 indicate that there was a slight variation in the soil profile between the two locations. In the top 12.2 m of boring 1, the sand strata was classified as a fine sand, while the soil in the top 12.2 m of boring 2 was classified as a silty fine sand. This difference in soil material was also reflected in the plot of the number of blows, N , of the standard penetration test (Cox et al, 1974). The N -values at boring 2 from 0 to 12.2 m are generally lower than those from boring 1. The sand from 0 to 6.1 m was classified as a medium dense sand, from 6.1 to 12.2 m as a dense sand, and from 15.2 m to 21.4 m as a dense sand. Laboratory tests were run on samples from boring 1 obtained using a piston sampler. More details of soil properties and the laboratory tests are documented in Cox et al (1974).

The angle of internal friction was found to be 39 degree and the submerged unit weight of sand was

10.3 kN/m³. The axial strain of the sand at 50 percent stress level, ϵ_{50} , characterized based on Fig. 2.14 was 0.003 based on the assessed sand.

Table 2. Soil Properties Employed in the SWM Program

Soil type	Thickness	Effective Unit Weight	Friction Angle, \mathbf{f}	ϵ_{50}
Medium dense	21 m	10.3 kN/m ³	39 degree	0.003

Figure 2.17 presents a comparison of field results versus SW model results and results obtained using the computer program COM624 (Reese 1977). Note that it is from this specific field test that the COM624 p-y curves for sand were derived and, therefore, a good correspondence between COM624 and measured results is to be expected. The SW model results of pile-head response shown in Fig. 2.17 are in excellent agreement at lower pile-head deflections (lower strain levels) and within 5 percent at higher levels of deflection (higher strain levels). The SW model predicted maximum moment of Fig. 2.17 is in excellent agreement with measured results throughout.

2.12.2 Pyramid Building at Memphis, Tennessee, Full-Scale Load Test on a Pile in Layered Clay Soil (Reuss et al. 1992)

A lateral load test was performed on a full-scale pile in downtown Memphis. In order to improve the lateral capacity of the piles associated with this building, 1.8 meters of soft soil around the piles was removed and replaced with stiff compacted clay. Since the improved soil profile consisted of different types of soil, the corresponding test represents a layered field case study.

Pile Configuration and Material Properties

A 400-mm-diameter reinforced concrete pile was installed to a total penetration of 22 meters. An inclinometer casing was installed in the pile to measure the lateral deflection. For a composite material such as reinforced concrete, the pile stiffness, EI, is a function of bending moment on the pile cross-section. The experimental values of EI as a function of the bending moment are reported by Reuss et al. (1992). The

selected value of EI lies, in general, between the uncracked EI value and the cracked EI value. An average value for EI equal to 38,742 m²-kN was characterized for the pile. Additional concrete was cast around the pile to restrain it against excessive deflection when it was reloaded, and the pile head was free to rotate.

Table 3. Pile Properties Employed in the SWM Program

Pile Type	Shape	Length	Diam.	Average Stiffness, EI	Head Fixity
R/C	Rounded	22 m	0.4 m	38,742 KN-m ²	Free-head

Foundation Material Characterization

The lateral load test conducted was performed at a location where the subsurface soil conditions could be approximated using information from a nearby soil boring. The soil profile, which consisted of different types of soils at this site, was the main advantage of this pile test. As documented by Reuss et al (1992), the top 1.8 meters of loose soil was replaced with a compacted gravelly clay for the lateral load test. The fill soil consisted of cinders, bricks, concrete, gravel, and sand intermixed with varying percentages of clay to 1.8 meters below the ground surface. The first soil stratum (fill soil) exhibited an undrained shear strength (S_u) of 47.9 kPa, a soil density (γ) of 18.08 kN/m³, and an ϵ_{50} of 0.005. The fill soil was underlain by soft to firm dark gray clay and silt clay with occasional silt and sand lenses. This soil layer (the second stratum) extended from approximately 1.8 to 13.1 meters below the ground surface. The second stratum of soil exhibited an S_u of 24 kPa, a γ of 9.11 kN/m³, and an ϵ_{50} of 0.02. Standard penetration N-values for stratum 2 varied from 3 through 10 with an average of about 5 blows per 0.3 meters. A third stratum between a depth of 13.1 meters and 19.9 meters below the ground surface had a reported S_u value of 38.3 kPa, γ of 9.11 kN/m³, and an ϵ_{50} value of 0.01 were reported. This stratum exhibited a greater frequency of silty and clayey sand lenses and increased strength as evidenced by penetration resistance N-values ranging from 4 to 16 and averaging 10. The fourth stratum lay a depth of 19.9 meters and consisted of stiff silty clay and silty sand lenses. This stratum exhibited an S_u value of 71.8 kPa, γ of 9.11 kN/m³, and ϵ_{50}

of 0.005.

Table 4. Soil Properties Employed in the SWM Program

Soil Layer #	Soil type	Thickness	Effective Unit Weight	ε_{50}	S_u
1	Sand mixed with clay, ciders and gravel	1.8 m	18.08 kN/m ³	0.005	47.9 kPa
2	Dark gray clay and silt clay	11.3 m	9.11 kN/m ³	0.02	24 kPa
3	Silty clay sand	6.8 m	9.11 kN/m ³	0.01	38.3 kPa
4	stiff silty clay	Below 19.9 m depth	9.11 kN/m ³	0.005	71.8 kPa

The soil properties of the fill soils and the second stratum (the natural clay soil) were modified by Reuss et al. (1992) to force good agreement between the results assessed with COM624 (Reese 1977) and the field results (see Fig. 2.18a). The measured values of the undrained shear strength of the first and second strata were increased by 40 percent and 20 percent, respectively, to achieve such agreement. The measured soil properties were employed with the SW model to analyze the response of the pile in the improved soil profile. Figure 2.18a shows good agreement between the measured values and SW model predicted pile-head response in the improved soil profile. Figure 2.18b shows the pile-head response predicted by COM624 and SW model analysis for the same pile in the original soil profile (natural clay at its measured undrained strength with no fill layer).

2.12.3 Sabine River Full-Scale Load Tests on a Pile in Soft Clay (Matlock 1970)

The benefit of the Sabine River tests derives from having load tests on piles of both free- and fixed-head conditions. Note that the results of the free-head test were performed to establish the p-y curve criteria for

piles in soft clay (Matlock 1970).

Pile Configuration and Material Properties

The same pile was driven twice, and two complete series of static and cyclic loading tests were performed at the Lake Austin site and then at the Sabine River site. Only the static loading tests are considered in this study. The driven pile was a steel pipe pile of 0.32-m-diameter and a 12.8-m embedded length. The pile maintained an approximate stiffness, EI, of 31,255 kN-m². The piles was tested under free-head conditions at both sites (Lake Austin and Sabine River) and fixed-head conditions at Sabine River site. The Sabine River tests were used to develop the p-y curves for short term static loading in soft clay.

Table 5. Pile Properties Employed in the SWM Program

Pile Type	Shape	Length	Diam.	Wall thick.	Stiffness, EI	Head Fixity
Steel Pipe	Rounded	12.8 m	0.32 m	12.75 mm	31,255 KN-m ²	Free-head (1) Fixed-head (2)

Foundation Material Characterization

As noted in Matlock et al (1970), extensive sampling and testing of the soils were undertaken at the Sabine River site. In-situ vane shear tests as well as laboratory triaxial compression tests were performed to determine stress-strain characteristics.

Sabine clay is typical of a slightly overconsolidated marine deposit, and exhibited lower Vane shear strengths averaging about 14.33 kPa in the significant upper zone. According to Matlock et al (1970), the values of ϵ_{50} for most clays may be assumed to be between 0.005 and 0.02. An intermediate value of 0.01 is probably satisfactory for most purposes. Average values of 0.012 and 0.007 for ϵ_{50} were estimated from the soil stress-strain curves at Sabine River.

Table 4. Soil Properties Employed in the SWM Program

Soil Layer #	Soil type	Thickness	Effective Unit Weight	ϵ_{50}	S_u
1	Soft clay	12.8 m	7.8 kN/m ³	0.007	14.33 kPa

As seen in Fig. 2.19a, the predicted free-head SW model results are in good agreement with the observed results for the Sabine River site. At higher levels of deflection, the results calculated using the SW model fall approximately 5 to 10 percent below those measured in the field. By comparison, the SW model predicted and the observed fixed-head pile response are in excellent agreement as shown in Fig. 2.19b. SW model results were established for two cases of the clay based on having a single average S_u and, separately, for a varying S_u .

2.13 SUMMARY

The SW model approach presented here provides an effective method for solving the problem of a laterally loaded pile in layered soil. This approach assesses its own nonlinear variation in modulus of subgrade reaction or p-y curves. The strain wedge model allows the assessment of the nonlinear p-y curve response of a laterally loaded pile based on the envisioned relationship between the three-dimensional response of a flexible pile in the soil to its one-dimensional beam on elastic foundation parameters. In addition, the strain wedge model employs stress-strain-strength behavior of the soil as established from the triaxial test in an effective stress analysis to evaluate mobilized soil behavior.

Compared to empirically based approaches which rely upon a limited number of field tests, the SW approach depends on well known or accepted principles of soil mechanics (the stress-strain-strength relationship) in conjunction with effective stress analysis. Moreover, the required parameters to solve the problem of the laterally loaded pile are a function of basic soil properties that are typically available to the designer.

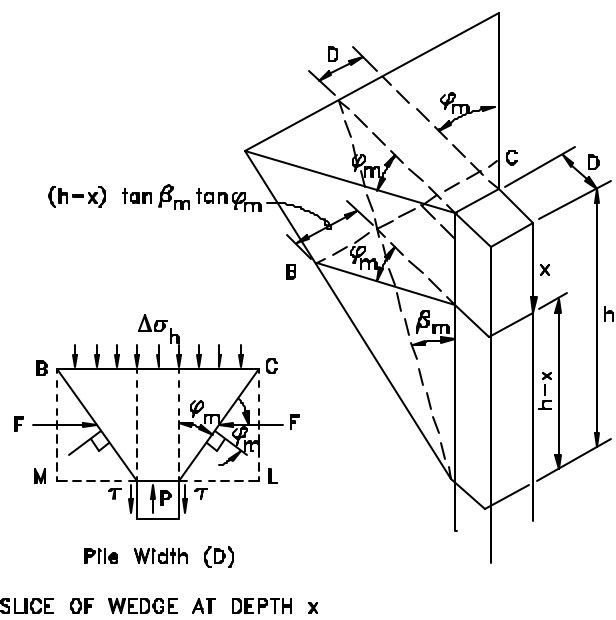


Fig. 2.1 The Basic Strain Wedge in Uniform Soil

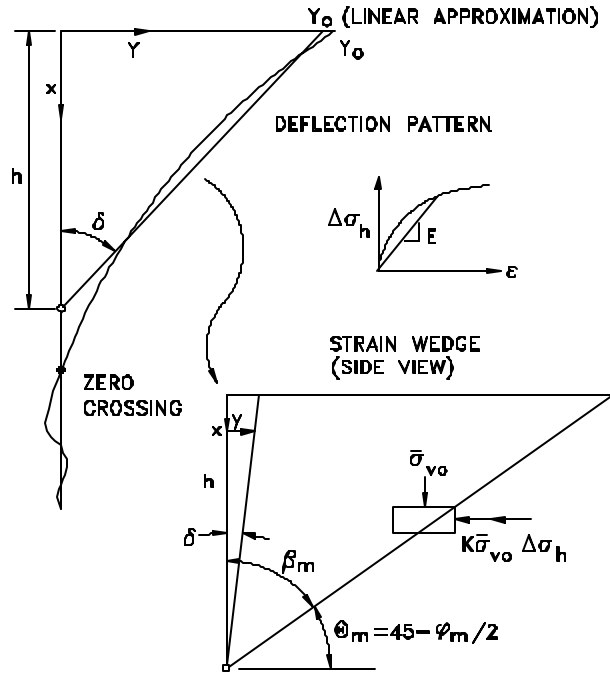


Fig. 2.2 Deflection Pattern of a Laterally Loaded Long Pile and the Associated Strain Wedge

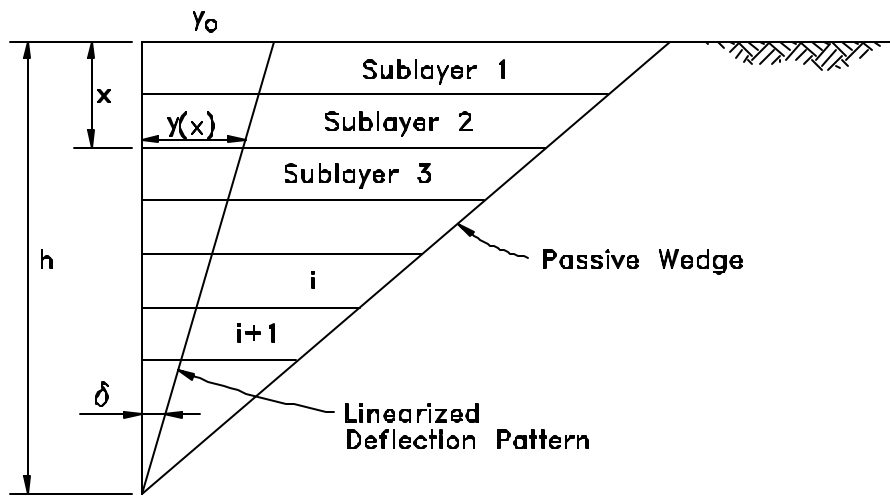


Fig. 2.3 The Linearized Deflection Pattern of a Pile Embedded in Soil Using the Multi-Sublayer Strain Wedge Model

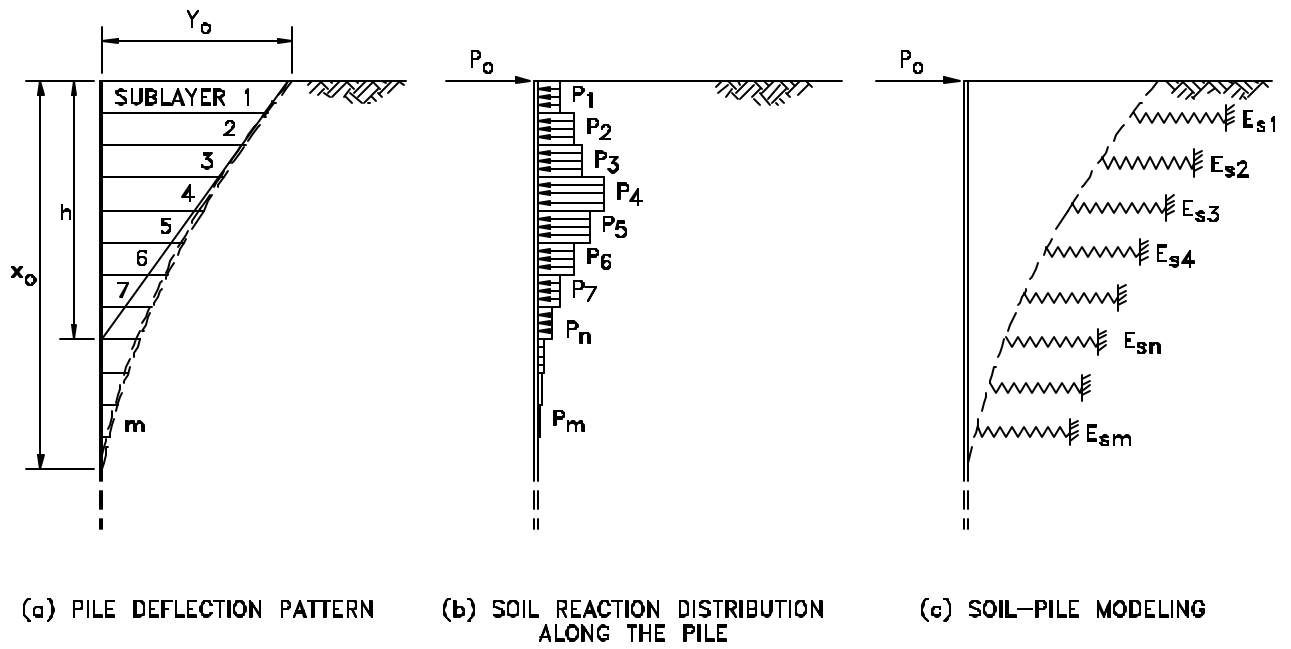
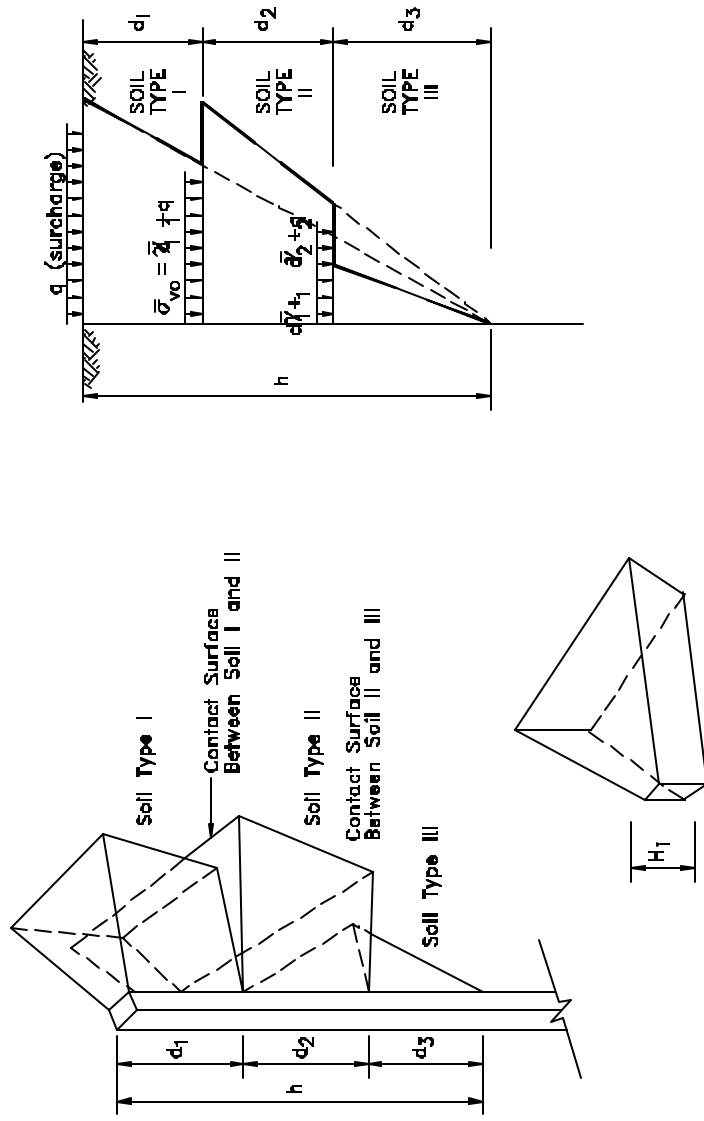


Fig. 2.4 Soil-Pile Interaction in the Multi-Sublayer Technique



The Geometry of Sublayer

Fig. 2.5 The Proposed Geometry of the Compound Passive Wedge

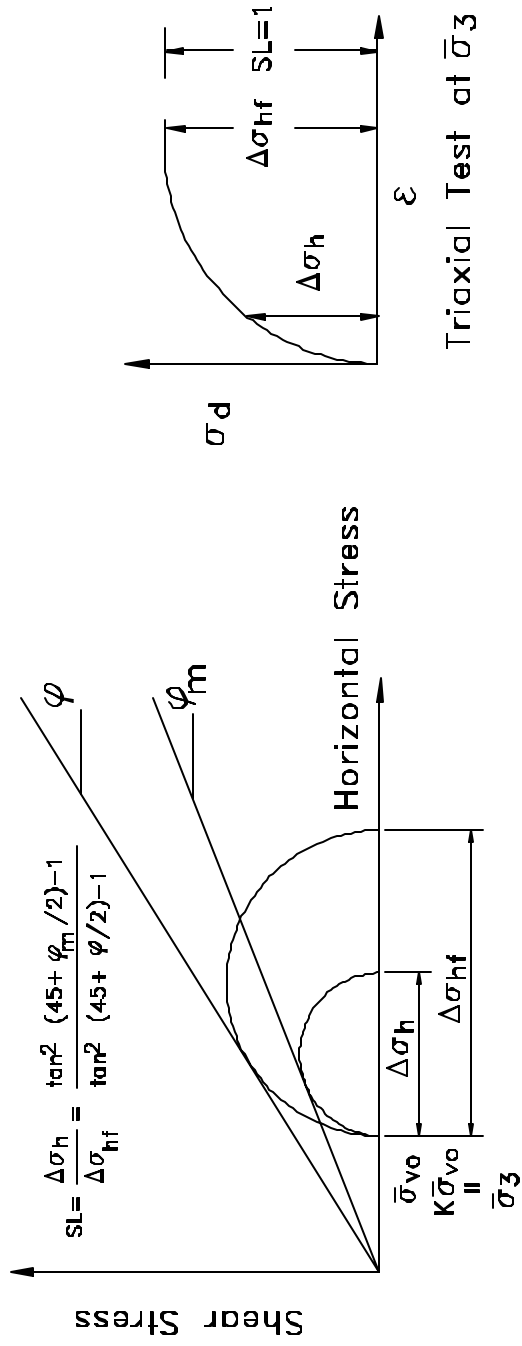
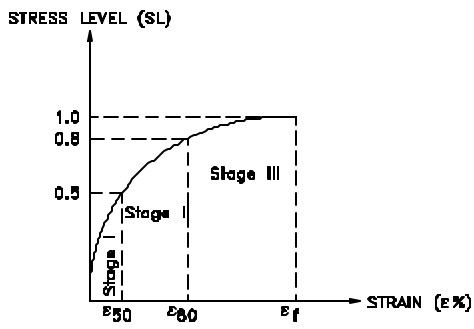
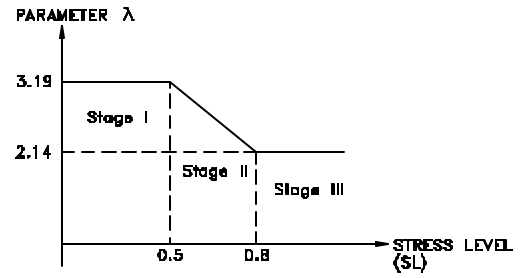


Fig. 2.7 Relationship Between Horizontal Stress Change, Stress Level, and Mobilized Friction Angle



(a) THE DEVELOPED HYPERBOLIC STRESS-STRAIN RELATIONSHIP IN SOIL



(b) THE VARIATION OF THE FITTING PARAMETER λ VERSUS STRESS LEVEL (SL)

Fig. 2.8 The Developed Stress-Strain Relationship in

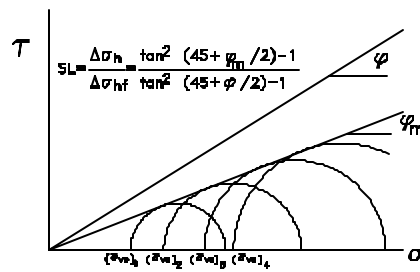
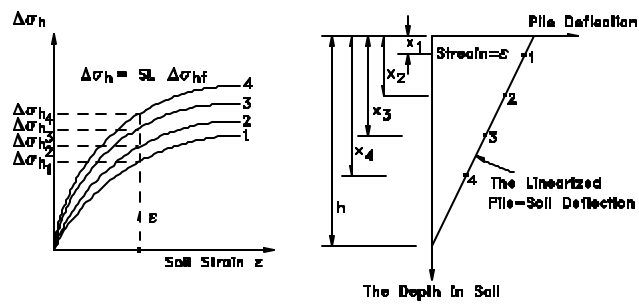


Fig. 2.9 The Nonlinear Variation of Stress Level Along the Depth of Soil at Constant Strain _

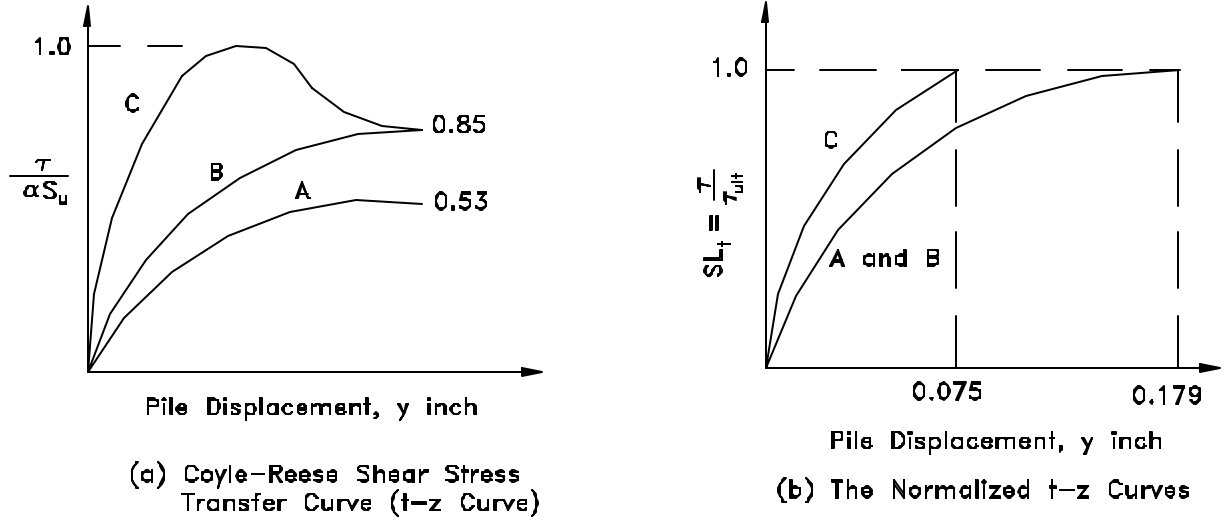


Fig. 2.10 The Employed Side Shear Stress-Displacement Curve in Clay

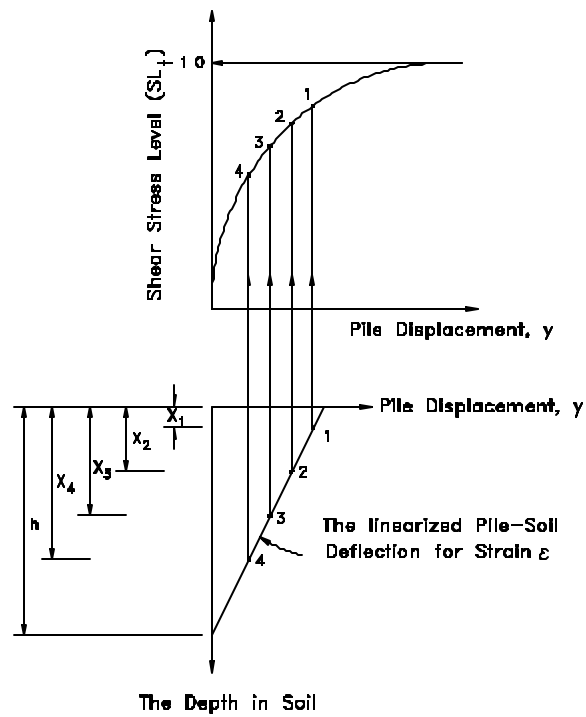


Fig. 2.11. The Nonlinear Variation of Shear Stress Level (SL_t) Along the Depth of Soil

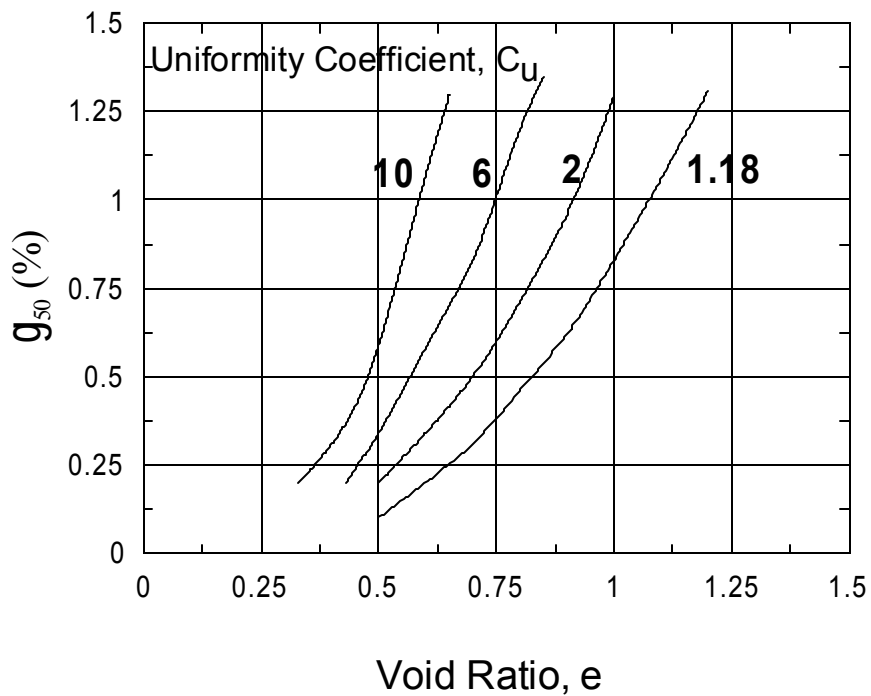


Fig. 2.12 Relationship Between ε_{50} , Uniformity coefficient (C_u) and Void Ratio (e) (Norris 1986)

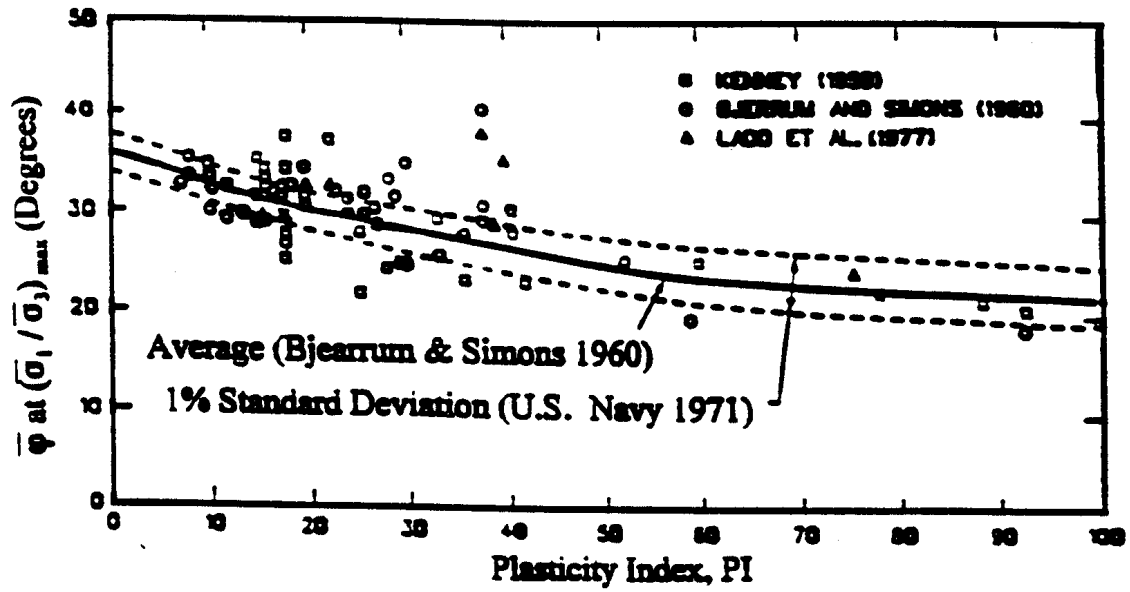


Fig. 2.13 Relationship Between Plasticity Index (PI) and Effective ϕ (US Army Corps of Engineers 1996)

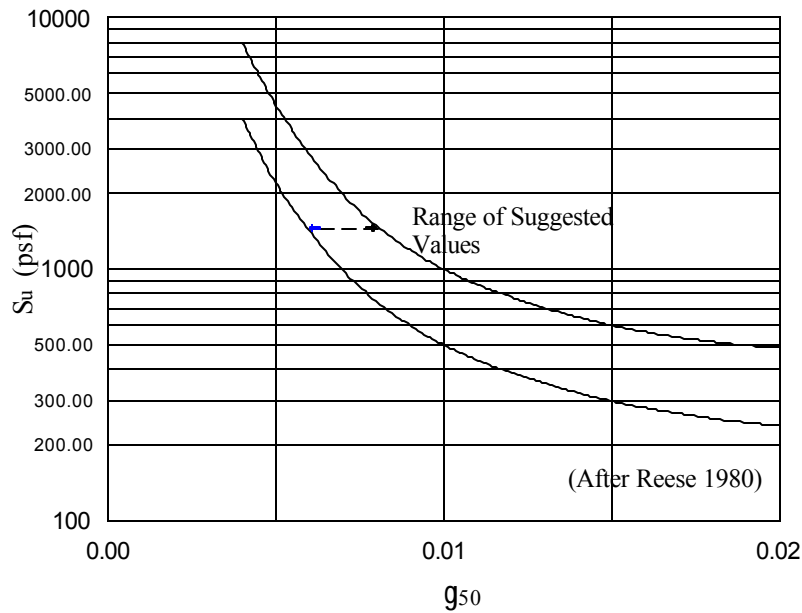


Fig. 2.14 Relationship Between ϵ_{50} and Undrained Shear Strength, S_u

(Evans and Duncan 1982)

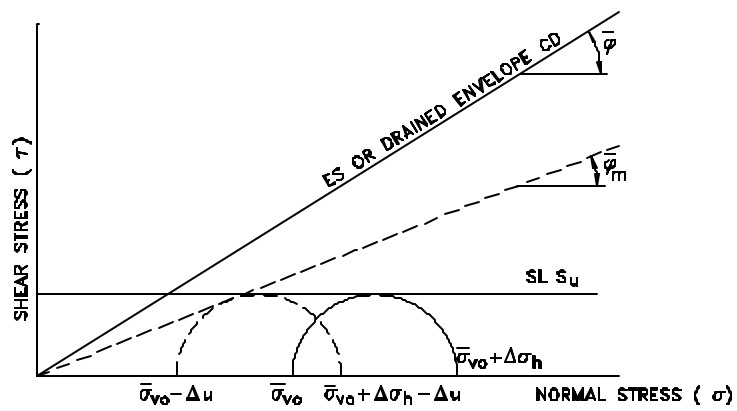
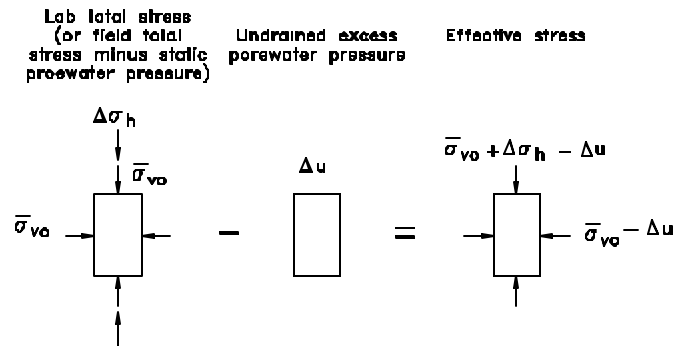


Fig. 2.15 Relationship Between Effective Stress and Total Stress Conditions

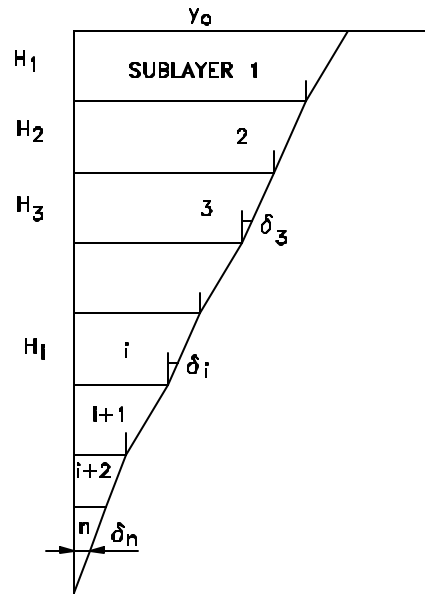


Fig. 2.16 The Assembling of Pile Head Deflection Using the Multi-Sublayer Technique

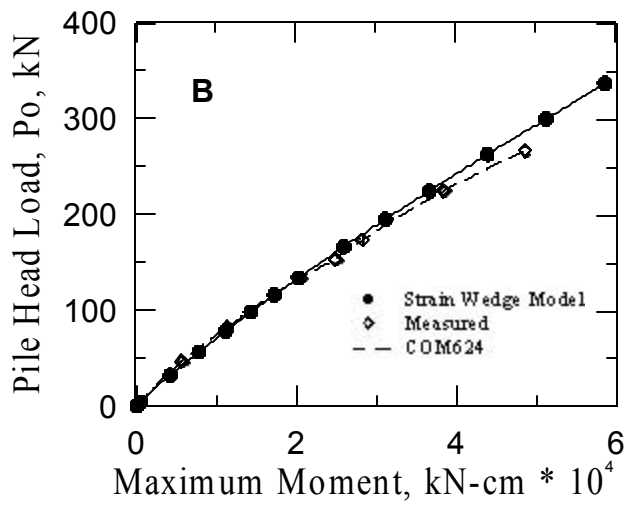
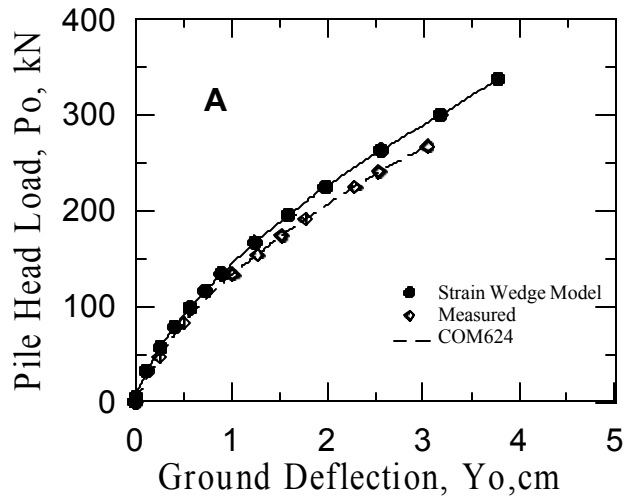


Fig. 2.17 The Measured and Predicted Response of a Laterally Loaded Pile in Sand at the Mustang Island Test.

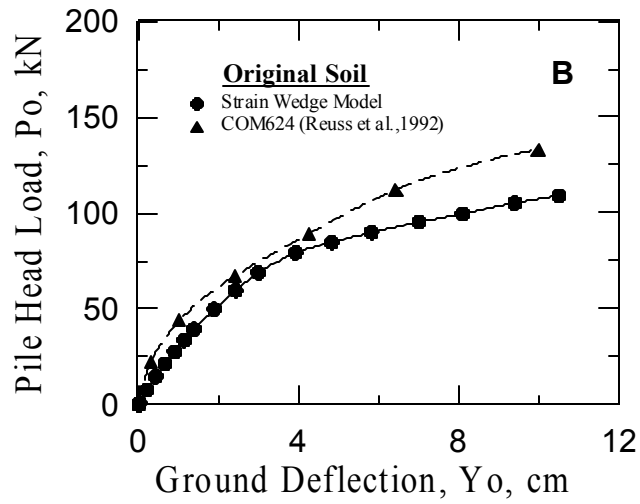
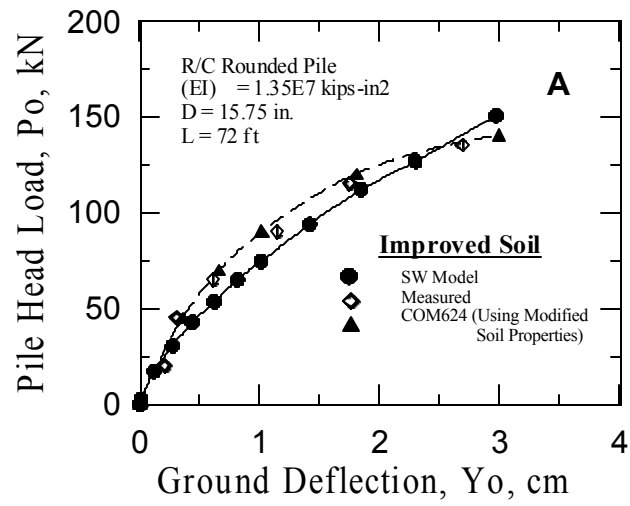


Fig. 2.18 The Measured and the Predicted Response of the Loaded Pile in the Improved and the Original Soils at the Pyramid Building, Memphis, Test.

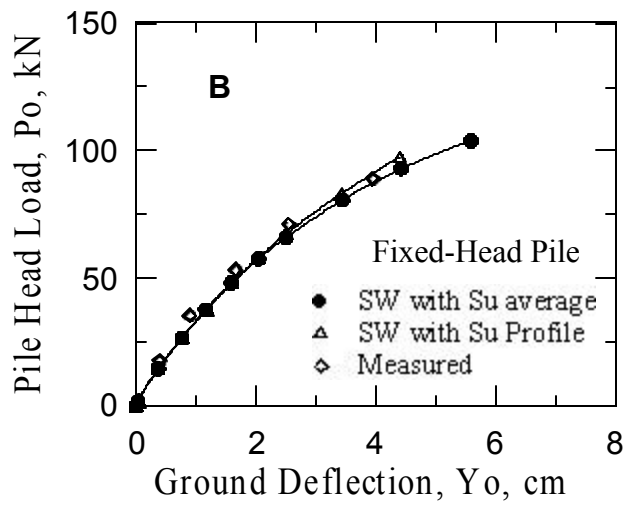
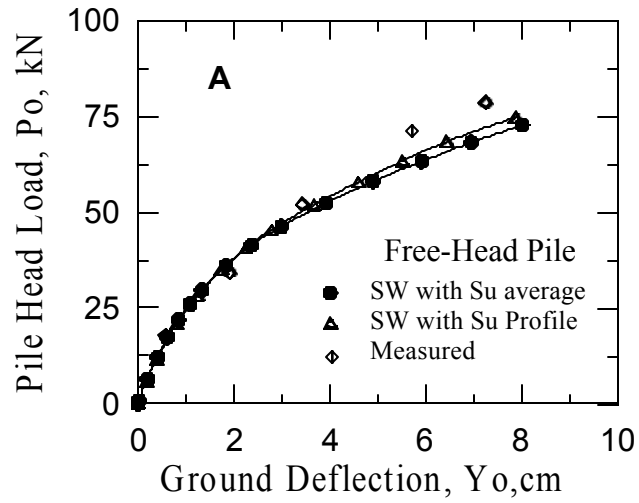


Fig. 2.19 The Measured and the SW Model Results of the Loaded Pile at the Sabine River Test.

CHAPTER 3

PILE GROUP IN LAYERED SOILS

3.1 INTRODUCTION

As presented in Chapter 2, the prediction of single pile response to lateral loading using the SW model correlates traditional one-dimensional beam on an elastic foundation (BEF) response to three-dimensional soil-pile interaction. In particular, the Young's modulus of the soil is related to the corresponding horizontal subgrade modulus; the deflection of the pile is related to the strain that exists in the developing passive wedge in front of the pile; and the BEF line load for a given deflection is related to the horizontal stress change acting along the face of the developing passive wedge. The three-dimensional characterization of the laterally loaded pile in the SW model analysis provides an opportunity to study the interference among the piles in a pile group in a realistic fashion. The influence of the neighboring piles on an individual pile in the group will be a function of soil and pile properties, pile spacing, and the level of loading. These parameters are employed together in the SW model analysis to reflect the pile-soil-pile interaction on pile group behavior.

The work presented illustrates the links between the single pile and the pile group analysis. The pile group procedure commonly used today employs the p-y multiplier technique (Brown et al. 1988). Such procedure is based on reducing the stiffness of the traditional (Matlock-Reese) p-y curve by using a multiplier ($f_m < 1$), as seen in Fig. 3.1. The value of the p-y curve multiplier should be assumed and is based on the data collected from full-scale field tests on pile groups which are few (Brown et al. 1988). Consequently, a full-scale field test (which is costly) is strongly recommended in order to determine the value of the multiplier (f_m) of the soil profile at the site under consideration. Moreover, the suggested value of the multiplier (f_m) is taken to be constant for each soil layer at all levels of loading.

In essence, this is quite similar to the traditional approach given in NAVFAC (DM 7.2, 1982) in which the subgrade modulus, E_s , is reduced by a factor (R_m) taken as a function of pile spacing ($R_m = 1$ at 8-diameter pile spacing varying linearly to 0.25 at 3 diameters). The difference is that f_m has been found to vary with pile row (leading, second, third and higher); and is taken to be constant with lateral pile displacement, y . By contrast, Davisson (1970) suggested that R_m should be taken constant with pile head load such that displacement y increases. In any case, neither f_m , nor R_m , reflects any change with load or displacement level, soil layering, pile stiffness, pile position (e.g. leading corner versus leading interior pile, etc.), differences in spacing both parallel and normal to the direction of load, and pile head fixity.

As seen in Fig. 3.2, the interference among the piles in a group varies with depth, even in the same uniform soil, and increases with level of loading as the wedges grow deeper and fan out farther. Therefore, the use of a single multiplier that is both constant with depth and constant over the full range of load/deflection would seem to involve significant compromise.

The assessment of the response of a laterally loaded pile group based on soil-pile interaction is presented herein. The strain wedge (SW) model approach, developed to predict the response of a long flexible pile under lateral loading (Ashour et al. 1998; and Ashour and Norris 2000), is extended in this paper to analyze the behavior of a pile group in uniform or layered soil. Several field and experimental tests reported in the literature are used to demonstrate the validity of the approach.

3.2 CHARACTERIZATION OF PILE GROUP INTERFERENCE

The pile group is characterized in terms of the three-dimensional pile-soil-pile interaction (Pilling 1997) and then converted into its equivalent one-dimensional BEF model with associated parameters (i.e. an ever changing modulus of sugrade reaction profile). Therefore, the interference among the piles in a group is determined based on the geometry of the developing passive wedge of soil in front of the pile in addition to the pile spacing. A fundamental concept of the SW model is that the size and shape (geometry) of the passive wedge of soil changes in a mobilized fashion as a function of

both soil and pile properties, at each level of loading, and is expressed as follows:

$$\beta_m = 45 + \frac{\varphi_m}{2} \quad (3.1)$$

$$\overline{BC} = D + (h - x) 2 \tan \beta_m \tan \varphi_m \quad (3.2)$$

As seen in Fig. 3.3, \overline{BC} is the width of the wedge face at any depth, x . D is the width of the pile cross section, h is the current depth of the passive wedge which depends on the lateral deflection of the pile and, in turn, on the pile properties such as pile stiffness (EI) and pile head fixity. φ_m is the mobilized fan angle of the wedge (also the mobilized effective stress friction angle of the soil) and is a function of the current stress level (SL) or strain (ϵ) in the soil as presented by (Ashour et al. 1998).

The overlap of shear zones among the piles in a group varies along the length of the pile as shown in Figs. 3.3 and 3.4. Also, the interference among the piles grows with the increase in lateral load.

The modulus of subgrade reaction, which is determined based on the SW model approach, will account for the additional strains (i.e. stresses) in the adjacent soil due to pile interference within the group (Figs. 3.4 and 3.5). Thus the modulus of subgrade reaction (i.e. the secant slope of the p-y curve) of an individual pile in a group will be reduced in a mobilized fashion according to pile and soil properties, pile spacing and position, the level of loading, and depth, x . No single reduction factor (f_m or R_m) for the p-y curve (commonly, assumed to be a constant value with depth and level of loading) is needed or advised. The SW model also allows direct evaluation of the nonlinear variation in pile group stiffness as required, for instance, for the seismic analysis of a pile-supported highway bridge.

The multi-sublayer technique developed by Ashour et al. (1996 and 1998) and presented in Chapter 2 provides a means to determine the interference among the passive wedges of piles in a group and the additional stress/strain induced in the soil in these wedges. As seen in Fig. 3.3, the soil around the piles in the group interferes horizontally with that of adjacent piles by an amount that varies with

depth. The multi-sublayer technique allows the SW model to determine the overlap of the wedges of neighboring piles in different sublayers over the depth of the interference as shown in Figs. 3.4 and 3.5.

This provides a great deal of flexibility in the calculation of the growth in stress (and, therefore, strain) in the overlap zones which increases with the growth of the passive wedges. The main objective in the calculation of the area of overlap among the piles is to determine the increase in soil strain within the passive wedge of the pile in question.

A value of horizontal soil strain (ϵ) is assumed for the soil profile within the developing passive wedge. The response of a single pile (similar to the piles in the group) in the same soil profile is determined at this value of soil strain. The shape and the dimensions of the mobilized passive wedge are assessed (i.e. ϕ_m , β_m , h and BC in $\overline{\text{Fig. 3.3}}$) as presented in Chapter 2. This will include the values of stress level in each soil sublayer i (SL_i), Young's modulus (E_i), and the corresponding modulus of subgrade reaction (E_s) $_i$.

Wedges will overlap and interact with the neighboring ones, as seen in Figs. 3.3 and 3.5. At a given depth (see Fig. 3.5), zones of overlap will exhibit larger values of soil strains and stresses. The increase in average soil strain attributable to the passive wedge of a given pile will depend upon the number and area of interfering wedges overlying the wedge of the pile in question (Fig. 3.6). Such interference depends on the position of the pile in the group. The type of pile (by position) is based on the location of the pile by row (leading/trailing row) and the location of the pile in its row (side/interior pile) as seen in Fig. 3.5.

The average value of deviatoric stress accumulated at the face of the passive wedge at a particular soil sublayer i (sand or clay) is

$$(\Delta\sigma_h)_g = SL_g \Delta\sigma_{hf} \quad (3.3)$$

The average stress level in a soil layer (SL_g) due to passive wedge interference is evaluated based on the following empirical relationship,

$$(SL_g)_i = SL_i (1 + \sum R_j)^{0.5} \leq 1 \quad (3.4)$$

where j is the number of neighboring passive wedges in soil layer i that overlap the wedge of the pile in question. R is the ratio between the length of the overlapped portion of the face of the passive wedge and the total length of the face of the passive wedge (\overline{BC}). R (which is less than 1) is determined from all the neighboring piles to both sides and in front of the pile in question (Fig. 3.6).

SL_g and the associated soil strain (ε_g) will be assessed for each soil sublayer in the passive wedge of each pile in the group. ε_g is $\geq \varepsilon$ of the isolated pile (no wedge overlap) and is determined based on the stress-strain relationship (σ vs. ε) presented in Chapter 2. It should be noted that the angles and dimensions of the passive wedge (φ_m , β_m , and \overline{BC}) obtained from Eqns. 3.1 through 3.4 will be modified for group effect according to the calculated value of SL_g and ε_g (Fig. 3.7).

For instance, the relationship between the corresponding stress level (SL_g) and the associated mobilized effective stress friction angle (φ_m) in a soil sublayer i is

$$(SL_g)_i = \left(\frac{(\Delta\sigma_h)_g}{\Delta\sigma_{hf}} \right)_i = \frac{\tan^2 \left(45 + \frac{(\varphi_m)_i}{2} \right) - 1}{\tan^2 \left(45 + \frac{\varphi_i}{2} \right) - 1} \quad (3.5)$$

where $(\Delta\sigma_h)_g$ is the current horizontal stress change (due to pile-head lateral load and pile group interference), and $\Delta\sigma_{hf}$ is the unchanged value of the deviatoric stress at failure for the full friction angle φ . The mobilized friction angle φ_m calculated in Eqn. 3.5 reflects the stresses in the soil (sand or clay) around the pile in question at depth x for the corresponding pile head (group) deflection with

consideration of the stresses from neighboring piles (Figs. 3.5 and 3.6). Consequently, the geometry of the passive wedge is modified according to the current state of soil stress and strain (Fig. 3.7). It should be noted that the behavior of clay is assessed based on the effective stress analysis in which the developing excess porewater pressure is evaluated in Chapter 2 and Ashour et al. (1996).

3.3 EVALUATION OF THE YOUNG'S MODULUS, E_g

The change in the soil Young's modulus and, therefore, the change in modulus of subgrade reaction in each sublayer due to group interference is assessed. Once the modified variation of the modulus of subgrade reaction along the individual pile is predicted, the pile is analyzed as an equivalent isolated pile (considering all piles in the group have the same pile head deflection). Based on the modified value of soil strain assessed at depth x (for the wedge of the pile of interest) at the current level of loading, the value of Young's modulus, $(E_g)_i$, of the soil sublayer i is expressed, i.e.

$$(E_g)_i = \frac{(SL_g)_i (\Delta\sigma_{hf})_i}{(\varepsilon_g)_i} \quad (3.6)$$

It should be noted the Young's modulus (E_g) calculated using Eqn. 3.6 results from the original strain in the passive wedge (ε) as an isolated pile and the additional soil strain ($\Delta\varepsilon$) which develops due to overlap zones between the pile in question and its neighboring piles (Fig. 3.8), i.e.

$$(\varepsilon_g)_i = \varepsilon_i + \Delta\varepsilon_i \quad (3.7)$$

According to the amount of interference among the piles in the group, the value of the Young's modulus (E_g) should be less or equal to the associated modulus (E) for the isolated pile.

3.4 EVALUATION OF THE MODULUS OF SUBGRADE REACTION, E_{sg}

Based on the concepts of the SW model, the modulus of subgrade reaction for an individual pile in a group can be expressed as

where x is the depth of a soil sublayer i below the pile head. δ is the linearized deflection angle of the deflection pattern as presented by Ashour et al. (1996). A_g is a parameter that governs the growth of the passive wedge and flow around failure, and is a function of soil and pile properties (Ashour and Norris 2000).

$$(A_g)_i = \left[\frac{p_i / D}{(\Delta \sigma_h)_g} \right]_i = \frac{\overline{BC}_i S_1}{D} + \left[\frac{2 \tau_i S_2}{(\Delta \sigma_h)_g} \right]_i \quad (3.9)$$

S_1 and S_2 are shape factors equal to 0.75 and 0.5, respectively, for a circular pile cross section, and equal to 1.0 for a square pile (Briaud et al. 1984). τ is the mobilized shear stress along the pile sides in the SW model (see Fig. 3.7) and is defined according to the soil type (sand or clay).

$$\tau_i = (\overline{\sigma}_{vo})_i \tan(\varphi_s)_i; \quad \text{where } \tan(\varphi_s)_i = 2 \tan(\varphi_m)_i \tan \varphi_i \quad \text{sand} \quad (3.10)$$

$$\tau_i = (SL_t)_i (\tau_{ult})_i \quad \text{clay} \quad (3.11)$$

Therefore,

$$(A_g)_i = S_1 \left[1 + \frac{(h - x_i) 2 (\tan \beta_m \tan \varphi_m)_i}{D} \right] + 2 S_2 \left[\frac{\overline{\sigma}_{vo} \tan \varphi_s}{(\Delta \sigma_h)_g} \right]_i \quad \text{sand} \quad (3.12)$$

$$(A_g)_i = S_1 \left[1 + \frac{(h - x_i) 2 (\tan \beta_m \tan \overline{\varphi}_m)_i}{D} \right] + S_2 \left[\frac{SL_t}{SL_g} \right]_i \quad \text{clay} \quad (3.13)$$

$$(E_{sg})_i = \frac{p_i}{y_i} = \frac{(A_g)_i D (\varepsilon_g)_i (E_g)_i}{\delta_i (h - x_i)} \quad (3.8)$$

φ_s is the mobilized side shear angle, SL_t is the stress level of shear along the pile sides, and τ_{ult} is

the ultimate shear resistance (Coyle-Reese 1966, and Ashour et al. 1998).

Compared to the case of a single pile, the developing passive wedge of a pile in a group will be larger than or equal to that of the single pile (depending on the amount of pile interference). However, the criteria presented in Chapter 2 and Ashour and Norris (2000) continue to govern the development of flow around failure; and variation of the BEF soil-pile reaction (p) and lateral deflection (y) in the single pile analysis continue to be employed in the pile group analysis.

It should be expected that the resulting modulus of subgrade reaction of a pile in a group, E_{sg} , is equal to or softer than the E_s of an isolated pile at the same depth (Fig 3.9). The value of E_s will vary with the level of loading and the growth of the soil stress in the developing passive wedge. Thus, there is no constant variation or specific pattern for changes in E_s of the individual piles in the pile group. Based on the predicted values of E_{sg} , the approach presented has the capability of assessing the p - y curve for any pile in the group.

The modulus of subgrade reaction of a pile in a group should reflect the mutual resistance between the soil and the pile. However, a portion of the pile deformation (Δy_i) results from the additional stresses in the soil (and, therefore, strains, $\Delta \epsilon$) which result from the effect of the neighboring piles (Figs. 3.5 and 3.6). Therefore, under a particular lateral load, the pile in the group will yield deflections more than those of the single pile. The additional deflection at any pile segment, (Δy_i), due to $\Delta \epsilon_i$ derives solely from the presence of neighboring piles, not the pile in question. The soil-pile reaction (p) is affected by the changes in stress and strain in the soil, and the varying geometry of the passive wedge.

Having reduced values of E_s along individual piles in the group, each pile is then analyzed as an equivalent isolated pile by BEF analysis. The piles in a group, at a particular step of loading, must experience equal deflections at the pile cap. For each pile in the group, the interference among the piles and the changes in the E_s profile (i.e geometry and dimensions of the passive wedge, and the internal stresses) will continue in an iterative process until the pile in question provides a pile-head

deflection equal to that of the group. As a reference, the group deflection is linked to the pile-head deflection (Y_0) of the isolated pile at the original soil strain (ϵ). This technique provides great flexibility to analyze each pile in the group independently in order to develop equal pile-head deflections (group deflection) which are the shared factor among the piles in a group.

3.5 CASE STUDIES

The original SW model program (Ashour et al. 1997 and 1998) for analyzing lateral loaded piles has been modified to incorporate the technique presented above. The modified SWM program allows the assessment of the lateral response (deflection, moment and shear force distribution) of an isolated pile and a pile group including the p-y curve along the length of the isolated pile and the individual piles in the pile group.

3.5.1 Full-Scale Load Test on a Pile Group in Layered Clay

A static lateral load test was performed on a full scale 3 x 3 pile group having a three-diameter center-to-center spacing (Rollins et al. 1998). The driven pipe piles were 0.305 m I.D., 9.5 mm wall thickness, and 9.1 m in length. The Young's modulus of the steel was 200 GPa, and the yield stress was 331 MPa. The soil profile along the length of the pile consisted of different types of clay and sand silt soils as described by Rollins et al. (1998).

Figure 3.10 shows good agreement between the measured and SWM program predicted response for the single pile and average pile in the group (pile group response is 9 times the average load at the same deflection). The P-Multiplier was used by Rollins et al. 1998 to differentiate between the average response of different piles by row. Accordingly, f_m values were varied arbitrarily to obtain the best match between the traditionally assessed p-y curve and averaged observed behavior. The predicted response assessed using SWM, averaged by pile row, shows reasonable agreement with the reported behavior as seen in Fig. 3.11. The deviation between predicted and observed behavior in the 10 to 40 mm range for the isolated pile carries over to that of the average pile in the group over the same range. SWM response was obtained based on the given pile and soil properties, and pile group layout; no adjustment was made to obtain better fit.

3.5.2 Full-Scale Load Test on a Pile Group in Sand

A full-scale lateral load test on a 3 x 3 pile group in sand overlying overconsolidated clay was conducted at the University of Houston, Texas (Morrison and Reese, 1986). The results obtained from this load test were used to develop values of f_m for use in the P-multiplier approach for laterally loaded pile groups in sand (Brown et al. 1988). This pile group of three diameter pile spacing was embedded in approximately 3 m of a dense to very dense uniform sand overlying an overconsolidated clay. The piles consisted of steel pipe with an outside diameter of 0.275 m, a wall thickness of 9.3 mm, a 13 m embedded length, and a bending stiffness (EI) of 1.9×10^4 kN-m². The soil properties, including the buoyant unit weight and the angle of internal friction suggested by Morrison and Reese (1986), were used in the SW model analysis.

Figures 3.12 and 3.13 show a comparison between the field data and the results obtained using the SWM program. As seen in Figs. 3.12 and 3.13, the observed and predicted responses of an average pile in the tested pile group are in good agreement. The good match of the predicted and observed behavior carries over to the average pile in the group.

3.5.3 Full-Scale Load Test on a Pile Group in Layered Clay

A full scale 3 x 3 pile group was driven in layered overconsolidated clay (Brown and Reese 1985). The pile group tested had a three diameter pile spacing and was laterally loaded 0.3 m above ground surface. The nine pipe piles tested had the same properties as the piles used in the preceding case study. The soil properties (ϵ_{50} , the soil unit weight, and the undrained shear strength of clay) evaluated by Brown and Reese were employed in the SW model analysis.

As shown in Figs. 3.14 and 3.15, the SW model provides good agreement with observed behavior for both the single and average pile in the group for pile-head load versus deflection and pile-head load versus maximum bending moment. It should be noted that this case represents a layered clay profile which exhibits different levels of wedge interference in each soil layer that then changes with the level of loading.

The procedure presented here has the capability to predict the pile head response, deflection, and bending moment for every individual pile in the group (type 1 through type 4 based on pile location, as seen in Fig. 3.5) not just the average pile response. Previous comparisons in terms of average pile in the group or average by row reflect what is reported in the literature. Likewise, the SWM program can assess the additional contribution to pile group resistance due to the presence of an embedded pile cap (not presented in this study) at any level of lateral loading. The effect of pile cap resistance on the lateral resistance of pile group can be judged from the following case study.

3.5.4 Full-Scale Load Test on a Pile Group with a Pile Cap in Layered Soil

A series of high amplitude load tests were performed on the Rose Creek bridge near Winnemucca, Nevada (Douglas and Richardson 1984). The stiffnesses of four pile groups, with pile caps of the foundation system were backfigured from system identification analysis of the collected accelerometer data. The soil profile and results of the tests are discussed by Norris (1994). Although the contribution of the embedded pile cap to the lateral resistance of the pile group has not been discussed in this paper, its effect on the lateral stiffness of pile groups is undertaken in the results predicted using the SWM program.

Piers 1 and 4 are each supported by a 3 x 5 pile group with 3-diameter pile spacings embedded in layered silt and clay soil, while piers 2 and 3 are each supported by a 4 x 5 pile group with 3-diameter pile spacings in the same layered silt and clay soil. Pile caps (4.57 x 2.75 m and 1.3 m thickness) associated with piers 1 and 4 are founded at 1.5 m depth below finished grade in a medium dense sand silt soil. Pile caps (4.57 x 3.65 m and 1.3 m thickness) associated with piers 2 and 3 are founded at 0.92 m below finished grade in a medium dense sand silt soil. The piers extend from the pile caps have a width of 1.22 m.

The piles are steel pipe piles of 0.32 m outer diameter backfilled with concrete and a bending stiffness of 3.38×10^4 kN-m². The piles associated with piers 1 through 4 were driven to 8, 7.8, 7.3 and 7 m below the bottom of the pile cap. All pile groups were loaded laterally in the direction

normal to length (long side) of the pile cap. Full details on soil and pile properties are presented by Norris (1994).

The pile heads are embedded 0.3 m into the pile cap. The piles in the group are treated as fixed head piles in the SW Model analysis. Even if the depth of pile head embedment into the pile cap was not adequate to provide complete restriction on the pile head rotation, the pile head in the group would exhibit fixed head conditions at the very low values of lateral deflection observed during the bridge load tests.

Figure 3.16 shows the agreement between the measured (backcalculated) and predicted pile group stiffnesses for groups 1 through 4 using the SWM program. It should be noted that the pile cap contribution to the total resistance of the group is a function of the pile cap dimensions and its embedment depth, properties of surrounding soil, and the level of lateral loading.

3.5.5 Model-Scale Load Test on a Pile Group in Loose and Medium Dense Sand

A series of load tests were performed using centrifuge tests on a model isolated pile, and on a model 3 by 3 pile group with piles spaced at 3 and 5 pile diameters within the group, embedded in a poorly graded loose ($D_r = 33\%$) and medium dense sand ($D_r = 0.55$) (McVay et al 1995). The prototype model piles, simulated using the centrifuge and a 1/45 (i.e. 45g) scale consisted of steel pipe piles with a diameter of 0.43 m and an overall length of 13.3 m. The pile had a bending stiffness, EI , of $72.1 \text{ MN}\cdot\text{m}^2$. The point of lateral load application to the pile groups was approximately 1.68 m above finished grade, while the point of lateral load application to the isolated pile was approximately 2.2 m above finished grade. Although a pile cap was associated with the pile group tests, McVay et al (1995) reported that the group tests simulated free-headed piles.

Very good agreement, between measured and predicted results, is shown in Figs. 3.17 and 3.18. Slight differences are observed between the measured and predicted capacity of the pile rows (leading, middle and trailing rows) in the group. It should be noted that the procedure presented herein has the capability of assessing the capacity of three different pile rows (leading, middle and

trailing rows). Therefore, 6 types of piles by position (instead of 4 types as seen in Fig. 3.5) should be analyzed. However, at low and medium level of pile head deflection, no significant differences are observed between the lateral resistance of the middle and trailing row.

3.6 SUMMARY

Assessment of the response of a laterally loaded pile group based on soil-pile interaction is presented. The behavior of a pile group in uniform and layered soil (sand and/or clay) is predicted based on the strain wedge (SW) model approach that was developed to analyze the response of a flexible long pile under lateral loading. Accordingly, the pile's response is characterized in terms of three-dimensional soil-pile interaction which is then transformed into its one-dimensional beam on elastic foundation equivalent with associated parameters (modulus of subgrade reaction). The interference among the piles in a group is determined based on the geometry and interaction of the mobilized passive wedges of soil in front of the piles in association with the pile spacing. The overlap of shear zones among the piles in the group varies along the length of the pile and changes from one soil layer to another in the soil profile. Also, the interference among the piles grows with the increase in lateral loading, and the increasing depth and fan angles of the developing wedges. The modulus of subgrade reaction determined will account for the additional strains (i.e. stresses) in the adjacent soil due to pile interference within the group. Based on the approach presented, the p-y curve for individual piles in the pile group can be determined. The reduction in the capacity of the individual piles in a group compared to the isolated pile is governed by soil and pile properties, level of loading, and pile spacing.

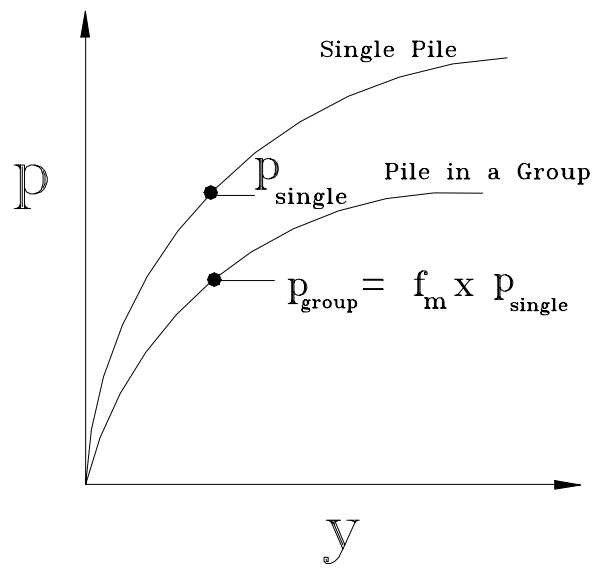


Fig. 3.1 P-Multiplier (f_m) Concept for Pile Group (Brown et al. 1988)

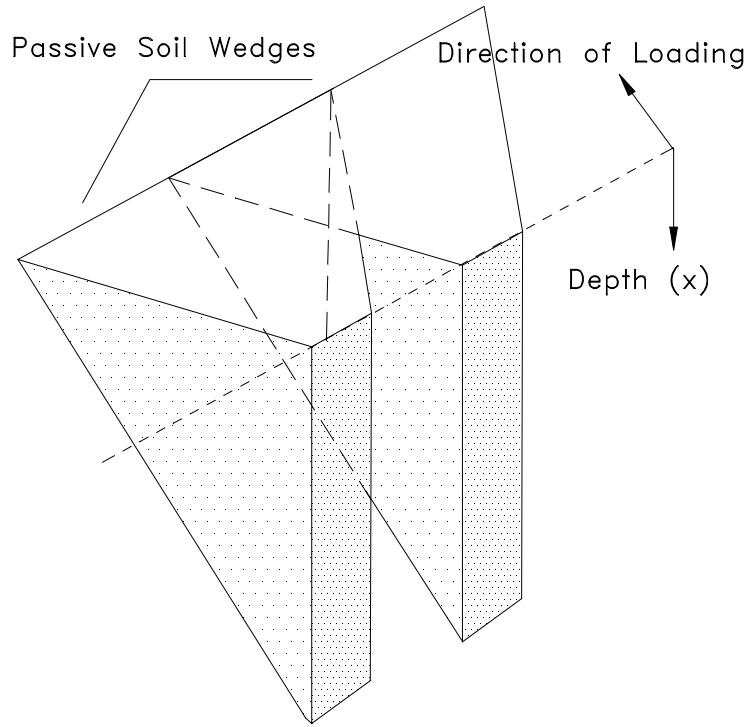


Fig. 3.2 Lateral Interference Between Two Neighboring Piles

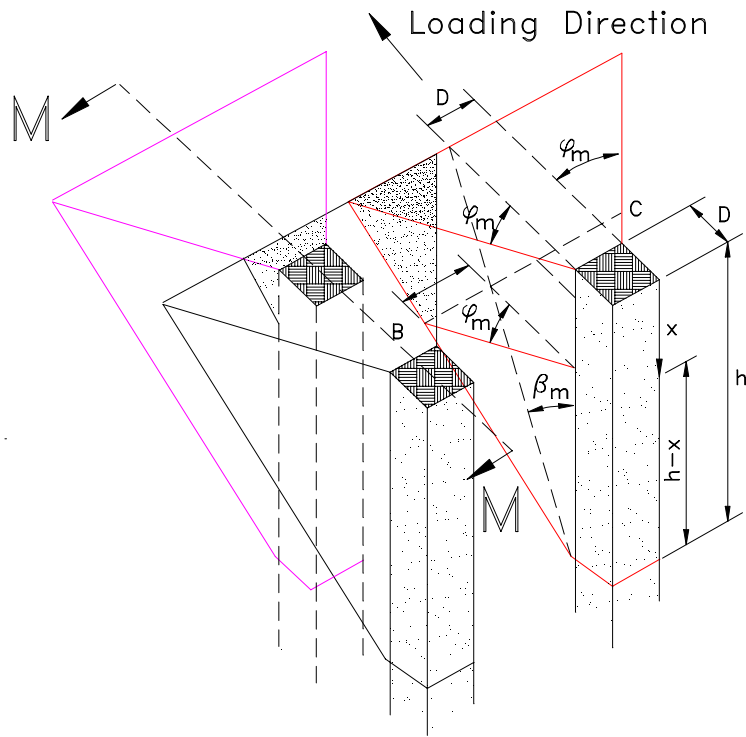


Fig. 3.3 Mobilized Passive Wedges and Associated Pile Group Interference

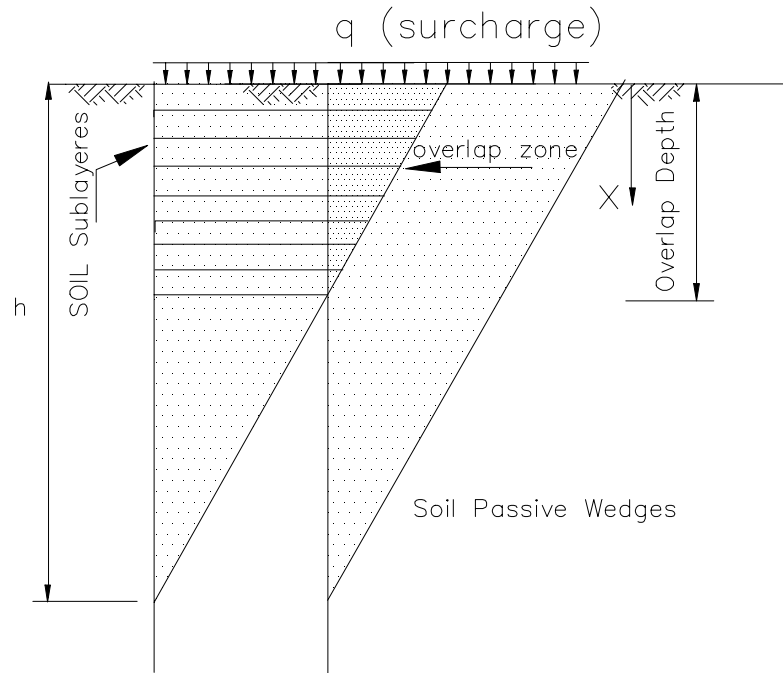
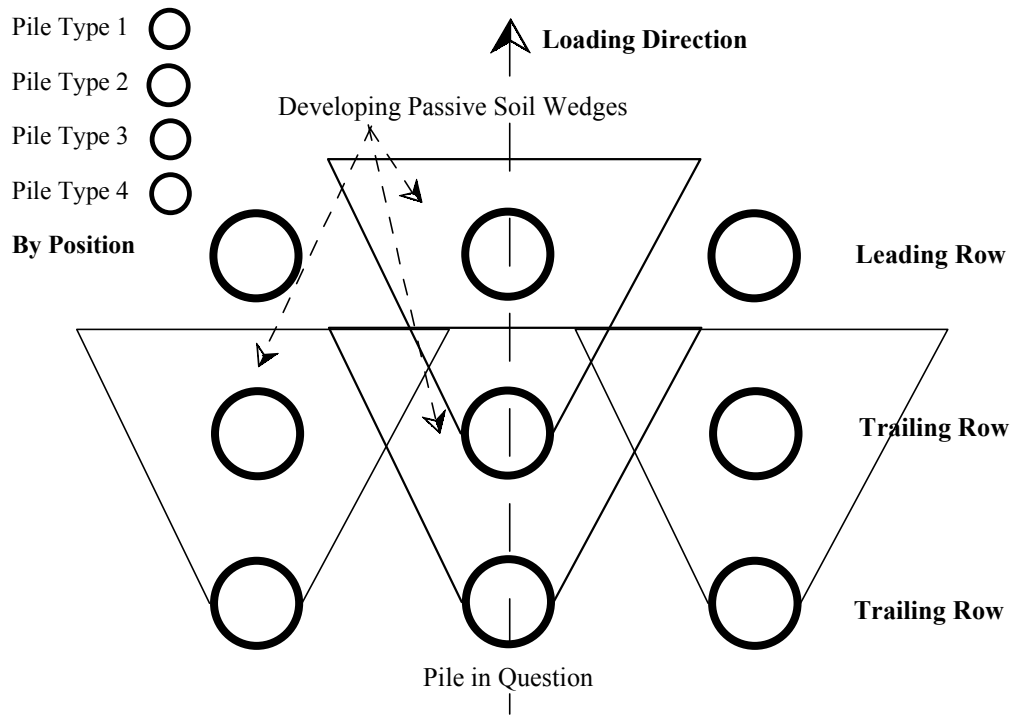


Fig. 3.4 Front Overlap Among Soil Sublayers in Two adjacent Passive Wedges (Section J-J in Fig. 3.3.)



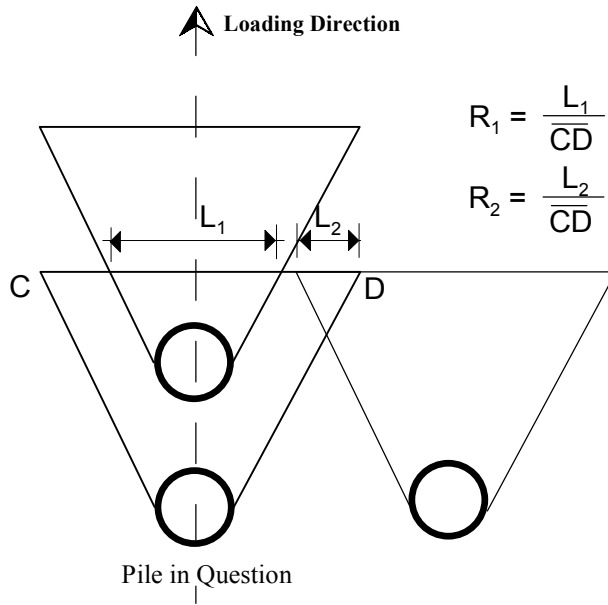
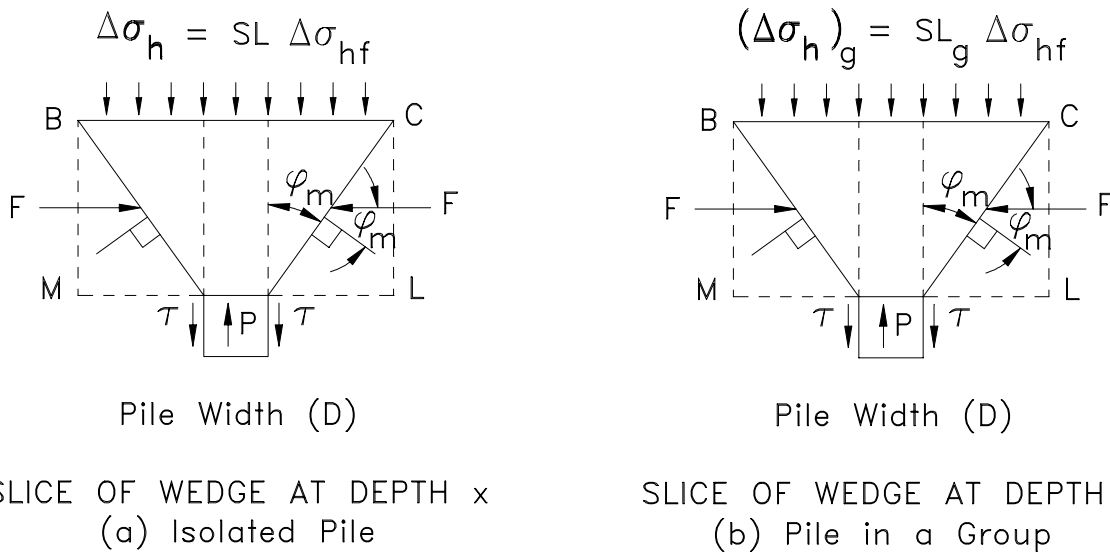


Fig. 3.5 The Initial Interference Among Piles in a Pile Group at a Given Depth

Fig. 3.6 Example of Overlap Ratio Calculation Among piles in a Pile Group



** At the same level of pile head deflection, f_m for an isolated pile is $\leq f_m$ for an individual pile in a pile group

Fig. 3.7 Stress and Geometry Change in a Slice of an Individual Pile in a Pile Group

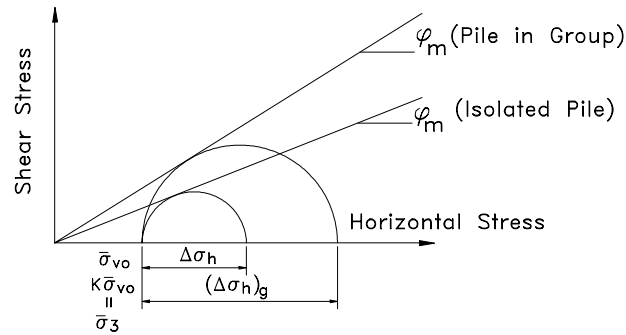
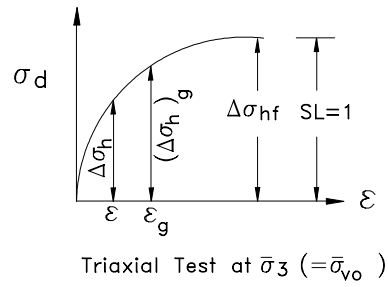


Fig. 3.8 Changes in Soil Young's Modulus Due to Pile Interference in a Pile Group at a Particular Level Of Loading

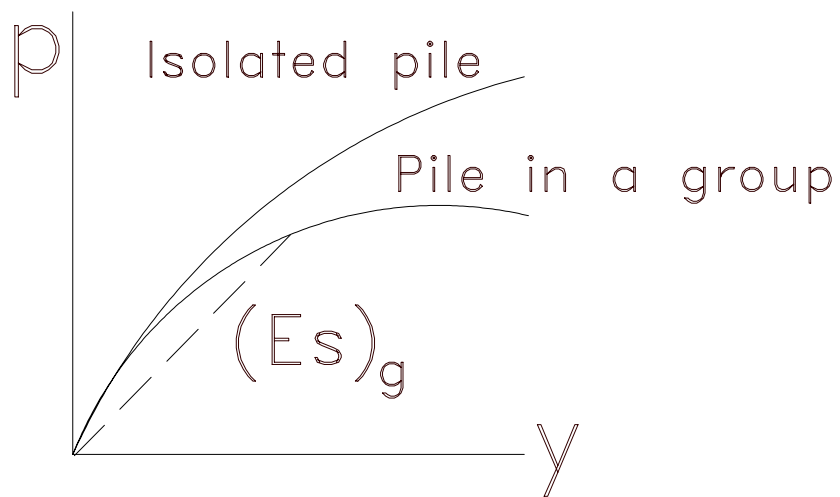


Fig. 3.9 Change in the Modulus of Subgrade Reaction (i.e. the p-y Curve) due to Pile Interference in the Pile Group at Different Levels of Loading according to the SW Model

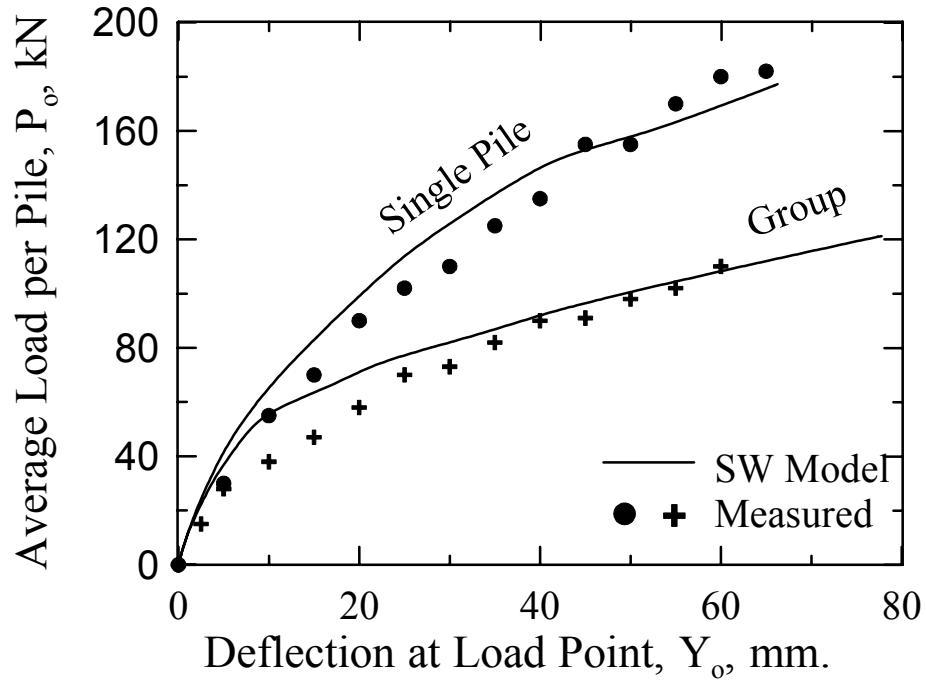


Fig. 3.10 Average lateral load versus deflection curves for isolated pile and average pile in a 3 x 3 group (after Rollins et al. 1998)

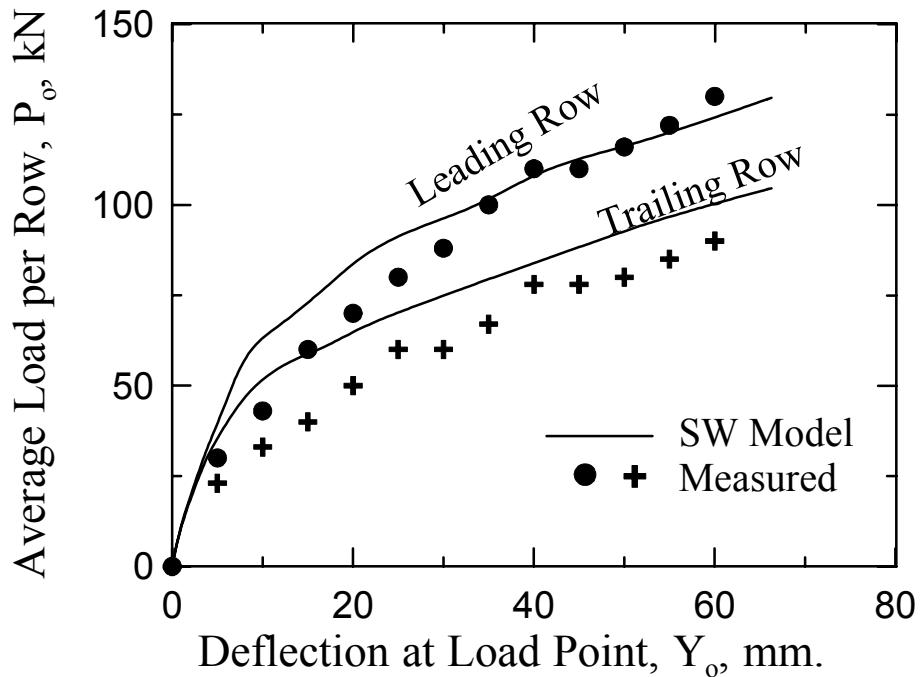


Fig. 3.11 Measured and predicted average lateral load per row versus deflection (after Rollins et al. 1998)

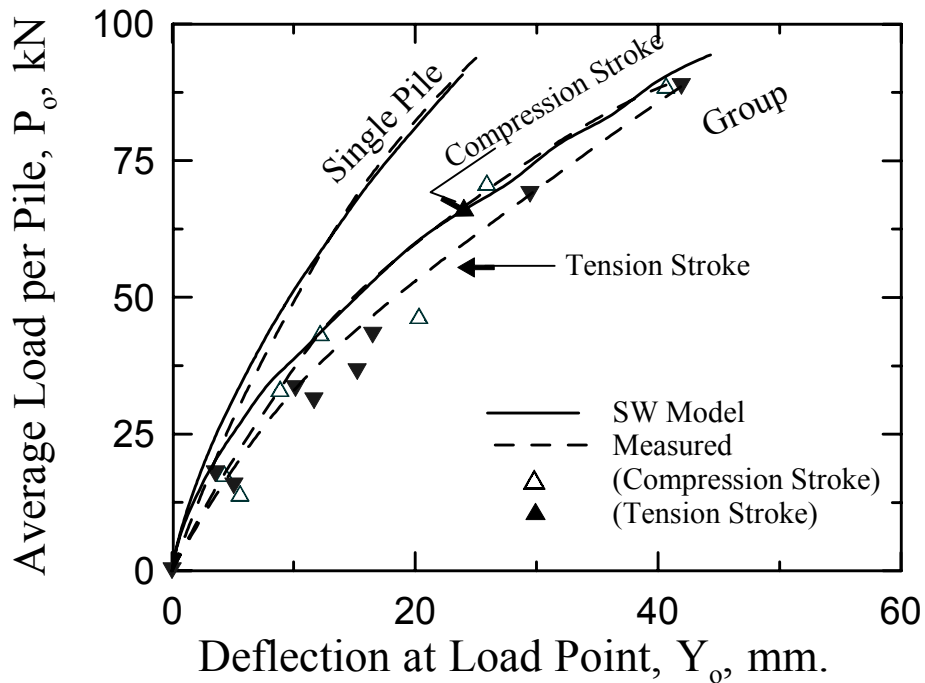


Fig. 3.12 Lateral pile-head lateral load vs. deflection for an isolated pile and an average pile in a 3 x 3 group in sand (after Morrison and Reese, 1986)

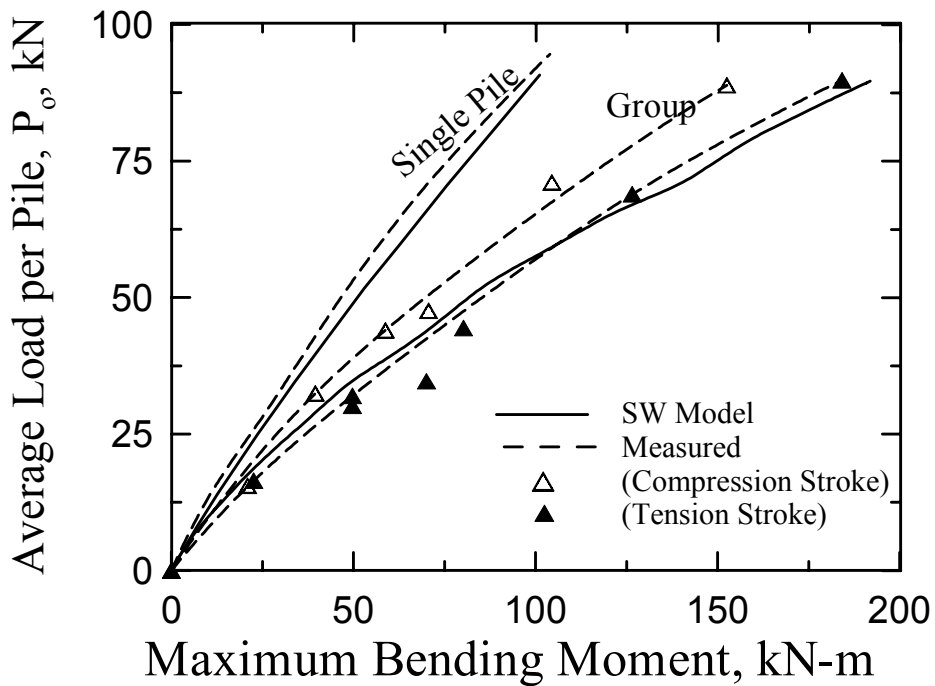


Fig. 3.13 Lateral load vs. maximum bending moment for isolated pile and an average pile in a 3 x 3 group in sand (after Morrison and Reese, 1986)

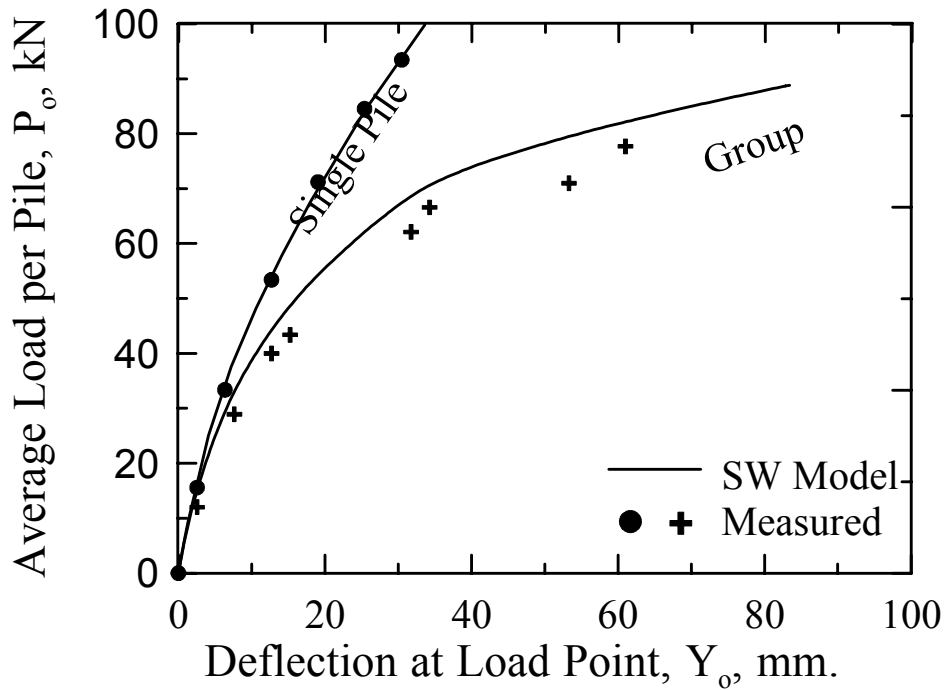


Fig. 3.14 Lateral load vs. deflection for isolated pile and an average pile in a 3 x 3 group in clay.(after Brown and Reese, 1985)

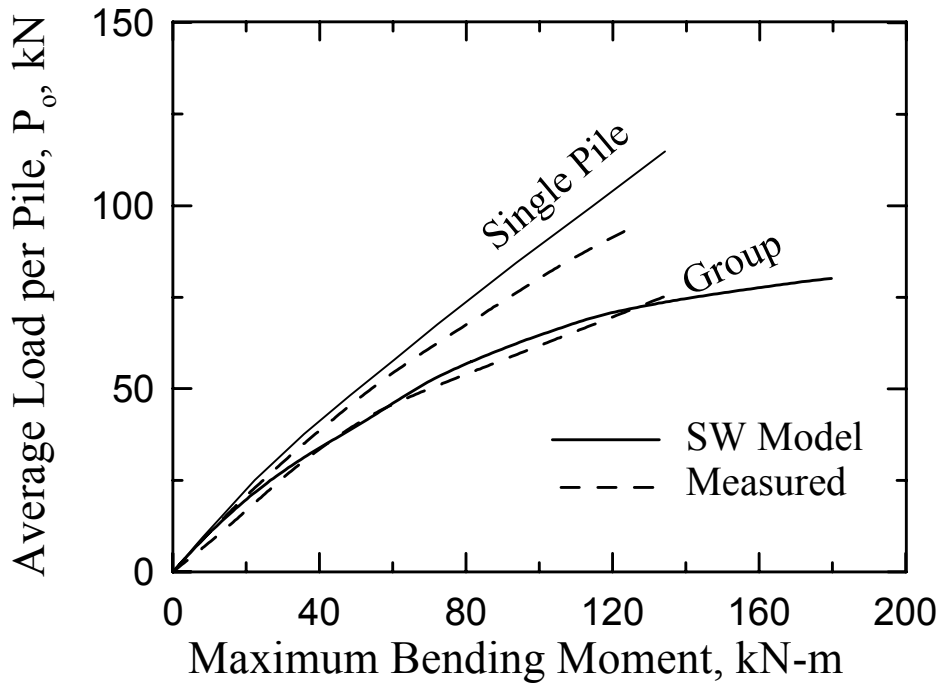
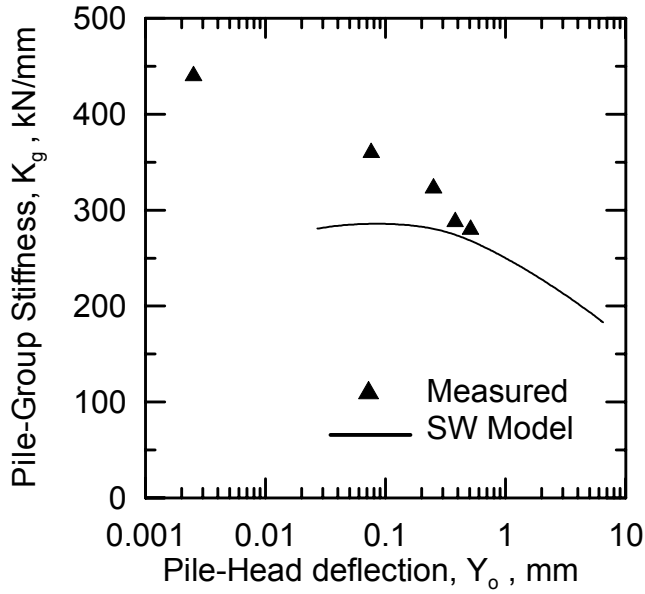
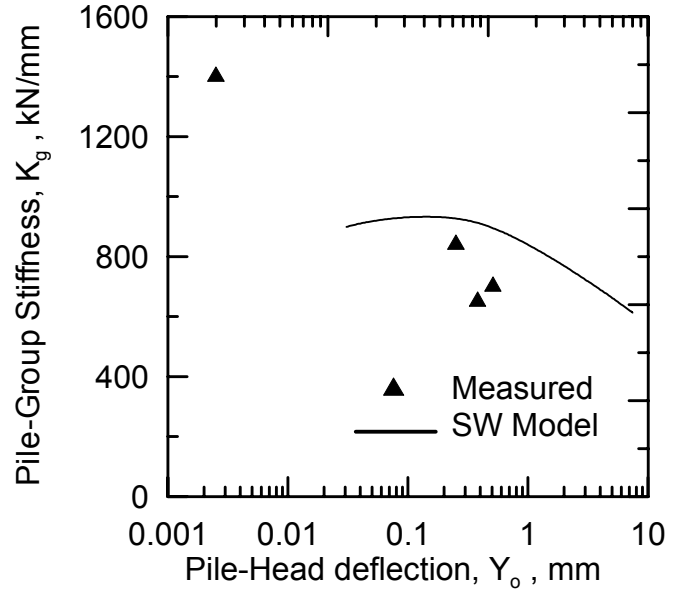


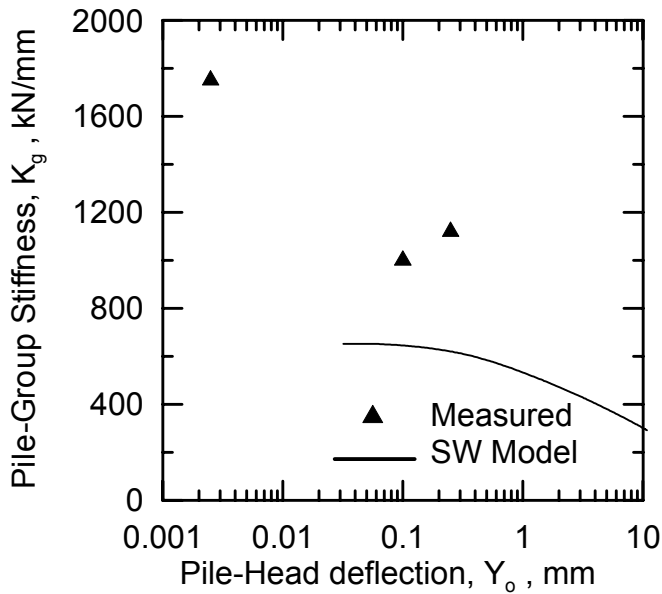
Fig. 3.15 Lateral load vs. maximum bending moment for isolated pile and an average pile in a 3 x 3 group in clay.(after Brown and Reese, 1985).



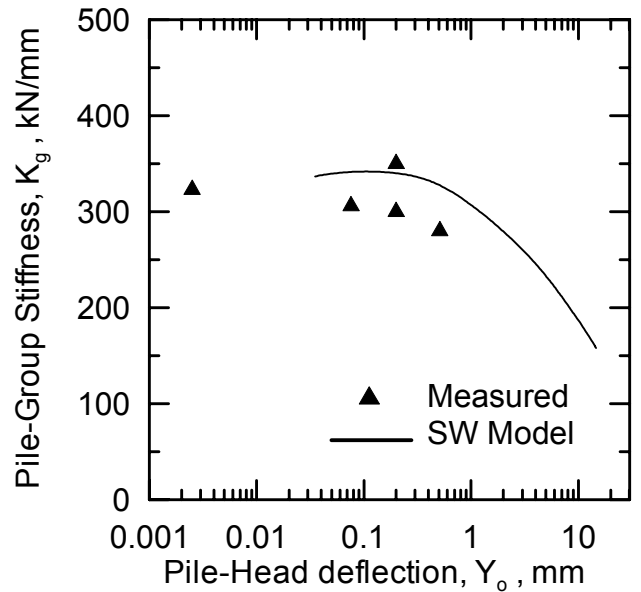
Measured and Predicted Stiffness of Pile Group 1



Measured and Predicted Stiffness of Pile Group 2



Measured and Predicted Stiffness of Pile Group 3



Measured and Predicted Stiffness of Pile Group 4

Fig. 3.16 Measured and Predicted Group Stiffness for Rose Creek Bridge Foundation (After Norris 1994)

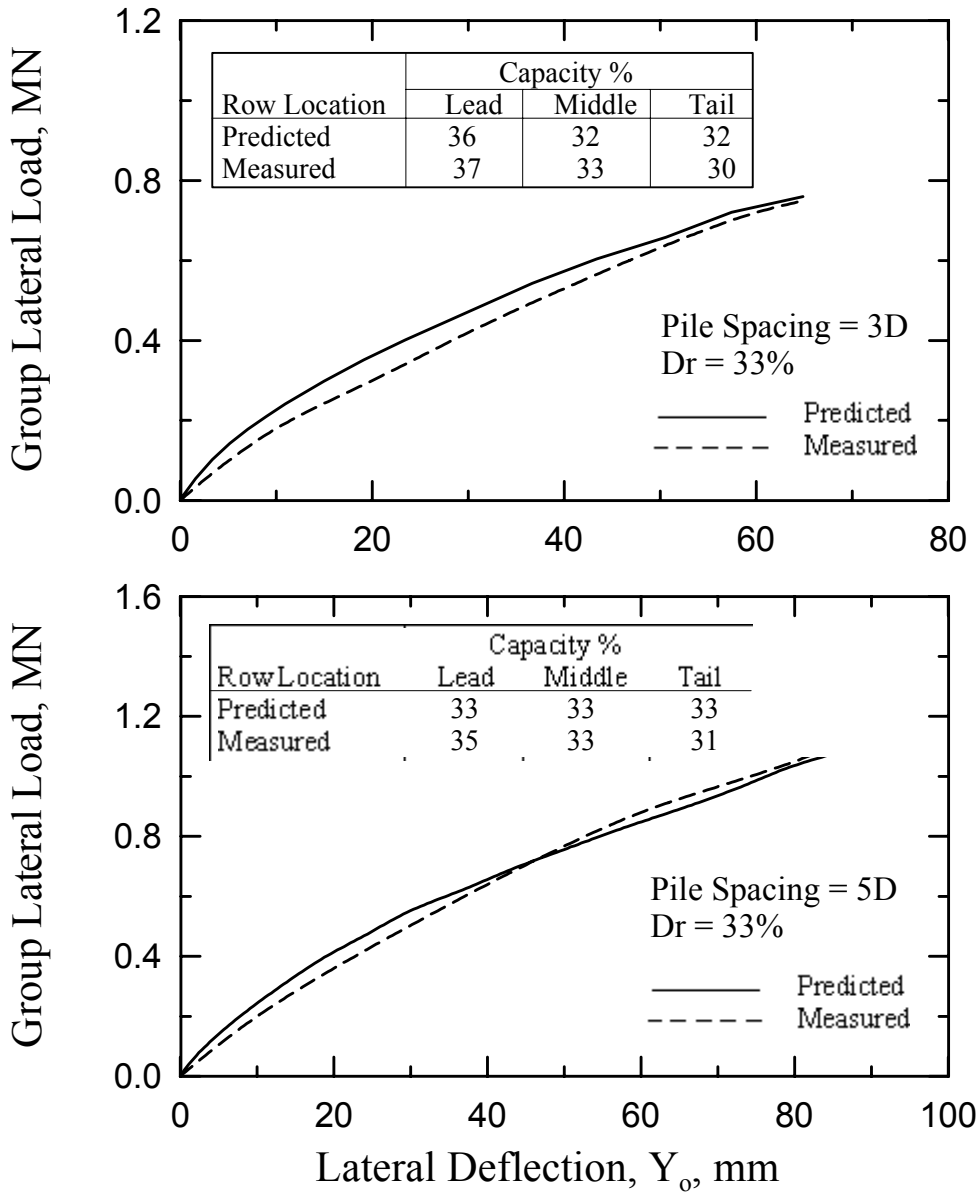


Fig. 3.17 A Pile Group Model (3x3) in Medium Loose Sand (after McVay et al. 1995)

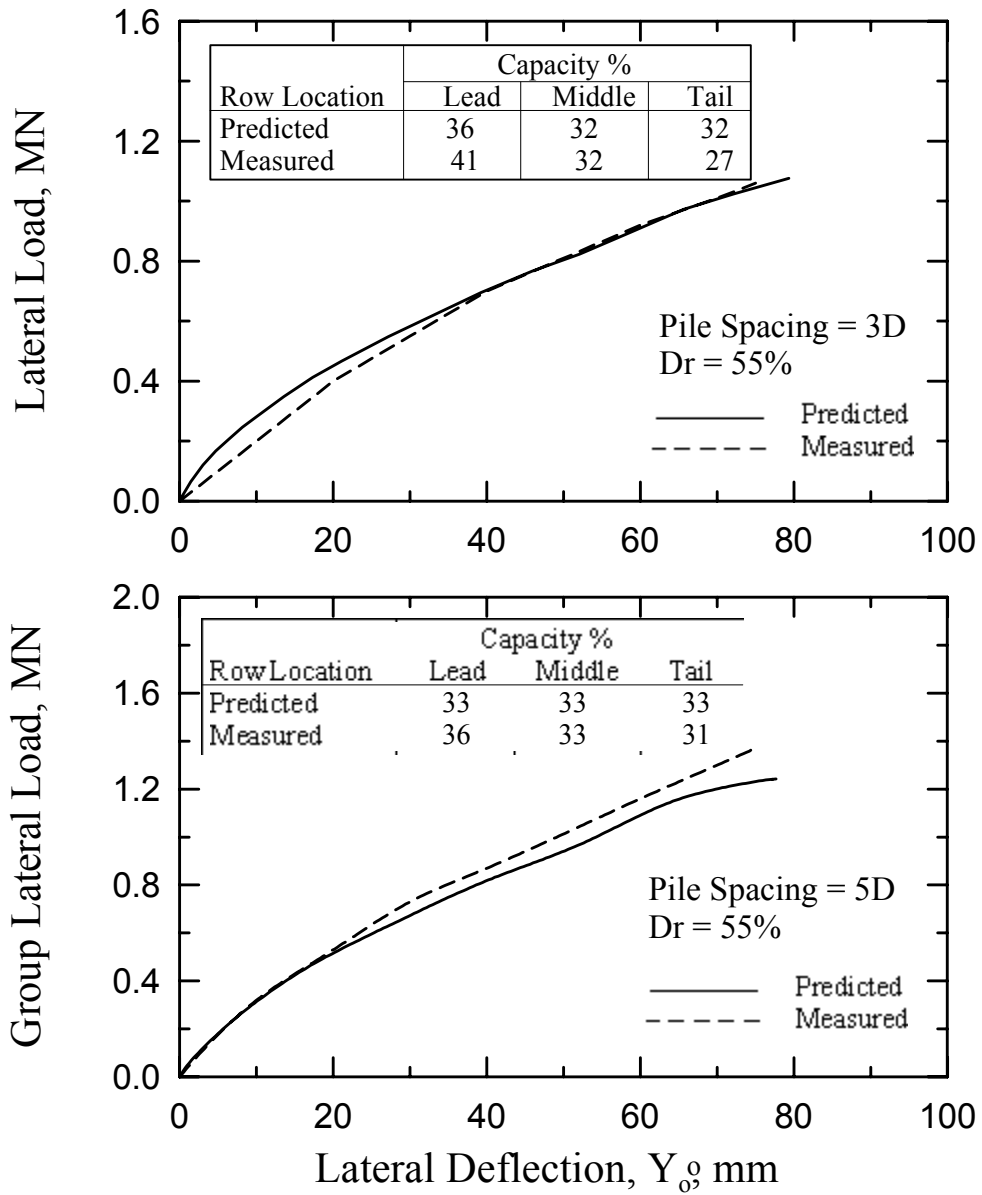


Fig. 3.18 A Pile Group Model (3x3) in Medium Dense Sand (after McVay et al. 1995)

CHAPTER 4

NUMERICAL MATERIAL MODELING

4.1 INTRODUCTION

Deformations in any structural element depend upon the characteristics of the load, the element shape and its material properties. With laterally loaded piles and shafts, the flexural deformations are based on the applied moment and the flexural stiffness of the pile at the cross section in question. In addition, the flexural stiffness (EI) of the pile is a function of the Young's modulus (E), moment of inertia (I) of the pile cross section and the properties of the surrounding soil. Given the type of material, concrete and/or steel, the properties of pile material vary according to the level of the applied stresses.

Behavior of piles under lateral loading is basically influenced by the properties of both the soil and pile (pile material and shape). The nonlinear modeling of pile material, whether it is steel and/or concrete, should be employed in order to predict the value of the lateral load and the realistic associated bending moment and pile deflection especially at large values of pile-head deflection and the onset of pile material failure. It is known that the variation in the bending stiffness (EI) of a laterally loaded pile is a function of the bending moment distribution along the pile (moment-curvature, $M-\Phi$, relationship) as seen in Fig. 4.1. Consequently, some of the pile cross sections which are subjected to high bending moment experience a reduction in bending stiffness and softer interaction with the surrounding soil. Such behavior is observed with drilled shafts and steel piles at advanced levels of loading and has an impact on the lateral response and capacity of the loaded pile. The pile bending stiffnesses along the deflected pile change with the level of loading, the $M-\Phi$ relationship of the pile material, and the soil reaction which affects the pattern of pile deflection. Therefore, the equilibrium among the distributions of pile deflection, bending moment, bending stiffness, and soil reaction along the pile should be maintained.

In the case of a steel pile, the Young's modulus remains constant (elastic zone) until reaching the yield stress, f_y (indicating the initial yielding), at which time the steel starts to behave elastic-plastically with different values of the secant Young's modulus. Once a plastic hinge develops, the pile cross section responds in plastic fashion under a constant plastic moment. But, in the case of a concrete pile or shaft, the stress-strain relationship varies in a nonlinear fashion producing a simultaneous reduction in Young's modulus and, in turn, the stiffness of the pile cross section. Furthermore, once it reaches a critical value of strain, the concrete ruptures catastrophically.

The technique suggested by Reese (1984), which employs the Matlock-Reese p - y curves, requires separate evaluation of the M - Φ relationship of the pile cross section and then adoption of a reduced bending stiffness (EI_r) to replace the original pile bending stiffness (EI). The suggested procedure utilizes this reduced bending stiffness (EI_r) over the full length of the pile at all levels of loading. Assuming a reasonable reduction in bending stiffness, particularly with drilled shafts, is a critical matter that requires guidance from the literature which has only limited experimental data. At the same time, the use of one constant reduced bending stiffness for the pile/shaft does not reflect the real progressive deformations and forces associated with the steps of lateral loading. However, this technique may work quite well with the steel H-pile which fails approximately once the pile flange reaches the yielding stage (occurs rapidly). In general, the response of the pile/drilled shaft (pile-head load vs. deflection, and pile-head load vs. maximum moment) is assessed based on a constant bending stiffness (EI_r) and is truncated at the ultimate bending moment of the original pile/drilled shaft cross section. The moment-curvature relationship, and thus the maximum bending moment carried by the pile cross section should be evaluated first.

Reese and Wang (1994) enhanced the technique presented above by computing the bending moment distribution along the pile and the associated value of EI at each increment of loading. Reese and Wang (1994) concluded that the bending moment along the pile does not depend strongly on structural characteristics and that the moment differences due to EI variations are small. It should be noted that the effect of the varying EI on the bending moment values along the drilled shaft was not obvious because the

EI of the drilled shaft had no effect on the p-y curves (i.e. modulus of subgrade reaction) employed in their procedure. Therefore, it was recommended that a single value of EI of the cracked section (constant value) be used for the upper portion of the pile throughout the analysis. Contrary to Reese and Wang's assumption, the variation in the value of EI has a significant effect on the nature of the p-y curve and modulus of subgrade reaction [Ashour and Norris (2000); Yoshida and Yoshinaka (1972); and Vesic (1961)] specially in the case of drilled shafts.

The main purpose in this chapter is to assess the moment-curvature relationship ($M-\phi$) of the loaded pile or shaft in a convenient and simplified fashion considering the soil-pile interaction. The prediction of the moment-curvature curve allows one to realistically determine the variation of pile stiffness (EI) as a function of bending moment.

The SW model allows the designer to include the nonlinear behavior of the pile material and, as a result, to find out the effect of material types on the pile response and its ultimate capacity based on the concepts of soil-pile interaction.

4.2 THE COMBINATION OF MATERIAL MODELING WITH THE STRAIN WEDGE MODEL

The bending moment distribution along the deflected length of a laterally loaded pile varies as shown in Fig. 4.1. This profile of moment indicates the associated variation of pile stiffness with depth if the stress-strain relationship of pile material is nonlinear. The strain wedge model is capable of handling the nonlinear behavior of pile material as well as the surrounding soil. The multi-sublayer technique, presented in Chapter 2, allows one to provide an independent description for each soil sublayer and the associated pile segment.

The effect of pile material is considered with the global stability of the loaded pile and the shape of the developing passive wedge of soil in front of the pile. During the iteration process using the SW model, the stiffness of each pile segment, which has a length equal to the depth of the soil sublayer, is a function of the

calculated bending moment at the associated pile segment, as seen in Fig. 4.1. Therefore, the pile is divided into a number of segments of different values of flexural stiffness under a particular lateral load.

In order to incorporate the effect of material nonlinearity, numerical material models should be employed with the SW model. A unified stress-strain approach for confined concrete has been employed with the reinforced concrete pile as well as the steel pipe pile filled with concrete. In addition, steel is modeled using an elastic perfectly plastic uniaxial stress-strain relationship which is commonly used to describe steel behavior. The procedure presented provides the implementation of soil-pile interaction in a fashion more sophisticated than that followed in the linear analysis with the SW model presented in Chapter 3.

The approach developed will allow one to load the pile to its actual ultimate capacity for the desired lateral load and bending moment according to the variation of pile material properties along the pile length.

4.2.1 Material Modeling of Concrete Strength and Failure Criteria

Based upon a unified stress-strain approach for the confined concrete proposed by Mander et al. (1984 and 1988), a concrete model is employed with circular and rectangular concrete sections. The proposed model, which is shown in Fig. 4.2, has been employed for a slow strain rate and monotonic loading. The longitudinal compressive concrete stress f_c is given by

$$f_c = \frac{f_{cc} x^r}{r - 1 + x^r} \quad (4.1)$$

where f_{cc} symbolizes the compressive strength of confined concrete.

$$x = \frac{\mathbf{e}_c}{\mathbf{e}_{cc}} \quad (4.2)$$

where ε_c indicates the axial compressive strain of concrete.

$$\mathbf{e}_{cc} = \mathbf{e}_{co} \left[1 + 5 \left(\frac{f_{cc}}{f_{co}} - 1 \right)^{\frac{2}{3}} \right] \quad (4.3)$$

where ε_{cc} is the axial strain at the peak stress. f_{co} and ε_{co} represent the unconfined (uniaxial) concrete strength and the corresponding strain, respectively. Generally, ε_{co} can be assumed equal to 0.002, and

$$r = \frac{E_c}{E_c - E_{sec}} \quad (4.4)$$

where

$$E_c = 57,000 (f_{co})^{0.5} \quad (p s i) \quad (4.5)$$

and

$$E_{\text{sec}} = \frac{f_{cc}}{e_{cc}} \quad (4.6)$$

E_c denotes the initial modulus of elasticity of the concrete under slowly applied compression load.

As mentioned by Paulay and Priestly (1992), the strain at peak stress given by Eqn. 5.3 does not represent the maximum useful strain for design purposes. The concrete strain limits occur when transverse confining steel fractures. A conservative estimate for ultimate compression strain (ϵ_{cu}) is given by

$$e_{cu} = 0.004 + \frac{1.4 r_s f_{yh} e_{sm}}{f_{cc}} \quad (4.7)$$

where ϵ_{sm} is the steel strain at maximum tensile stress (ranges from 0.1 to 0.15), and ρ_s is the volumetric ratio of confining steel. Typical values for ϵ_{cu} range from 0.012 to 0.05. f_{yh} represents the yield stress of the transverse reinforcement.

In order to determine the compressive strength of the confined concrete (f_{cc}), a constitutive model (Mander et al. 1988) is directly related to the effective confining stress (f_l) that can be developed at the yield of the transverse reinforcement.

$$f_{cc} = f_{co} \left[-1.254 + 2.254 \left(1 + \frac{7.94 f_l}{f_{co}} \right)^{0.5} - \frac{2 f_l}{f_{co}} \right] \quad (4.8)$$

For circular and square section of concrete, f_t is given by

$$f_t = 0.95 r_s f_{yh} \quad (4.9)$$

- **Monotonic tensile loading**

Although concrete tension strength is ignored in flexural strength calculation, due to the effect of concrete confinement it would be more realistic if it were considered in the calculation. As suggested by Mander et al. (1988), a linear stress-strain relationship is assumed in tension up to the tensile strength (f_{tu}). The tensile stress is given by

$$f_t = E_c e_c \quad \text{for } f_t \leq f_{tu} \quad (4.10)$$

and

$$e_{tu} = \frac{f_{tu}}{E_c} \quad (4.11)$$

where

$$f_{tu} = 9 (f_{co})^{0.5} \quad (psi) \quad (4.12)$$

If tensile strain ϵ_t is greater than the ultimate tensile strain (ϵ_{tu}), f_t is assumed to be equal to zero.

4.2.2 Material Modeling of Steel Strength

There are different numerical models to represent the stress-strain relationship of steel. The model employed for steel in this study is linearly elastic-perfectly plastic, as shown in Fig. 4.3. The complexity of this numerical model is located in the plastic portion of the model which does not include any strain hardening (perfectly plastic).

The elastic behavior of the steel is limited by the linearly elastic zone of this model at which the strain is less than the yield strain

$$\epsilon_y = \frac{f_y}{E_{so}} \quad (4.13)$$

where f_y is the yield stress of steel, and ϵ_y is the value of the steel strain at the end of the elastic zone where the stress is equal to f_y . E_{so} is the elastic Young's modulus of steel which is equal to 29,000 kips/inch².

When the value of steel stress (f_s) at any point on the cross section reaches the yield stress, the Young's modulus becomes less than E_{so} of the elastic zone. The initial yielding takes place when the stress at the farthest point from the neutral axis on the steel cross section (point A) becomes equal to the yield stress (f_y), as shown in Fig. 4.4a.

The initial yielding indicates the beginning of the elastic-plastic response of the steel section. By increasing the load, other internal points on the cross section will satisfy the yield stress to respond plastically under a constant yield stress (f_y), as seen in Figure 4.4b. Once all points on the steel section satisfy a normal stress (f_s) equal to the yield stress (f_y) or a strain value larger than the yield strain (ϵ_y), the steel section responds as a plastic hinge with an ultimate plastic moment (M_p) indicating the complete yielding of the steel section, as presented in Fig. 4.4c.

During the elastic-plastic stage (after the initial yielding and before complete yielding) some points on the steel section respond elastically ($f_s \leq f_y$) and the others respond plastically ($f_s = f_y$) with different values of Young's modulus (E_s), as presented in Fig. 4.3. The values of normal strain are assumed to vary linearly over the deformed cross section of steel.

If the strain at any point on the steel cross section is larger than the yield strain (ϵ_y), the plastic behavior will be governed by the flow of the steel under a constant stress (f_y) at the point in question. Regardless of whether the section is under elastic, elastic-plastic or plastic states, the strain is linearly distributed over the whole steel section. In addition, the strain at any point is controlled by the values of strain at other locations in order to keep the strain distribution linear. Generally, the external and internal moments over the steel section should be in a state of equilibrium.

4.3 MOMENT-CURVATURE (M-F) RELATIONSHIP

The aim of developing the moment-curvature relationship of the pile material is to determine the variation of the flexural stiffness (EI) at every level of loading. The normal stress (σ_x) at any cross section along the pile length is linked to the bending moment (M) and curvature (ϕ) by the following equations:

$$EI \frac{d^2 y}{d x^2} = M \quad (4.14)$$

$$EI \mathbf{f} = \frac{EI}{\mathbf{r}} = M \quad (4.15)$$

$$\mathbf{f} = \frac{d^2 y}{d x^2} = \frac{\mathbf{e}_x}{z} \quad (4.16)$$

$$\mathbf{e}_x = -\frac{z}{\mathbf{r}_o} \quad (4.17)$$

where

$$\mathbf{s}_x = E \mathbf{e}_x = E \mathbf{f} z \quad (4.18)$$

z = the distance from the neutral axis to the longitudinal fiber in question

ρ_o = the radius of curvature of the deflected axis of the pile

ϵ_x = the normal strain at the fiber located z -distance from the neutral axis.

The above equations are based on the assumption of a linear variation of strain across the pile cross section.

In addition, the pile cross section is assumed to remain perpendicular to the pile axis before and after deforming, as shown in Fig. 4.5.

4.4 SOLUTION PROCEDURE

The solution procedure adopted consists of calculating the value of bending moment (M_i) at each cross section associated with a profile of the soil modulus of subgrade reaction which is induced by the applied load at the pile top. Then, the associated curvature (ϕ), stiffness (EI), normal stress (σ_x) and normal strain

(ε_x) can be obtained. This procedure depends on the pile material. The profile of moment distribution along the deflected portion of the pile is modified in an iterative fashion along with the values of the strain, stress, bending stiffness and curvature to satisfy the equilibrium among the applied load and the associated responses of the soil and pile. Based on the concepts of the SW model, the modulus of subgrade reaction (i.e. p-y curve) is influenced by the variations in the pile bending stiffness at every pile segment. This procedure guarantees the incorporation of soil-pile interaction with the material modeling. The technique presented strives for a more realistic assessment of the pile deflection pattern under lateral loading and due to the nonlinear response of pile material and soil resistance.

4.4.1 Steel Pile

Steel piles involved in this study have either circular (pipe) or H-shape cross sections, as seen in Fig. 4.6. The cross section of the steel pipe pile is divided into a number of horizontal strips (equal to a total of 2m) parallel to the neutral axis. Each strip has a depth equal to the thickness of the pipe pile skin, as seen in Fig. 4.7. The cross section of the steel H-pile is divided into horizontal strips of a width equal to one half the thickness of the H-section flange, as seen in Fig. 4.7. The moment applied over the cross section of the pile segment (i) is M_i , and the normal stress at a strip (n) is $(f_s)_n$ ($1 \leq n \leq m$).

Using Eqns. 4.17 and 4.18, the stress and strain distributions over the cross section of each pile segment can be determined as

$$\mathbf{f}_i = \frac{M_i}{(EI)_i} \quad (4.19)$$

$$(\mathbf{e}_s)_n = z_n \mathbf{f}_i \quad 1 \leq n \leq m \quad (4.20)$$

$$(f_s)_n = (E_s)_n (\epsilon_s)_n \quad (4.21)$$

where $E_s \leq E_{s0}$; ϕ_i is the curvature at pile segment (i) which is constant over the steel cross section at the current level of loading; z_n indicates the distance from the neutral axis to the midpoint of strip n; $(\epsilon_s)_n$ represents the strain at strip n; $(EI)_i$ represents the initial stiffness of the pile segment (i); I is the moment of inertia of the steel cross section of the pile segment (i) which is always constant; and E_{s0} symbolizes the elastic Young's modulus of the steel.

1. Elastic Stage

The Young's modulus of any strip of the steel section (i) is equal to the steel elastic modulus (29×10^6 psi) as long as the stress $(\epsilon_s)_n$ is less or equal to the yield strain. Consequently, there is no change in the stiffness value of the pile segment (i) if ϵ_s at the outer strip ($n = 1$) is less than or equal to ϵ_y . This stage is similar to the linear analysis (constant EI) of the SW model presented in Chapter 3.

2. The Elastic-Plastic Stage

Once the calculated strain at the outer strip based on Eqn. 4.20 is larger than ϵ_y , the stress $(f_s)_n$ determined at the outer strip ($n = 1$) using Eqn. 4.21 will be equal to the yield stress. Therefore, initial yielding occurs and the elastic-plastic stage begins. During the elastic-plastic stage, the strips of the steel cross section experience a combination of elastic and plastic responses with different values of the secant Young's modulus (E_s) . Some strips behave elastically ($\epsilon_s \leq \epsilon_y$ and $f_s \leq f_y$), and the others behave plastically ($\epsilon_s > \epsilon_y$ and $f_s = f_y$) with different values of the secant Young's modulus (E_s) , as shown in Figs. 4.3, 4.4 and 4.8.

The normal stresses on the steel cross section are redistributed in order to generate a resisting moment $(M_R)_i$ that balances the applied moment (M_i) and satisfies the following equation:

$$M_i = (M_R)_i = (M_e)_i + (M_y)_i \quad (4.22)$$

where $(M_e)_i$ and $(M_y)_i$ represent the internal elastic and plastic moments induced over the steel cross section (i).

The internal elastic moment $(M_e)_i$ represents the internal moment exerted by the strips (m_1) which behave elastically and can be obtained as

$$(M_e)_i = \sum (f_s)_j A_j z_j \quad (1 \leq j \leq m_1) \quad (4.23)$$

The internal plastic moment $(M_y)_i$ is the moment generated by the yielded strips (m_2) which respond plastically and can be calculated using the following equation:

$$(M_y)_i = \sum f_y A_k z_k \quad (1 \leq k \leq m_2) \quad (4.24)$$

where A is the area of the steel strip, and

$$2m = m_1 + m_2 \quad (4.25)$$

For the first iteration of the solution in this stage, the steel cross section experiences a resisting internal moment $(M_R)_i$ less than the external moment (M_i) . Therefore, the steel cross section of the pile segment (i) should maintain a modified stiffness value for the pile segment in question, i.e. $(EI)_{i,mod}$. This reduced

$$(\mathbf{f}_i)_{mod} = \mathbf{f}_i \frac{M_i}{(M_R)_i} \quad (4.26)$$

value of stiffness at pile segment (i) is associated with an increase in the value of curvature such that the new value of curvature, $(\phi_i)_{\text{mod}}$, is

The modified stiffness value at pile segment (i) can be computed using the following equation,

$$(EI)_{i,\text{mod}} = \frac{M_i}{(\mathbf{f}_i)_{\text{mod}}} \quad (4.27)$$

The above procedure should be performed with all the unbalanced segments along the deflected portion of the loaded pile at each step of loading.

The global stability problem of the laterally loaded pile is resolved under the same level of loading and soil resistance using the modified values of stiffness of the pile segments (Eqn. 4.27). Consequently, the new moment distribution (M_i) along the pile length is assessed during each iteration. The modification for pile curvature and, therefore, stiffness values at the unbalanced segments continues until Eqn. 4.22 is satisfied over all the deflected segments of the pile.

3. Plastic Stage

The elastic-plastic stage continues until the steel cross section reaches a condition of complete yield. Thereafter, all strips of the steel section will be subjected to the yield stress (f_y) and strain values larger than ϵ_y , as presented in Fig. 4.9. At this level of pile head load, the steel section exhibits a plastic moment (M_p) which represents the ultimate moment that can be carried by the steel section. Once the steel section reaches the plastic moment, a plastic hinge develops to indicate the beginning of the plastic stage at the pile segment in question. The plastic moment is expressed as

$$M_p = \Sigma f_y A_n z_n \quad (4.28)$$

Equations 4.26 and 4.27 are employed in order to obtain the desired values of curvature and the associated stiffness at the plastic section is

$$(EI)_{i,\text{mod}} = \frac{M_p}{(\boldsymbol{f}_i)_{\text{mod}}} \quad (4.29)$$

During the plastic stage, the moment capacity and the stress over the steel section are restricted to the plastic moment (M_p) and the yield stress (f_y), respectively. However, the strain and curvature values are free to increase in order to produce reduced stiffnesses with the higher level of loading.

The resisting moment of the completely yielded section (plastic hinge) is always equal to M_p . If the external moment (M_i) which is calculated from the global stability is larger than M_p , Eqns. 4.26, 4.28 and 4.29 will be employed. The iteration process continues until satisfying an external moment value equal to the plastic moment at the pile segment in question.

The development of the plastic hinge on the pile does not mean the failure of the pile but leads to a limitation for the pile-head load. After the formation of the plastic hinge, the pile deflects at a higher rate producing larger curvatures and smaller stiffnesses to balance the applied load. Therefore, another plastic hinge may develop at another location on the pile. If the soil has not failed at the development of the plastic hinge, the pile may exhibit a lateral load capacity slightly larger than the load associated with the plastic hinge formation due to increase in soil resistance. The laterally loaded pile is assumed to fail when the outer strip at any pile segment experiences a strain value larger than 0.15.

4.4.2 Reinforced Concrete Pile and Drilled Shaft

The reinforced concrete pile is assumed to have a circular or square shape cross section and to be divided

into a total number of horizontal strips of (2m) as seen in Fig. 4.10. Unlike the cross section of a steel pile, the cross section of the reinforced concrete pile is not symmetrical around the neutral axis as a result of the different behavior of concrete under tensile and compressive stresses. The incorporation of concrete tensile strength reflects the actual response of the reinforced concrete pile. As presented in Section 4.2.1, the employment of concrete confinement has a significant influence on the concrete behavior (strength and strain values).

The resistance of the concrete cover (outside the confined core of concrete) is neglected. Therefore, the initial stiffness of the whole concrete cross section $(EI)_i$ represents the effective concrete section which is the confined concrete core. The curvature (ϕ_i) at the concrete section (i) is initially determined based on the applied external moment M_i and the initial stiffness of the reinforced concrete cross section $(EI)_i$, i.e.

$$\mathbf{f}_i = \frac{M_i}{(EI)_i} \quad (4.30)$$

Based on a linear distribution of strain (ϵ) over the reinforced concrete cross section, the strain at any strip (n) can be obtained using Eqn. 4.20 and is expressed as

$$(\mathbf{e})_n = z_n \mathbf{f}_i \quad 1 \leq n \leq m \quad (4.31)$$

Eqns. 4.1 and 4.21, which represent the numerical models of the compressive stress of confined concrete and tensile stress of steel, respectively, are used to calculate the associated concrete stress (f_c) and steel stress (f_s) at each strip (n). In this study, the tensile stress (f_t) is assumed to be equal to the compressive stress (f_c) if the tensile strain $(\epsilon_t)_n$ is less than ϵ_{tu} , which is more conservative than Eqn. 4.10. Therefore, the reinforced concrete cross section remains symmetric (the center line represents the neutral axis) as long

as ε_t at the outer strip ($n = 1$) is less than ε_{tu} . Under the conditions of a symmetric reinforced concrete section, the moment equilibrium and stiffness modification at any pile segment (i) can be expressed as

$$(M_R)_i = \Sigma 2 [(f_c A_c)_n z_n + (f_s A_s)_n z_n] \quad (1 \leq n \leq m) \quad (4.32)$$

Once the value of the tensile strain at the outer strip of any pile cross section exceeds ε_{tu} , the outer strip on the tension side fails and the cross section becomes unsymmetric. Thereafter, the neutral axis is shifted towards the compression side as shown in Fig. 4.10. In order to accurately estimate the new position of the neutral axis, the cross section should be in equilibrium under the compressive and tensile forces (F_{com} and F_{ten}) or

$$(F_{com})_i = (F_{ten})_i \quad (4.33)$$

where

$$(F_{com})_i = \Sigma (A_c f_c + A_s f_s)_n \quad 1 \leq n \leq n_1 \quad (4.34)$$

and

$$(F_{ten})_i = \Sigma (A_c f_t + A_s f_s)_n \quad 1 \leq n \leq n_2 \quad (4.35)$$

n_1 and n_2 are the numbers of strips in the compression and tension zones of the concrete cross section, respectively. At any strip in the tension zone, f_t is equal to zero when the tensile strain is greater than ε_{tu} .

Having the values of n_1 and n_2 ($2m = n_1 + n_2$) and using Eqns. 4.33 through 4.35, the location of the neutral

axis can be identified, and the resisting moment can be determined as

$$(M_R)_i = (M_{com} + M_{ten})_i \quad (4.36)$$

where

$$(M_{com})_i = \sum [(f_c A_c + f_s A_s)_n (z_c)_n] \quad (1 \leq n \leq n_1) \quad (4.37)$$

$$(M_{ten})_i = \sum [(f_t A_c + f_s A_s)_n (z_t)_n] \quad (1 \leq n \leq n_2) \quad (4.38)$$

where z_c and z_t are the distance from the neutral axis to the strip in question in the compression and tension zones, respectively.

In addition, the behavior of steel bars in the compressive and tensile zones is subjected to the steel model presented in Section 4.2.2. Once the strain of any steel bar is greater than or equal to ϵ_y , f_s will be equal to f_y in Eqns. 4.34 through 4.38. The equations above are influenced by the ultimate values of concrete strength and strain (ϵ_{cu} and f_{cu}) that are associated with concrete confinement as presented in Section 4.2.1.

If the calculated moment $(M_R)_i$ is less than the external moment M_i , the cross section curvature will be modified to obtain new values for the curvature and stiffness to balance the applied moment, i.e.

$$(f_i)_{mod} = f_i \frac{M_i}{(M_R)_i} \quad (4.39)$$

The modified stiffness value at pile segment (i) can be computed using the following equation,

$$(EI)_{i,\text{mod}} = \frac{M_i}{(\boldsymbol{f}_i)_{\text{mod}}} \quad (4.40)$$

By iteration, Eqns. 4.33 through 4.40 are employed to obtain the desired values of the curvature and the stiffness of the pile segment (i) in order to generate a resisting moment $(M_R)_i$ equal to the external moment (M_i) . The above procedure should be performed with all unbalanced segments along the deflected portion of the loaded pile at each level of loading.

The global stability problem of the laterally loaded pile is solved again under the same level of loading and using the modified values of stiffness of the pile segments. Consequently, the bending moment (M_i) is redistributed along the pile length.

Once any concrete strip under compressive stress reaches the ultimate strain ε_{cu} (Eqn. 4.7), the strip fails and is excluded from the resisting moment. The steel bars fail when the steel strain reaches a value of 0.15. The strength of a failed strip is assumed to be equal to zero in Eqn. 4.28. However, the pile fails when the stiffness of any pile segment diminishes to a small value that does not provide equilibrium between the external and the resisting moments.

4.4.3 Steel Pipe Pile Filled with Concrete (Cast in Steel Shell, CISS)

In the current case, the pile cross section is treated as a composite section similar to the reinforced concrete pile. The pile cross section (steel and concrete) is divided into a number of strips (equal to 2m) as shown in Fig. 4.9. The thickness of each strip is equal to the thickness of the steel shell (t_s). Both numerical material models presented in Section 4.2 are employed here using an iterative technique governed by the deformation criteria of the numerical models.

The normal strain is assumed to vary linearly over the pile cross section which is perpendicular to the pile axis, as shown in Fig. 4.11. Therefore, the curvature is constant over the whole composite section. The applied bending moment (M_i) at pile segment (i) generates initial values for curvature, stresses and strains in both the steel pipe and the concrete section as described in Section 4.2. Similar to the reinforced concrete section, the concrete resistance in the tension zone is considered. It should be noted that the steel pipe provides large concrete confinement resulting in large values of concrete strength and strain.

The composite cross section of pile behaves symmetrically as long as the tensile strain at the outer strip of concrete ($n = 2$) is less than ϵ_{tu} . The strain values of steel and concrete are obtained using Eqns. 4.30 and 4.31. Then the associated stress values of concrete and steel are calculated based on Eqns. 4.1 and 4.21. Generally, the stiffness the composite cross section is modified according to the equilibrium between the external and internal moments as expressed by Eqn. 4.32 for the symmetric section.

When the tensile strain of the outer strip of concrete ($n = 2$) exceeds ϵ_{tu} , the composite cross section is no longer symmetric and the neutral axis location is shifted towards the compression zone and should be determined by using an iterative technique which includes Eqns. 4.36 through 4.39. It should be noted that the concrete tensile stress (f_t) at any failed strip in the tension zone is equal to zero. In addition, at any strip, the steel stress is equal to f_y if the strain is equal to or larger than ϵ_y . If the calculated resisting moment $(M_R)_i$ does not match the external moment (M_i) , the stiffness of the pile segment in question is modified using Eqn. 4.40.

The above procedure is performed with all pile segments under the same level of loading. This procedure is repeated in an iterative way using the modified stiffness values to solve the problem of the laterally loaded pile (global stability). The iteration process continues until there is equilibrium between the external and resisting moments at all pile segments. The distribution of bending moment (M_i) , along the length of the pile, and the deflection pattern is based on the modified pile stiffnesses and the resistance of the surrounding soil.

It should be noted that the concrete section will not fail before a plastic hinge develops. This occurs because the steel yields at a strain (ϵ_y) much less than the ultimate strain of concrete (ϵ_{cu}). However, the failed strips of concrete (in either the tension or compression zones) are subtracted from the composite section resulting in a faster drop in the stiffness of the pile segment in question. It should be emphasized that there is no sudden failure for the concrete portion of the composite section because of the steel shell.

The stiffness of the loaded pile and the effective area of the deflected pile cross section vary according to the level of loading. Therefore, the actual moment-curvature relationship and the ultimate moment carried by a reinforced concrete pile or a steel pipe pile filled with concrete should be calculated using the technique presented.

4.4.4 Steel Pipe Pile Filled with Reinforced Concrete (Cast in Steel Shell, CISS)

Similar to the pile cross section presented in Section 4.4.3, the pile cross section is treated as a composite section. The pile cross section (steel and reinforced concrete) is divided into a number of strips (equal to 2m) as shown in Fig. 4.9. The thickness of each strip is equal to the combined thickness of the steel shell (t_s) and the thickness equivalent to the longitudinal reinforcement, A_s [$t_r = A_s / 3.14 / (Z_s - t_s)$]. Both numerical material models presented in Section 4.2 are employed here using an iterative technique governed by the deformation criteria of the numerical models.

The normal strain is assumed to vary linearly over the pile cross section which is perpendicular to the pile axis, as shown in Fig. 4.12. Therefore, the curvature is constant over the whole composite section. The applied bending moment (M_i) at pile segment (i) generates initial values for curvature, stresses and strains in both the steel pipe and the concrete section as described in Section 4.2. The current pile cross section (Fig. 4.12) is analyzed by following the procedure applied to the CISS section presented in Section 4.4.3.

4.5 ILLUSTRATIVE EXAMPLES

The examples presented have been reported by Reese (1984) to demonstrate the capability of the computer programs (COM624 and PMEIX) in the design process. The results provided by these two programs are compared to the approach presented to show the drawbacks of using these two programs together and the capability of the technique developed in the present study.

4.5.1 Example Problem, a Fixed-Head Steel Pile Supporting a Bridge Abutment

As reported by Reese (1984), a steel pile of H-shape cross section is driven in stiff clay. The loaded pile is subjected to an axial load of 50 kips, and it is desired to find the lateral load that would cause a soil or pile failure. The pile head was assumed to be fixed against rotation and to have the following properties: 14HP89, depth = 13.83 in., width = 14.70 in., stiffness (EI) = 2.621×10^{10} lb-in², t_w = 0.615 in., f_y = 40,000 psi, plastic moment = 5.8×10^6 lb-in., and length = 50 ft.

The surrounding soil is assumed to have a unit weight of 119 pcf, an undrained shear strength equal to 2016 psf, and an ε_{50} of 0.007.

Figure 4.13 shows the response of the loaded pile assessed using COM624 and the nonlinear analysis of the SW model. The pile response assessed using COM624 was based on a constant value of pile stiffness which is equal to the initial value of EI . Once the calculated moment at any cross section on the loaded pile develops a moment equal to the plastic moment, the moment-load curve is truncated at that value to give the associated lateral load (ultimate lateral load, P_{ult}), as seen in Fig. 4.13. In order to predict the maximum value of pile-head deflection, the load-deflection curve of the pile head, assessed using COM624 is also truncated at a value of a lateral load equal to P_{ult} .

The procedure used by Reese (1984) does not include any variation in the steel pile stiffness. It limits the capacity of pile-head load when any section on the pile experiences a moment (using a constant stiffness equal to the initial stiffness) equal to the plastic moment which is a very crude assumption. The approach presented provides a pile head load capacity twice as much as the value computed using Reese's

procedure, as seen in Fig. 4.13. Furthermore, the pile-head deflection determined using the SW model is approximately four times larger than the deflection assessed by Reese (1984).

4.5.2 Example Problem, a Free-Head Drilled Shaft Supporting a Bridge Abutment

This example was selected by Reese (1984) to demonstrate the difference in the method of analysis of a drilled shaft as compared to the analysis of a steel section. The proposed shaft is surrounded by the same soil (stiff clay) presented in the previous example. The drilled shaft is assumed to have a 30-inch outer diameter, 12 No. 8 rebars (steel area = 9.48 in²) placed on a 24-inch diameter circle. The ultimate strength of the concrete is assumed to be 4000 psi, and the yield strength of steel is 60,000 psi. The shaft exhibits a stiffness value (EI) of 1.89 x 10⁸ kips-in² and is subjected to an axial load of 50 kips. It is desired to find the lateral load that would cause a soil or shaft failure under free and fixed shaft-head conditions.

The interaction diagram (axial load versus ultimate bending moment) for the drilled shaft is calculated using program PMEIX. The predicted ultimate bending moment (M_{ult}) under the applied axial force and at a concrete strain of 0.003 is 6.78 x 10⁶ lb-in. PMEIX is also used to assess a relationship between the stiffness values of the shaft cross section and the associated moments (M_i) under the 50-kip axial load. It is suggested that the designer choose a reduced value of shaft stiffness, $(EI)_{red}$, at M_i / M_{ult} equal to 0.13. This reduced stiffness is equal to 6.96 x 10⁷ kips-in² and is used as a new constant stiffness value for the drilled shaft with COM624.

Figure 4.14 shows the variation in the free-head shaft response using material modeling compared with the shaft response based on constant values of pile stiffness (linear analysis). The assumed values of shaft stiffness range from the initial stiffness (1.89 x 10⁸ kips-in²) to a reduced stiffness equal to 3 x 10⁷ kips-in² which represents 16 percent of the initial stiffness. The shaft responses predicted using both linear and nonlinear analysis at low levels of loading under free-head conditions are the same. Once the shaft material behaves nonlinearly, the shaft response begins to intersect the curves which describe the response of the shaft using the linear analysis at the reduced stiffness values as shown in Fig. 4.14. This figure shows that

there is no single reduction ratio for pile/shaft stiffness (as suggested by Reese 1983) that can be employed in order to predict the pile response based on pile/shaft material properties because pile response varies according to pile and soil properties.

The results computed using COM624 are shown in Fig. 4.15 and compared with the results calculated using the SW model for the free-head drilled shaft. According to the technique presented in this chapter, the effect of concrete confinement is considered. In addition, the transverse steel ratio is assumed to be 0.003 of the whole cross section area. The ultimate lateral load determined using the SW model is 38 percent larger than the value predicted by using STIFF1 and COM624. In addition, the associated pile head deflection is approximately three times as much as the deflection computed using COM624.

It should be noted that the locations of maximum moment cross section on the free-head shaft using the material modeling vary in a different fashion from that predicted using a constant stiffness value. Moreover, unlike the steel cross section, the cross section area of the reinforced concrete pile is not constant during the solution process. Therefore, the shaft head load-maximum moment curve (Fig. 4.15) is not smooth as it is in the linear analysis. However, the load-deflection curve in Fig. 4.15 shows a smooth variation.

4.5.3 Example Problem, a Fixed-Head Drilled Shaft Supporting a Bridge Abutment

The shaft described in the previous example was employed by Reese (1984) to demonstrate the response of a fixed-head pile/shaft including the nonlinear behavior of the reinforced concrete. Similar to the previous example (a free-head shaft), a fixed-head drilled shaft has been solved using the SW model (linear analysis) considering different stiffness values. The assumed stiffness values range from the initial stiffness ($EI = 1.89 \times 10^8$ kips-in²) to a low stiffness of 10^7 kips-in² which represents 0.053 percent of the initial stiffness. As seen in Fig. 4.16, the response of the laterally loaded fixed-head shaft using the material modeling intersects the curves which represent the response of the shaft using different constant stiffness values through linear analysis.

In the case of the fixed-head drilled shaft, the location of the maximum moment section on the shaft is always at the shaft head. Therefore, The shaft head load-maximum moment curve presented in Fig. 4.17 is a smooth relationship.

The ultimate capacity of the shaft head-load defined by Reese (1984) was determined using the same procedure presented in the previous example and is shown in Fig. 4.17. The SW model nonlinear analysis provides an ultimate moment value for the drilled shaft similar to the value calculated by Reese (1984), as seen in Fig. 4.17. However, the associated the lateral load and shaft head deflection predicted using the SW model are approximately twice and eight times larger than the values calculated by Reese, respectively.

4.6 SUMMARY

A technique for the inclusion of nonlinear material modeling for steel, concrete, and composite steel concrete piles has been developed and demonstrated in this chapter. The strain wedge model exhibits the capability of predicting the response of a laterally loaded pile based on the nonlinear behavior of pile material. The technique presented allows the designer to evaluate the location of a plastic hinge developed in the pile, and to determine the realistic values of the ultimate capacity and the associated deflection of the loaded pile.

The nonlinear behavior of the pile/shaft material has an influence on the lateral response and capacity of the pile/shaft. This effect is dependent on the values of bending moment (level of loading). In turn, the modulus of subgrade reaction (i.e. the p-y curve) is affected by the changed bending moment, the reduced bending stiffnesses, and the changed deflection pattern of the pile/shaft. Without the appropriate implementation of material modeling, the pile/shaft capacity, and the associated deflection pattern and bending moment distribution will be difficult to predict with any degree of certainty.

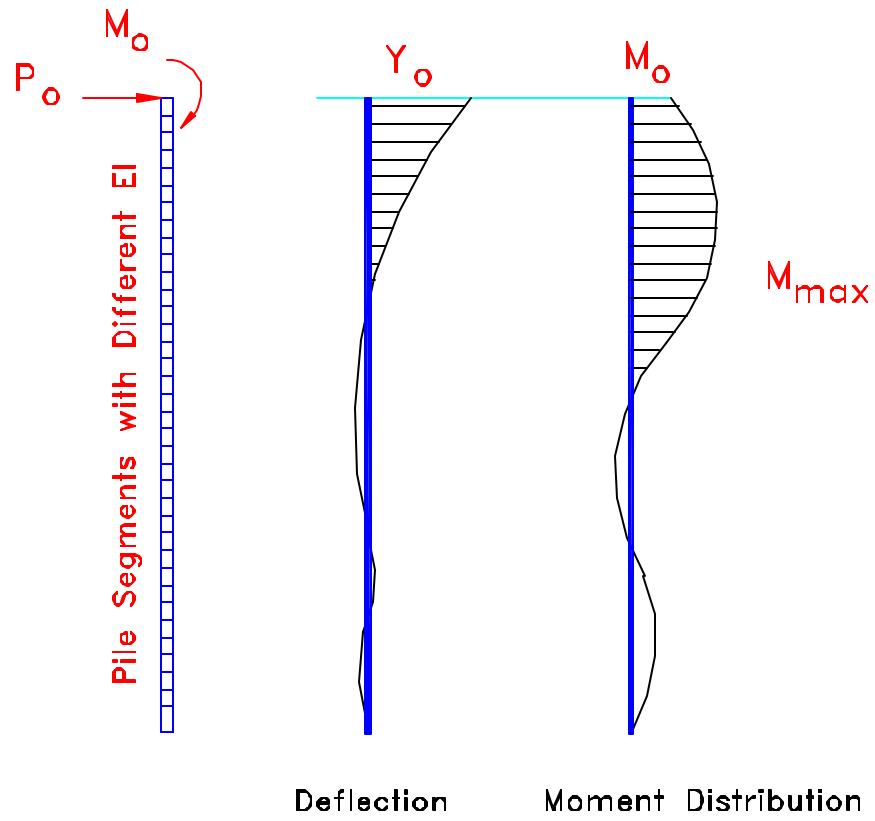


Fig. 4.1 Deflection and Moment Distributions in a Laterally Loaded Pile

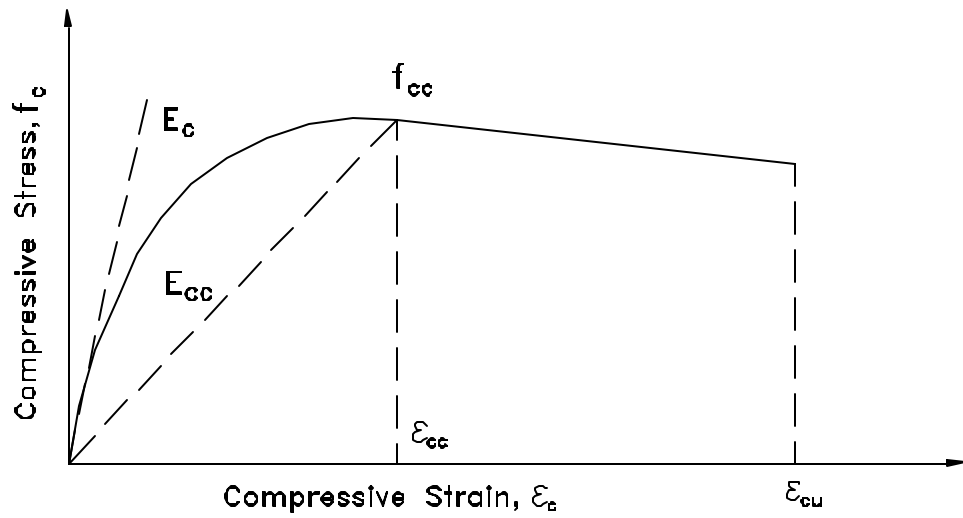


Fig. 4.2 Stress-Strain Model for Confined Concrete in Compression (Mander et al. 1984 and 1988)

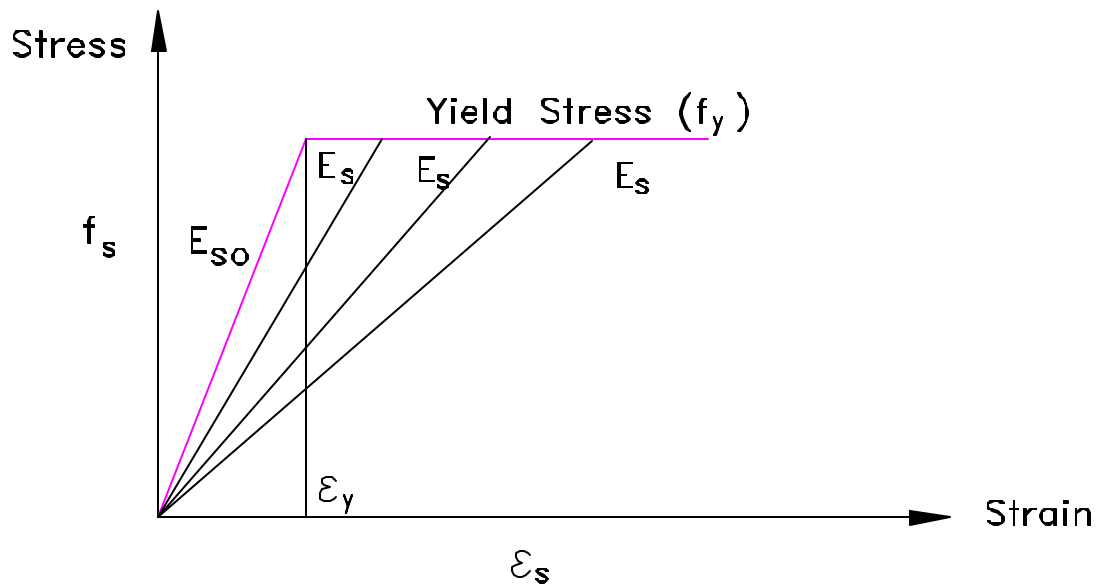


Fig. 4.3 Elastic-Plastic Numerical Model for Steel

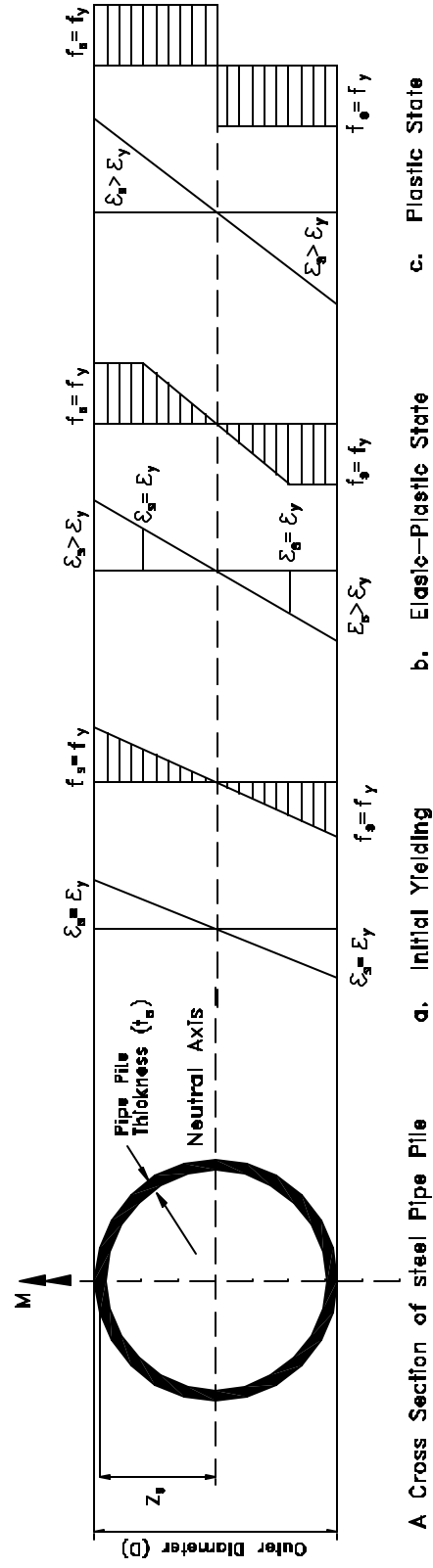
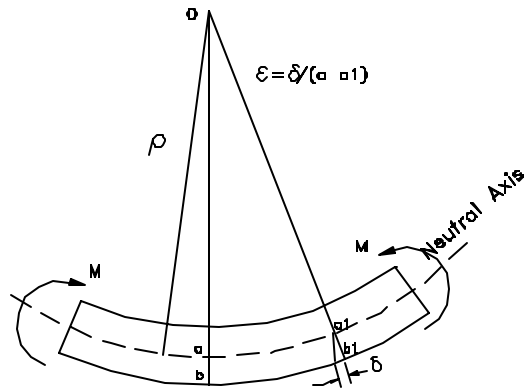
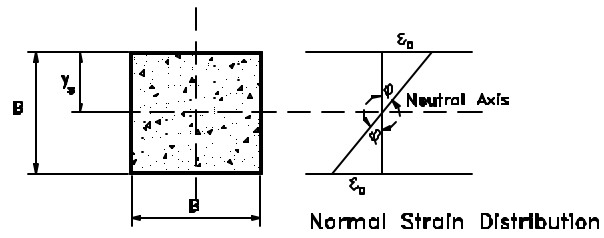


Fig. 4.4 Different stages of Normal Stresses Over a Steel Section

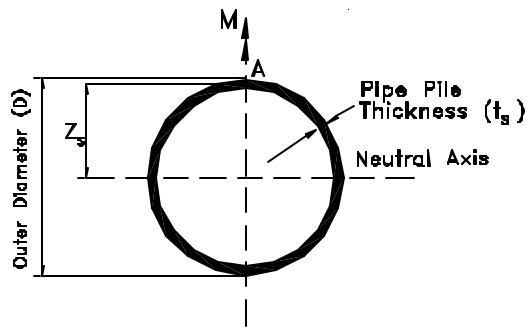


A Pile Segment Subjected to bending Moment

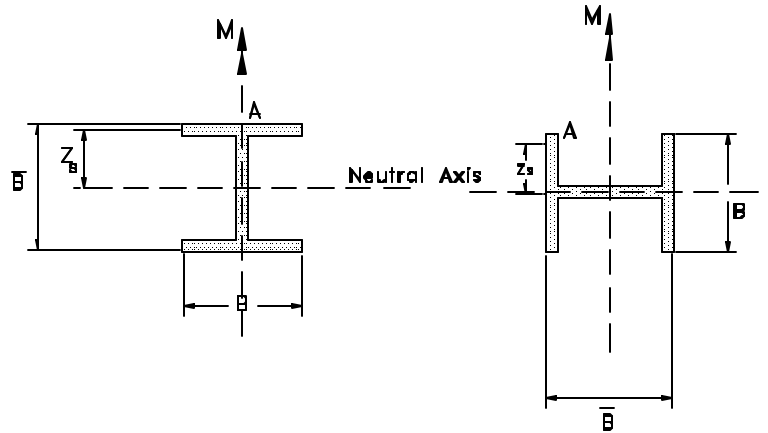


A Cross section of a Concrete Pile Under Bending Moment

Fig. 4.5 Flexural Deformations of a Pile Segment subjected to Bending Moment

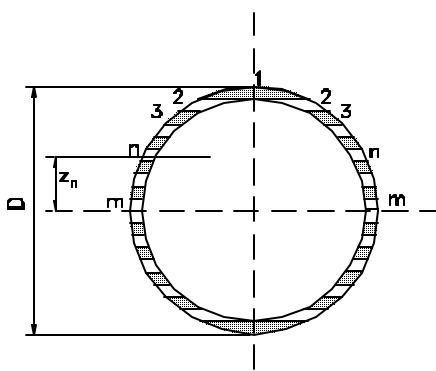


A Cross Section of steel Pipe Pile

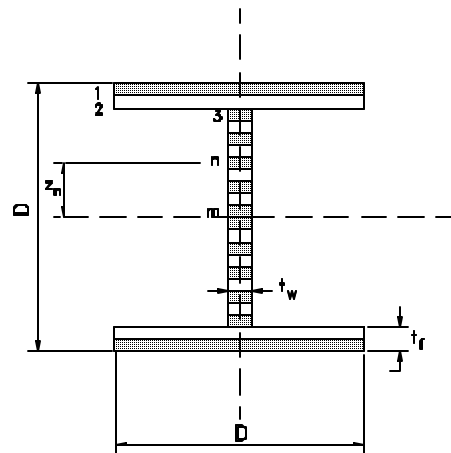


A Cross Section of H-Shape Steel Pile

Fig. 4.6 Different Cross Sections of Steel Piles



A Cross Section of steel Pipe Pile



A Cross Section of H-Shape steel Pile

Fig. 4.7 Steel Sections Divided into Horizontal Strips

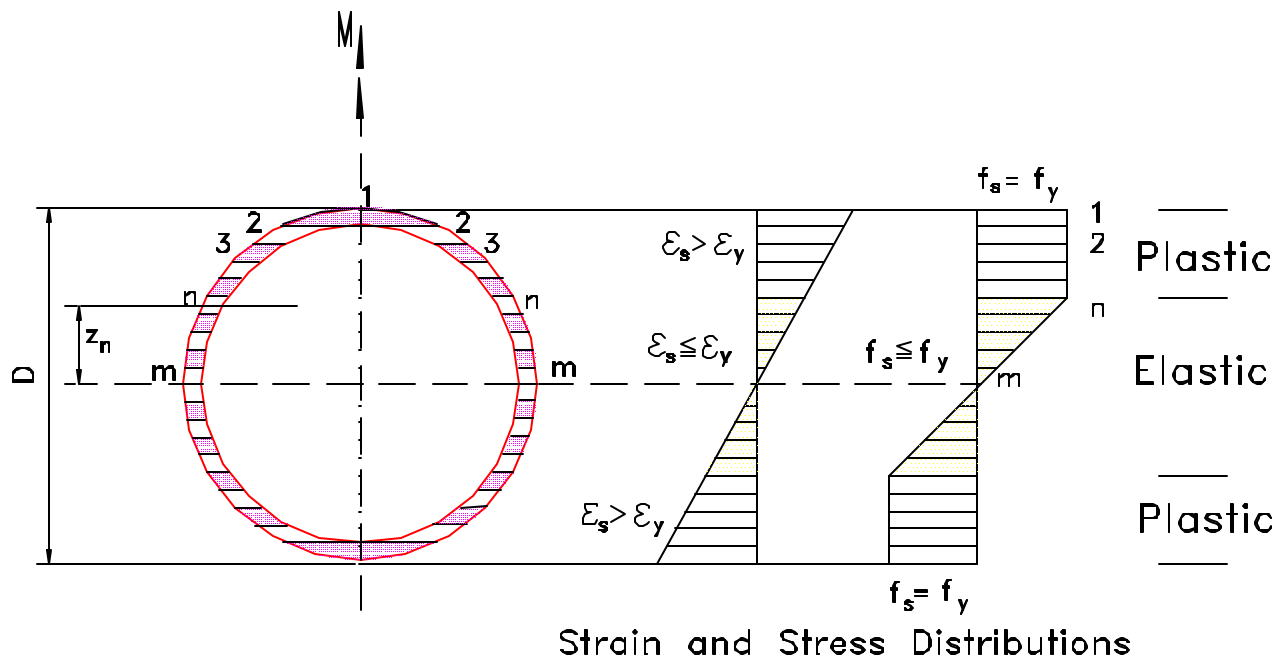


Fig. 4.8 Behavior of Steel Pile Cross Section in the Elastic-Plastic Stage

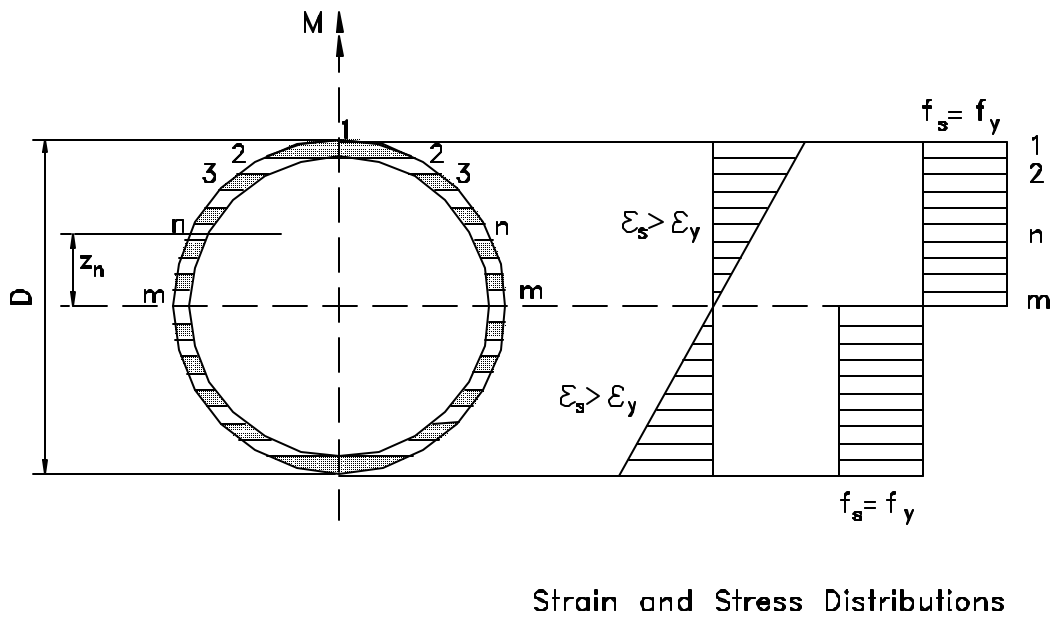
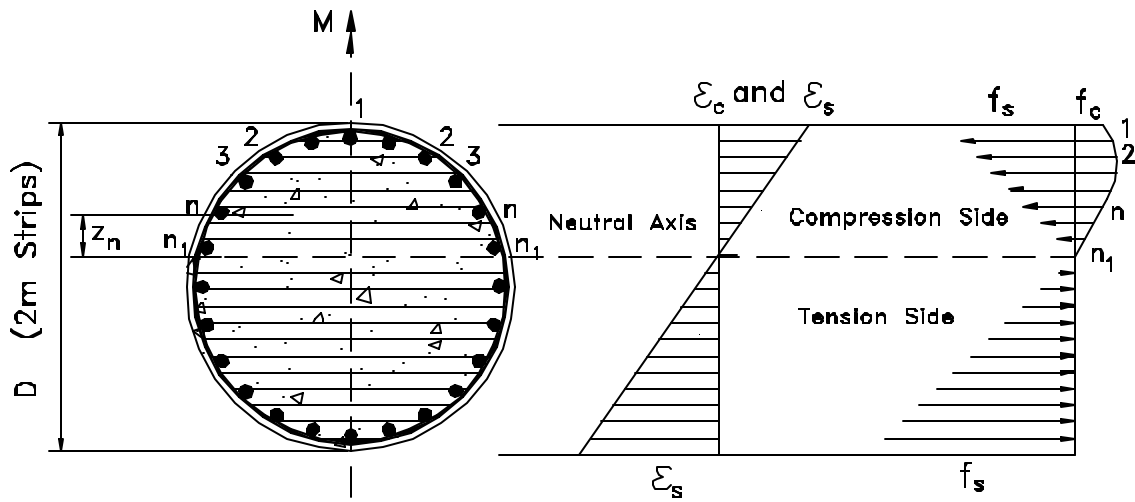
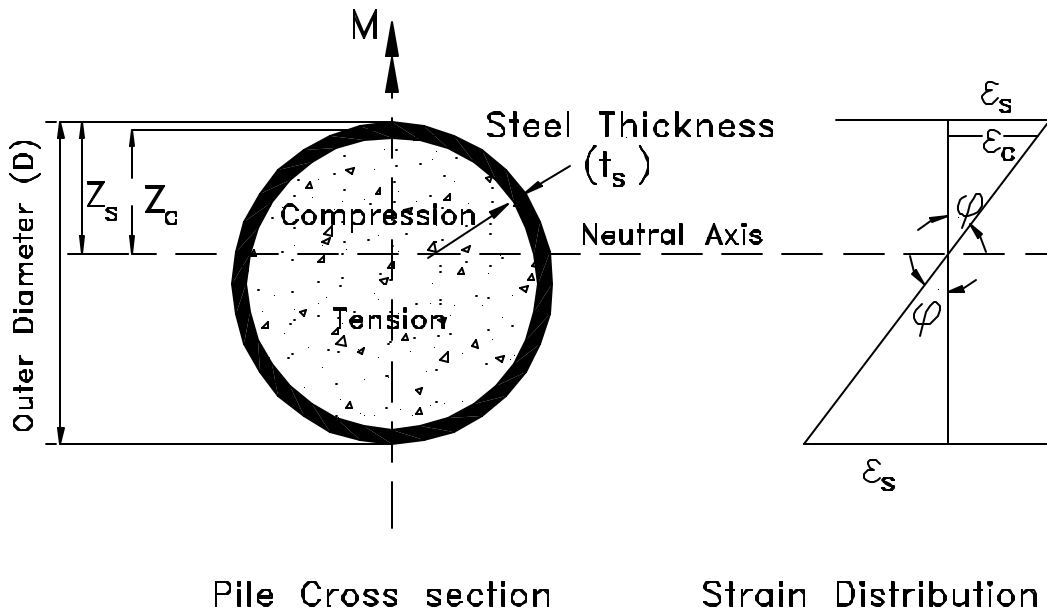


Fig. 4.9 Behavior of Steel Pile Cross Section in the Plastic Stage



Strain and Stress Distributions

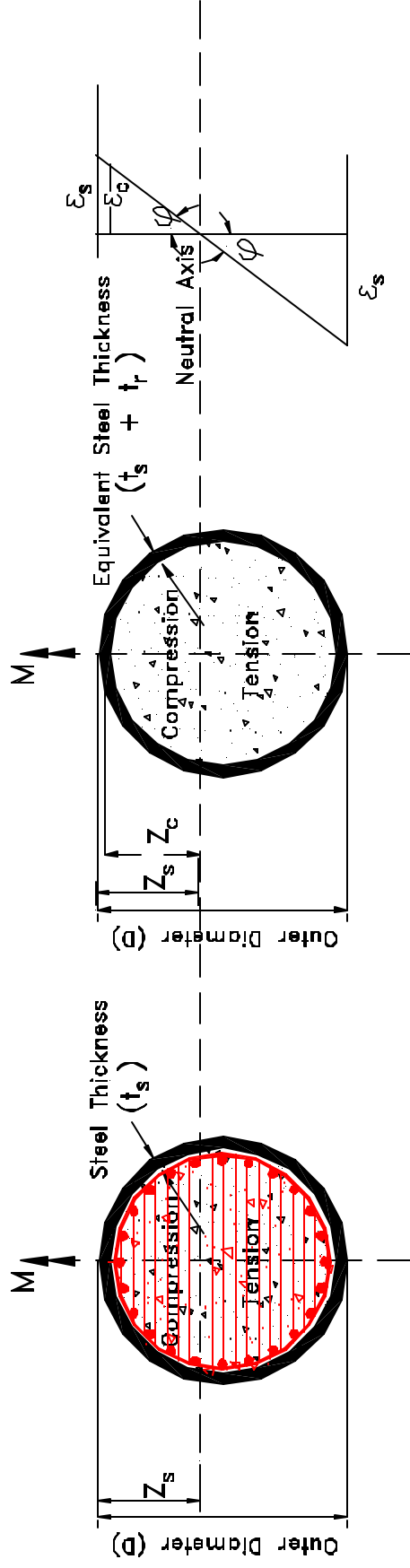
Fig. 4.10 Behavior of a Reinforced Concrete Pile Cross Section Divided into Strips



Pile Cross section

Strain Distribution

Fig. 4.11 Composite Cross Section of a Steel Shell-Concrete Pile (CISS)



Pile Cross section

Equivalent CISS Pile Cross section

Strain Distribution

Fig. 4.12 A Pile Cross Section of Reinforced Concrete Cast in Steel Shell

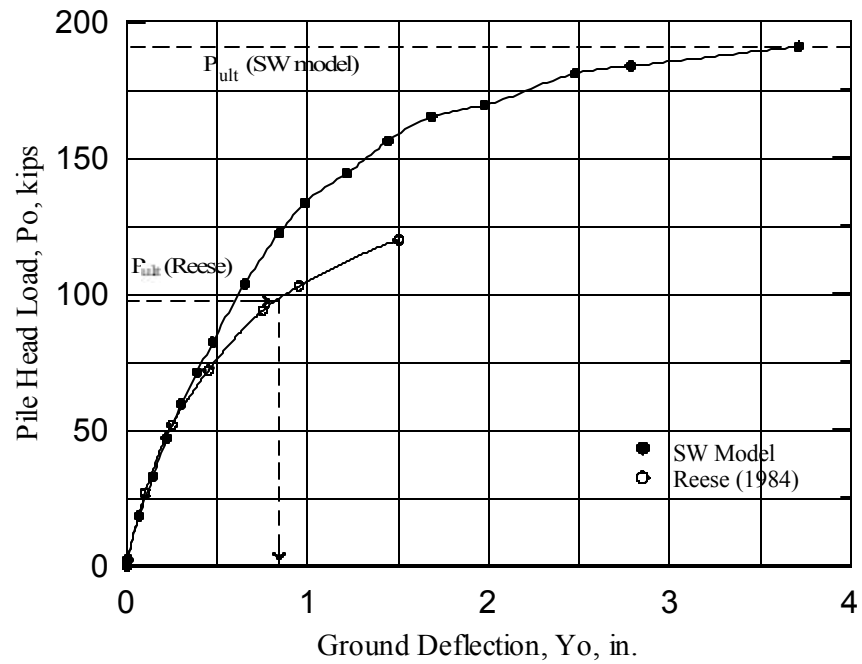
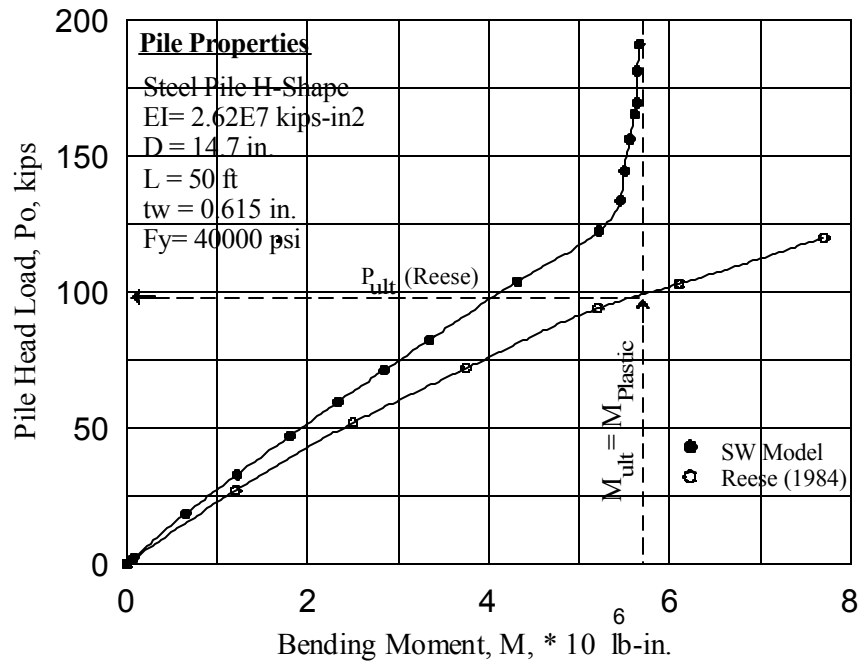


Fig. 4.13 Response of a Laterally Loaded Steel Pile with Fixed-Head Conditions Based on Modeling the Pile Material

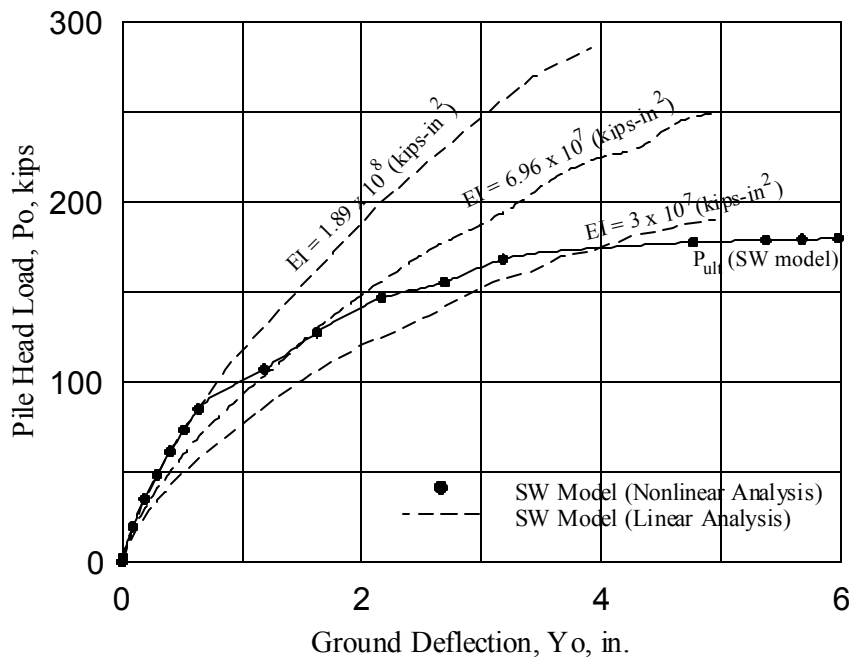
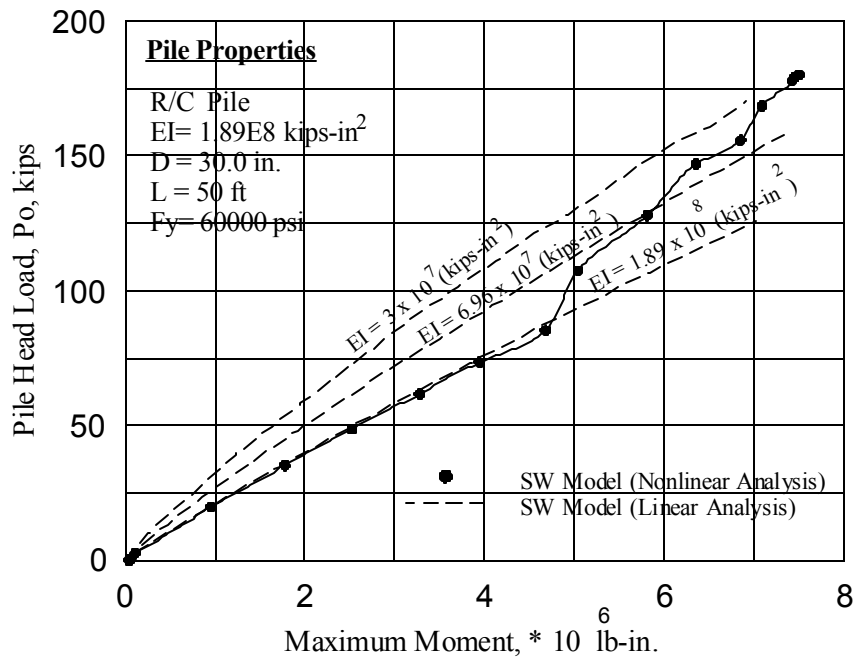


Fig. 4.14 Response of a Laterally Loaded Reinforced Concrete Pile with Free-Head Conditions Based on Pile Material Modeling

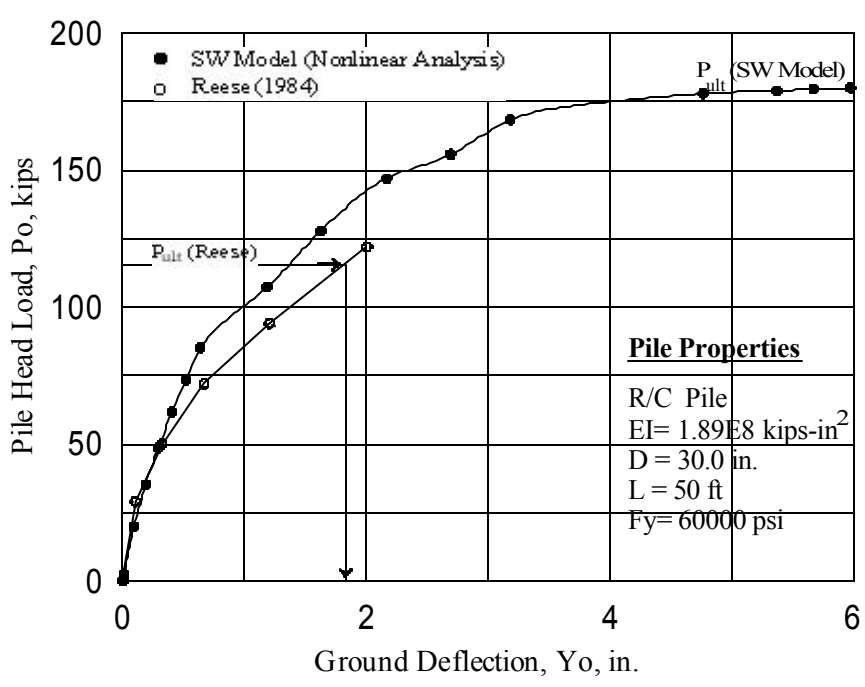
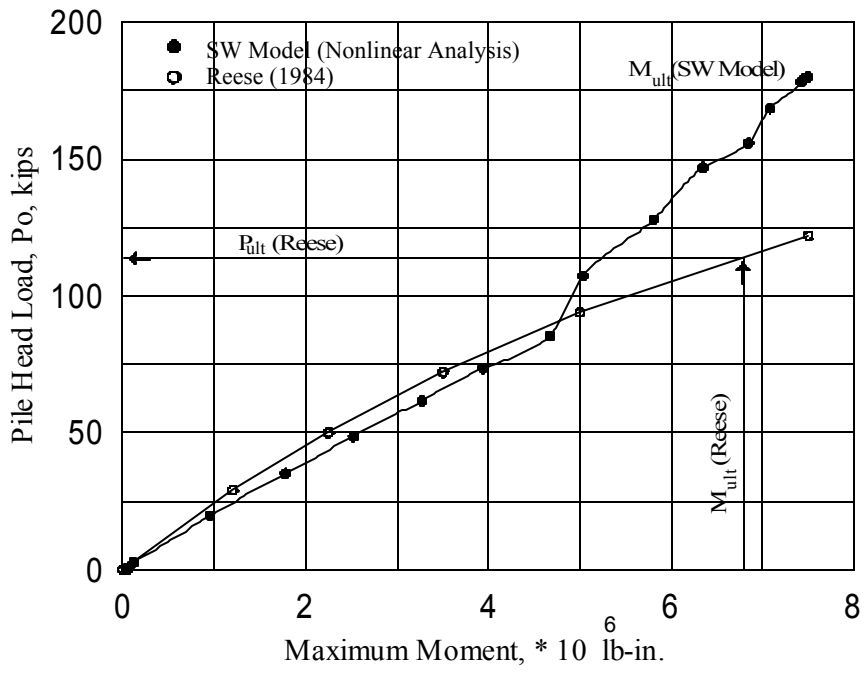


Fig. 4.15 Response of a Laterally Loaded Reinforced Concrete Pile with Free-Head Conditions Based on Pile Material Modeling

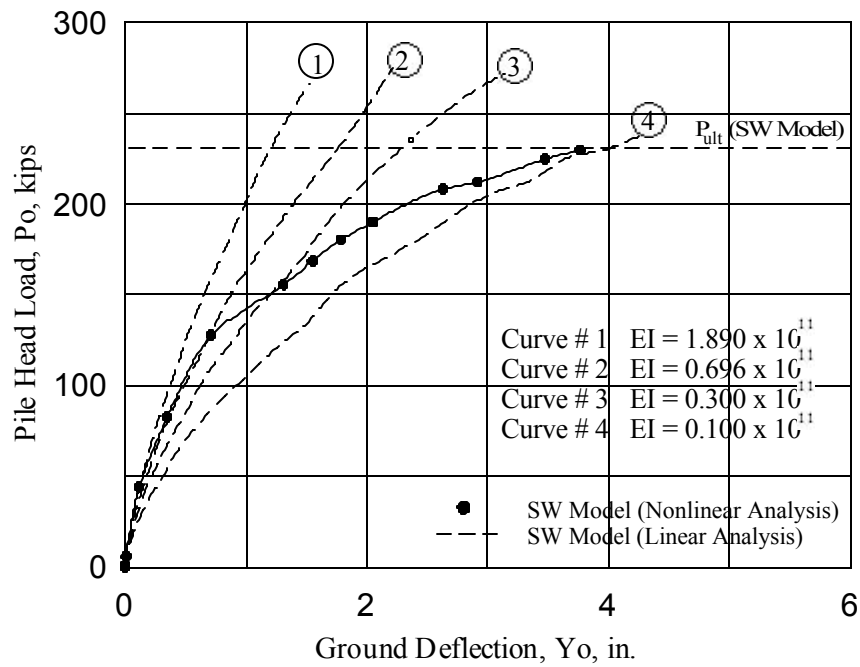
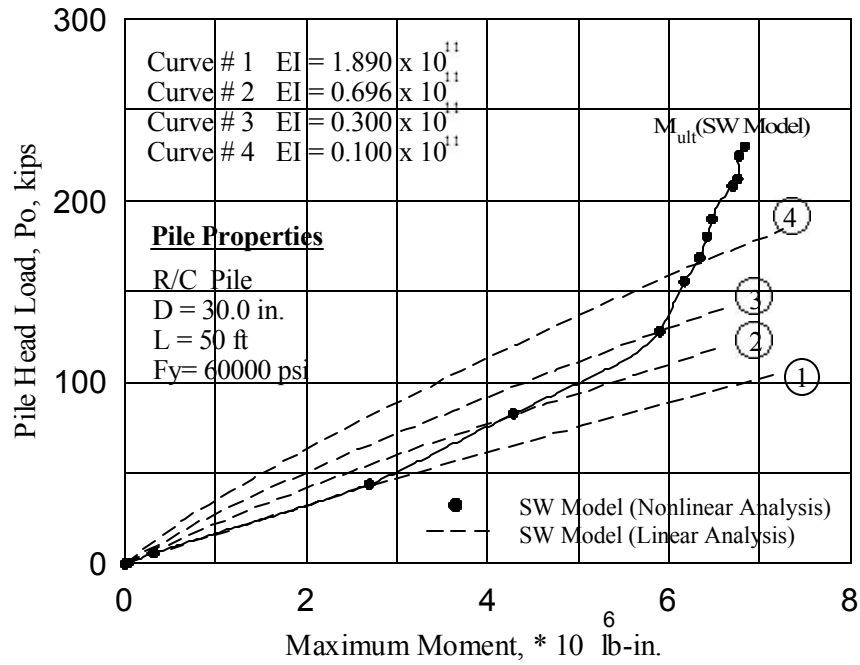


Fig. 4.16 Response of a Laterally Loaded Reinforced Concrete Pile with Fixed-Head Conditions Based on Pile Material Modeling

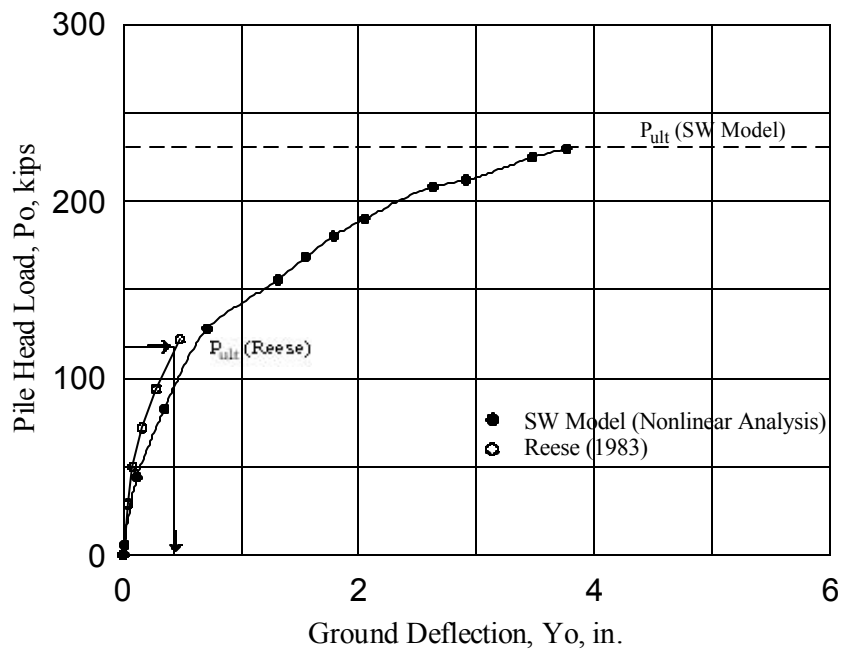
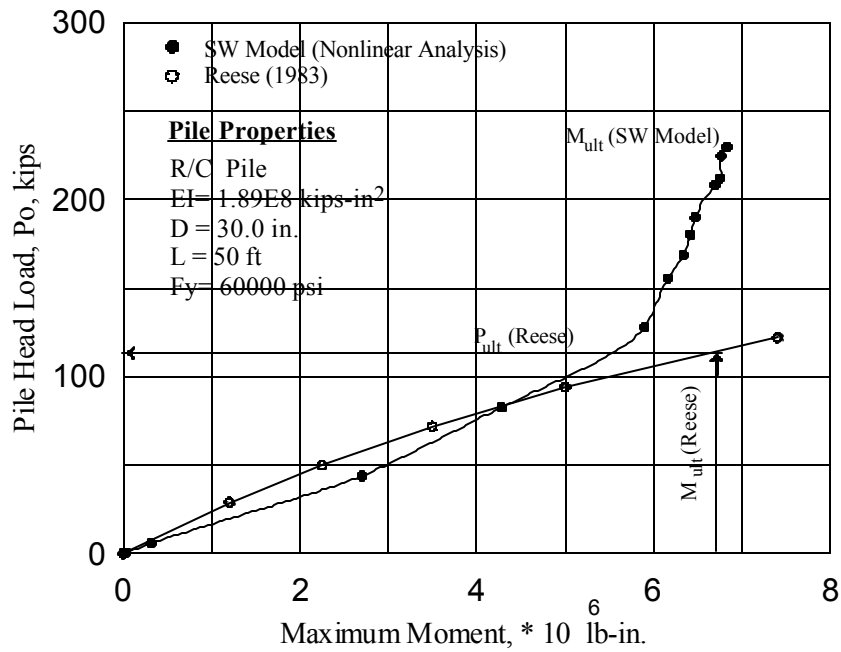


Fig. 4.17 Response of a Laterally Loaded Reinforced Concrete Pile with Fixed-Head Conditions Based on Pile Material Modeling

CHAPTER 5

EFFECT OF NONLINEAR BEHAVIOR OF PILE MATERIAL ON PILE AND PILE GROUP LATERAL RESPONSE

5.1 INTRODUCTION

The problem of a laterally loaded pile is often solved as a beam on an elastic foundation (BEF) involving nonlinear modeling of the soil-pile interaction response (p-y curve). Currently employed p-y curve models were established/verified based on the results of field tests in uniform soils such as the Mustang Island (Reese et al. 1974), Sabine River (Matlock 1970) and Houston (Reese and Welch 1975) tests, and adjusted mathematically using empirical parameters to extrapolate beyond the soil's specific field test conditions. The traditional p-y curve models developed by Matlock (1970) and Reese et al. (1974) are semi-empirical models in which soil response is characterized as independent nonlinear springs (Winkler springs) at discrete locations. Therefore, the effect of a change in soil type of one layer on the response (p-y curve) of another is not considered. In addition, the formulations for these p-y curve models do not account for a change in pile properties such as the pile bending stiffness (nonlinear behavior of pile material).

Soil-pile interaction or p-y curve behavior is not unique but a function of both soil and pile properties. It would be prohibitively expensive to systematically evaluate all such effects through additional field tests. Terzaghi (1955) and Vesic (1961) stated, the subgrade modulus, E_s (and, therefore, the p-y curve), is not just a soil but, rather, a soil-pile interaction (and, therefore, a pile property dependent) response.

The SW model approach, which has been developed to predict the response of a flexible pile under lateral loading, has the capability to carry out such an analysis. The SW model allows the assessment of the (soil-pile) modulus of subgrade reaction (i.e. the secant slope of the p-y curve) based on soil and pile properties which includes the pile bending stiffness. Therefore, the

assessed modulus of subgrade reaction will be affected by the changes in the bending stiffness of the pile at any pile cross section, particularly when the drop in bending stiffness is significant.

In addition to soil and pile properties (Ashour and Norris 2000), the shape of the developed p-y curve is influenced by variations in the pile bending stiffness (i.e. the M- ϕ -EI relationship) and the interference among the passive wedges of soil in the case of a pile group. The p-y curves assessed using the SW model are no longer independent Winkler springs. They are a group of dependent springs that are affected by soil and pile properties, pile group interference, and the nonlinear response of pile material.

5.2 EFFECT OF PILE MATERIAL NONLINEAR RESPONSE ON THE P-Y CURVE

As presented by Ashour et al. (1996 and 1998), the SW model parameters are related to an envisioned three-dimensional passive wedge of soil developing in front of the pile. The basic purpose of the SW model is to relate stress-strain-strength behavior of the layered soil in the wedge to one-dimensional Beam on Elastic Foundation (BEF) parameters in order to solve the following differential equation:

$$EI \frac{d^4 y}{d^4 x} + E_s(x)y + P_v \frac{d^2 y}{d^2 x} = \quad (5.1)$$

$$M \frac{d^2 y}{d^2 x} + E_s(x)y + P_v \frac{d^2 y}{d^2 x} = 0 \quad (5.2)$$

where

M = Bending moment

P_v = Axial load

y = Pile lateral deflection

x = Location of pile section below pile head

The SW model is able to provide a theoretical link between the more complex three-dimensional soil-pile interaction and the simpler one-dimensional BEF characterization. The SW model links the nonlinear variation in the Young's modulus ($E = \frac{d\sigma_h}{d\epsilon}$) of the soil to the nonlinear variation in the modulus of subgrade reaction ($E_s = p/y$) associated with BEF characterization as illustrated in detail in Chapter 2. As presented by Vesic (1961), the bending stiffness (EI) is one of the parameters which affects the modulus of subgrade reaction (E_s). Ashour and Norris (2000) presented a study, based on the SW Model, that showed the influence of the variation in the pile bending stiffness (EI) on the nature of the resulting p-y curve, assuming a constant elastic EI for the whole pile.

As seen by Eqn. 5.1, the response of the laterally loaded pile is a function of M and EI . Using nonlinear modeling for the strength of the pile material (concrete and/or steel) leads to a softer response (less Young's modulus, E , and/or a cracked R/C section which, in turn, means less moment of inertia, I) with increasing pile-head load and moment at a given depth. The SW Model has the capability to account for this reduction in EI on the response of the laterally loaded pile and the associated p-y curves.

As derived and presented in Chapters 2 and 3, the variation in E_s and E_{sg} with depth is a function of the geometrical shape (i.e. the size) of the developing and ever changing three-dimensional passive wedge of soil in front of the pile, the stress level (SL) in the soil (and the associated variation in soil E), and the corresponding deflection pattern of the loaded pile. This combination of soil and pile properties is presented in Eqns. 5.3 and 5.4. Compared to the isolated pile at the same value of pile-head deflection, the overlap among neighboring passive wedges of soil within the pile group affects the values of E_g , ϵ_g , A_g , h and E_{sg} . Also, the size of the passive wedge of soil in front of an individual pile in the pile group will be greater than that of the isolated pile.

The difference in subgrade moduli of the isolated pile versus the pile in the group is as follows:

$$(E_s)_i = \frac{p_i}{y_i} = \frac{A_i D \mathbf{e} E_i}{\mathbf{d}(h - x_i)} = \frac{A_i}{(h - x_i)} D \Psi_s E_i \quad (\text{An Isolated Pile}) \quad (5.3)$$

$$(E_{sg})_i = \frac{p_i}{y_i} = \frac{(A_g)_i D (\mathbf{e}_g)_i (E_g)_i}{\mathbf{d}_i (h - x_i)} \quad (\text{Individual Pile in a Pile Group}) \quad (5.4)$$

where i is the number of soil sublayer or pile segment; p and y are the soil-pile reaction and the pile's lateral deflection, respectively, at each pile segment. As presented in Chapter 2, soil parameter \mathcal{O}_s varies with the Poisson's ratio and stress level (SL) of the soil. Parameter A in the SW model links the BEF p to the horizontal stress change ($\Delta\sigma_h$) in the soil at the face of the passive wedge. h is the current depth of the mobilized passive wedge. Subscript g signifies an individual pile within the pile group. From Eqns 5.2 through 5.4, it is obvious that any change in EI will have an impact on the lateral deflection (y), the associated shape of the passive wedge (h , $\bar{\alpha}$, and n_m), and soil dependent parameters (E , \mathcal{O}_s , and A) as illustrated in Chapter 2 and Section 5.2.1.

5.2.1 Steps for Constructing the p - y Curve in the SW Model Analysis

1. For a particular value of lateral strain (ε) in the developing passive wedge of soil in front of the pile, the increase in horizontal stress ($\Delta\sigma_h$), the stress level (SL) and the associated Young's modulus ($E = \Delta\sigma_h/\varepsilon$) are determined based on the stress-strain relationship of soil (Chapter 2) as assessed from conventional triaxial testing.
2. The associated geometry of the passive wedge of soil (mobilized fan angle, ϕ_m , base angle, β_m , and width of the wedge face, \overline{BC}) is assessed according to an assumed initial value (h) of the passive wedge depth (Fig. 5.1) which is related to the depth (X_0) of the zero deflection point ($y = 0$). The soil layers within the depth h are divided into thin sublayers, and steps 1 and 2 are applied to each sublayer (Fig. 5.2).

3. Based on the current shape and size of the passive wedges, the geometrical overlap of the wedges is evaluated for a pile in a group in each soil sublayer. As a result, the size of the passive wedge in front of the pile in question will increase. A larger stress level and strain (SL_g and ϵ_g), and reduced moduli (E_g and E_{sg}) will develop in the overlapping regions. Therefore, a softer p-y curve results.
4. The current variation of soil-pile line load (p) along depth h (Fig. 2.4) is obtained as a function of soil and pile parameters ($\Delta\sigma_h$, BC , D and τ) and the pile cross-section shape (Eqns 2.32 and 3.9). D is the pile width and τ is the mobilized shear resistance along the pile sides (Fig. 5.3).
5. Pile deflection (y) along the depth of the passive wedge is determined as a function of Poisson's ratio, SL , and the size of the passive wedge (Chapter 2). As a result, the associated profile of $E_s = p/y$ or E_{sg} can be predicted as given in Eqn. 5.3 or Eqn 5.4.
6. Based on the current profile of E_s (isolated pile) or E_{sg} (a pile within the group), the laterally loaded pile is analyzed as a BEF under an arbitrary pile-head lateral load (P_o). The values of pile-head deflection (Y_o) and X_o (i.e. h) assessed using BEF analysis are compared to those of the SW model analysis.
7. Through several iterative processes for the same value of soil strain, converged values of h (i.e. geometry of the passive wedge), Y_o and P_o are obtained. In addition, P_o is modified as a function of the values of Y_o from both the BEF and SW model analyses $[(P_o)_{\text{modified}} = (Y_o)_{\text{SW Model}} (P_o / Y_o)_{\text{BEF}}]$
8. For the next step of loading, a larger value for the horizontal soil strain (ϵ) is used, and steps 1 through 7 are repeated.

Using the nonlinear models for pile material presented in Chapter 4, the bending moment along the pile and the associated EI are calculated by iteration at each step. The solution procedure consists of calculating the value of bending moment (M_i) at each cross section associated with a profile of the modulus of subgrade reaction (E_s) which is induced by the applied load at the pile

top (P_o) . Then, the associated curvature (ϕ), stiffness (EI), normal stress (σ_x) and normal strain (ϵ_x) can be obtained.

This procedure depends on the pile material. The profile of moment distribution along the deflected portion of the pile is modified in an iterative fashion along with the values of the strain, stress, stiffness and curvature to satisfy the equilibrium between the applied load and the associated responses of the soil and pile. This procedure guarantees the incorporation of soil-pile interaction with material modeling. The technique presented strives for a more realistic assessment of the pile deflection pattern under lateral loading due to the nonlinear response of the pile material and the consequent soil resistance.

It should be noted that employment of pile/shaft material modeling is very important in predicting the ultimate capacity, lateral deflection, and the associated moment of the loaded pile/shaft. The simplified procedure of using a single EI of the cracked section can be used to predict the response of the laterally loaded pile/shaft, but with much less certainty. The influence of the variation in EI on the assessed p - y curve will be obvious and especially significant over the zone of large bending moment. For the case of fixed-head conditions, the critical zone will be at the pile/shaft head, where a plastic hinge will develop reducing the pile's capacity.

The SW model has the capability of analyzing the behavior of laterally loaded piles beyond the development of the first plastic hinge. The pile fails when pile stiffnesses at several sections (critical sections under large moment) drop to small values at which time the equilibrium between pile and soil resistances, and the external loads is not satisfied.

5.2.2. Effect of Material Modeling on the p - y Curve Ultimate Resistance (p_{ult})

The influence of the pile bending stiffness on the nature of the resulting p - y curve can be demonstrated via the SW model approach. Based on the SW model analysis, pile properties have a significant effect on the shape and geometry of the developing passive wedge and, hence, the values of p_{ult} and A_{ult} in flow-around failure.

In order to address this issue, consider a pile of the same diameter ($D= 0.33$ m, original $EI= 3.13$ kN-m²) driven in the same soft clay as the Sabine River test (Matlock 1970) but of different bending stiffnesses (different materials). Fig. 5.4 presents the free-head SW model p-y curves at 0.915 m below the ground surface for different EI values. It is noted that the ultimate resistance of soil-pile reaction is controlled by the soil-pile combination as given in Eqns 2.47 and 2.48, and represented by Eqns 5.5 and 5.6 ($p_{ult} = 14.35$ kPa and $A_{ult} = 4.25$, respectively).

$$(p_{ult})_i = (\Delta \mathbf{s}_{hf})_i \overline{BC}_i S_1 + 2(\mathbf{t}_f)_i D S_2 = 10(S_u)_i D S_1 + 2(S_u)_i D S_2 \quad (\text{clay}) \quad (5.5)$$

$$(A_{ult})_i = \frac{(p_{ult})_i}{(\Delta \mathbf{s}_{hf})_i} = \frac{(p_{ult})_i}{D 2(S_u)_i} = 5 S_1 + S_2 \quad (\text{clay}) \quad (5.6)$$

$$p_i = (\Delta \mathbf{s}_h)_i \overline{BC}_i S_1 + 2 \mathbf{t}_i D S_2 = SL_i (2 S_u)_i (5 S_1 + S_2) D \quad (5.7)$$

$$\dots = SL_i (p_{ult})_i ; \dots \text{at} \dots A_i = (A_{ult})_i \dots (\text{clay})$$

A very stiff pile (10 EI) in this soft clay does not interact well with the soil, and a deep and large passive wedge at higher stress levels (SL and SL_i) quickly develops. Consequently, as A_i (given by Eqn 2.35) reaches its ultimate value at A_{ult} , flow around failure occurs at this depth and the soil-pile reaction, p , ceases at a value (when $A_i = A_{ult}$) less than p_{ult} (Eqn. 5.7).

Flow around failure in clay will occur in clay at $p = p_{ult}$ as given by either Eqn 5.5 ($SL = 1$) or Eqn 5.7 ($SL < 1$ but $A = A_{ult}$). However, a plastic hinge can develop in the pile when the pile material reaches its ultimate resistance at a time when $SL_i < 1$ in the soil. In this case, h becomes fixed, and BC_i and p_i will be limited when SL_i in the soil reaches 1 or A_i equals A_{ult} . The plastic hinge may develop in the pile before the development of flow around failure in the case of dense sand and stiff clay. In other words, the chance of developing plastic hinges in a pile before the occurrence of flow around failure increases with softer piles in stiffer soils.

As seen in Fig. 5.4, reducing the bending stiffness of the pile to that of the original steel pipe pile (EI) yields an increase in A_i (compared to the first case) and an increase in the range of soil-

pile interaction until flow around failure again occurs at $A = A_{ult}$ for $p < p_{ult}$. A greater reduction in pile stiffness (similar to a R/C pile of $0.1EI$) increases the ductility of the p-y curve resulting in approximately the same value of p at flow around failure ($A = A_{ult}$). The previous three cases reflect the characteristics of the p-y curve when the pile has large resistance compared to that of the surrounding soil. However, for a very flexible pile (a timber pile of $0.01EI$) in this soft clay, very large deflection is required before the soil-pile reaction reaches p_{ult} at $A = A_{ult}$. This is because of the very slow growth of the passive wedge and parameter A .

Fig. 5.5 presents the interaction between pile and sand at a depth of 1.83 m for conditions similar to the Mustang Island test (Cox et al. 1974). Changing the pile stiffness results in very different p-y curves. Because the surrounding sand is dense, increasing the pile stiffness causes the p-y curve to become stiffer. The p-y curve in the sand would cease to grow due to the development of a plastic hinge (yield moment) well before any flow-around failure. Note that the effect of yield moment is shown only for the Mustang Island test and the SW model (EI) p-y curve (for linear elastic material modeling, i.e. a constant EI). It should be noted that reaching the value of the plastic moment at any point on the pile results in the cessation in the growth the p-y curve at p_{ult} as shown in Fig. 5.5.

The incorporation of the material modeling for pile material in the SW model analysis allows the designer to control the lateral ductility of the pile foundations. This can be accomplished by choosing the appropriate material (steel and/or reinforced concrete) for a pile in a particular soil profile in order to delay or quicken the development of plastic hinges in the loaded pile. Such analysis can be further enhanced by using nonlinear material modeling as described in Chapter 4.

5.3 CASE STUDIES

5.3.1 PYRAMID BUILDING AT MEMPHIS, TENNESSEE, FULL-SCALE LOAD TEST ON A PILE IN LAYERED CLAY SOIL

As documented by Reuss et al. (1992), a lateral load test was performed on a full-scale pile in downtown Memphis, Tennessee. An arena of the shape of a pyramid was constructed at the site between 1989 and 1991. The site bordered the Mississippi river until the early 1900's, then, the

channel changed with the formation of a sand bar or mud island that diverted the flow of the river. To improve the lateral capacity of piles associated with this building, 1.8 meters of soft soil around the piles were removed and backfilled with compacted stiff clay. A full-scale loading test was conducted to measure the pile responses after the soil improvement. The field testing also included the measurement of the pile deflections under sustained loading and the flexural rigidity of the tested pile. The results reported for the pile test occurred before and after the soil improvement.

Pile Configuration and Foundation Material Properties

As documented by Reuss et al. (1992), a 400-mm-diameter reinforced concrete pile was installed to a total penetration of 22 meters. An inclinometer casing was installed in the pile to measure the lateral deflection. For a composite material such as reinforced concrete, the pile stiffness, EI, is a function of bending moment on the pile cross-section. The experimental values of EI as a function of the bending moment are reported by Reuss et al. (1992) as shown in Fig. 5.7. The selected value of EI lies, in general, between the uncracked EI value (initial EI = 1.75×10^7 kips-in² or 50,220 m²-kN) and the cracked EI value. An average value for EI equal to 1.35×10^7 kips-in² (38,742 m²-kN) was used for the pile in the material linear elastic analysis. Concrete was cast around the pile to restrain it against excessive deflection when it was reloaded, and the pile head was free to rotate.

The different types of soils at this site allowed the comparison of the SW model predicted versus observed response for a layered soil case. The top 1.8 meters of the soft soil was replaced by a compacted gravely clay pad for the lateral load test. Figure 5.6 provides a description for the improved soil profile as documented by Reuss et al. (1992) and employed with the SW model analysis and LPILE. The soil properties given in Fig. 5.6 were modified as seen in Fig. 5.7 to obtain good agreement between the measured data and the pile response predicted using LPILE (Reuss et al. (1992)).

Comparison of Results of Load Test with Results Predicted by the SW Model

As mentioned above, the soil properties of the fill soil and the second stratum were modified by Reuss et al. (1992) to obtain good agreement between the values predicted using LPILE and the

field results. The unmodified soil properties were employed with the SW model to analyze the response of the tested pile for the original and improved soil profiles. The SW model employs material modeling of the reinforced concrete pile as explained in Chapters 2 (linear analysis) and 4 (nonlinear material modeling). As a result, the moment-stiffness relationship can be obtained and compared with the measured values as shown in Fig. 5.8. The concrete tensile strength is considered in the nonlinear SW model material analysis. The moment-stiffness relationships shown in Fig. 5.8 were obtained by first considering the concrete tensile strength and then by neglecting it. The results shown in Fig. 5.9 were obtained using an average value of pile stiffness (1.35×10^7 kips-in²) with the linear SW model and LPILE analysis, and an initial stiffness value (1.75×10^7 kips-in²) with the nonlinear SW model analysis. In Fig. 5.8, note the wide range of measured values of pile stiffness, especially, at the lower values of bending moment, which indicates the inconsistency of the reinforced concrete response at various pile cross sections.

Figure 5.9 demonstrates the good agreement between the measured and the SW model results for pile head response in the improved soil profile. The effect of the nonlinear behavior of the concrete and steel is noticed at the higher levels of deflection where linear and nonlinear SW model analyses separate. The LPILE response based on measured soil properties (Fig. 5.6), rather than properties modified to enhance fit (Fig. 5.7), is too soft for deflections greater than 0.2 inches. This is due to LPILE's difficulty in approaching appropriately modeling p-y curves in a layered soil profile.

A comparison of the predicted pile head responses in the original soil profile (no compacted gravelly clay pad) using the SW model (linear and nonlinear analyses) and LPILE is presented in Fig. 5.10. The LPILE and SW model linear analysis results are in good agreement. This indicates that, for basically the single layer soil profile of soft clay (with silt and sand lenses), LPILE and the linear SW model analyses are comparable. For this case, the unmodified properties of this layer (from Fig 5.6) were employed, not the increased value (from Fig. 5.7) needed for better LPILE fit for the layered case (improved soil profile with pad on place).

Figure 5.10 (original soil profile) shows a greater difference of the more accurate nonlinear SW model response compared to linear SW model and LPILE responses than between linear and nonlinear SW model responses for the layered case (Fig. 5.9, improved soil profile)

Corresponding to the results of Fig. 5.10, Fig. 5.11 indicates the influence of soil and pile properties on the nature of the associated p-y curve (3 ft below ground surface). p_{ult} is governed at this depth by the development of flow around failure in soft clay that takes place before the development of a plastic hinge as addressed in Section 5.2.2.

5.3.2 HOUSTON FULL-SCALE LOAD TEST ON A REINFORCED CONCRETE SHAFT IN STIFF CLAY

As published by Reese and Welch (1975) and Reese (1983), a laterally loaded shaft was tested at a site located in Houston, Texas. The testing site was near the intersection of State Highway 225 and Old South Loop East. The aim of the test was to develop criteria for predicting the behavior of stiff clay around a deep foundation subjected to short-term static or cyclic loading. The test involved the lateral loading of an instrumented long shaft to measure the bending moment along the length of the foundation.

Pile Configuration and Foundation Material Properties

A loading test was performed on a drilled shaft constructed by drilling an open hole of 30 inches diameter to a depth of 42 feet below the ground surface. An instrument column and a reinforcing steel cage were placed in the hole and concrete was poured.

The shaft extended 2 feet above the ground surface. The instrument column was steel pipe with a wall thickness of 0.25 inch and outer diameter of 10.75 inches. The wall thickness was selected to provide flexural stiffness for the instrument column equal to the flexural stiffness of the concrete it replaced.

To install strain gages for measuring the bending moment in the drilled shaft, the pipe of the instrument column was split longitudinally, and two strain gages were mounted on each half of the pipe at each gage level. At each level, the four gages were connected in a bridge circuit to

provide the maximum sensitivity to bending. The strain gages were spaced at 15 inch intervals for the top two-thirds of the shaft, and at 30 inch intervals for the bottom one-third.

It should be mentioned that difficulty was encountered in filling the hole with concrete. Because the close spacing of the reinforcing steel, a cavity formed near the top of the shaft, as reported by Reese (1983). The diameter and properties of the drilled shaft were not precisely known because of the construction procedure. The stiffness of the shaft had to be established before the bending moment could be assessed from the measured bending strains (Reese and Welch 1975). The variation of initial shaft stiffness with depth is shown in Fig. 5.12. The average linear value of shaft stiffness employed in this study is 1.47×10^{11} pounds-inch², as suggested by Reese (1983).

The soil profile at the site consisted of 28 feet of stiff to very stiff red clay, 2 feet of interspersed silt and clay layers, and very stiff tan silty clay to a depth of 18 feet below the ground surface. Isotropically consolidated-undrained triaxial compression tests (ICU) were performed on undisturbed samples taken at the test site with confining pressure equal to the effective overburden pressure. In order to define the resulting stress-strain relationships in nondimensional terms, the SL (applied principal stress difference divided by the maximum principal stress difference) was plotted against the strain divided by the strain at fifty percent of the maximum stress (ϵ_{50}). The average value of ϵ_{50} was 0.005 as calculated by Reese and Welch (1975). More information and details are presented by Reese and Welch (1975).

Direct measurement of the relationship between bending moment and bending strains was considered the most suitable method to determine the stiffness, especially with the nonlinear response of the reinforced concrete. To measure the stiffness of the shaft, the soil around the shaft was excavated to a depth of 20 feet and loaded as a cantilever. Bending strain readings were taken at various depths versus load levels. Four sets of readings were taken, and the average values assumed to define the stiffness. The moment-curvature relationship ($M-\phi$) was developed to define the flexural stiffness as a function of the applied load. The curvature was determined by measuring bending strains assuming a linear strain distribution over a cross section perpendicular to the axis. There was a significant change in stiffness with depth, due to

the defects in the shafts. A theoretical $M-\phi$ curve was generated and compared with the measured $M-\phi$ as shown in Fig. 5.13

Comparison of Results of Load Test with Results Predicted by the SW Model

The moment-curvature ($M-\phi$) curve predicted using the SW model based on the properties of the shaft material presented in Fig. 5.12 are compared to the measured and theoretical values assessed by Reese and Welch (1975) (Fig. 5.13). The SW model $M-\phi$ curve shows very good agreement with the measured and the theoretical values at each level of loading.

A comparison between the measured and predicted values of shaft response is presented in Figs. 5.14 and 5.15. The plotted values for the laterally loaded shaft, using the SW model, are based on a constant average shaft stiffness in linear analysis and varying shaft stiffnesses in the nonlinear analysis. The influence of nonlinear behavior of concrete controls the ultimate capacity of the loaded shaft, $(P_o)_{ultimate}$ and $M_{ultimate}$, as shown in Figs. 5.14 and 5.15. It should be noted that the uncertain value of diameter has a significant effect on the response of the shaft.

Figure 5.15 provides a comparison of the measured values of maximum bending moment versus the applied lateral load and that assessed using the SW model linear and nonlinear analyses. The moment capacity (7584×10^3 kips-in) of the shaft calculated using the nonlinear SW model is based on the given properties of the shaft material.

The nonlinear material modeling for the steel and concrete with the nonlinear SW model allows realistic assessment of an ultimate value of lateral load. The SW model predicts an ultimate value 25 percent larger than the value calculated by Reese and Welch (1975).

The $p-y$ curve presented in Fig. 5.16 clearly shows the effect of the nonlinear response of pile material (R/C) on the nature of the associated $p-y$ curve. Once a plastic hinge develops at that depth (5 ft below ground), the $p-y$ curve ceases to grow due to a large, quick reduction in pile stiffness at that particular section.

5.3.3 LAS VEGAS TEST ON DRILLED SHAFTS AND SHAFT GROUP IN A CALICHE LAYER

Lateral load tests on drilled shafts of different diameter were performed at the US 95 and I-15 interchange in Las Vegas (Zafir and Vaderpool 1998). The primary purpose of the load test program was to verify the higher design values of both vertical and lateral resistance of drilled shaft foundations for the partially to fully cemented (caliche) soils generally found in the Las Vegas valley.

Pile Configuration and Foundation Material Properties

The test presented in this study was performed at site # 1 that had two layers of stiff clay in the upper 13.5 ft as seen in Table 5.1. A 7.5 ft caliche layer with shear strength of 690,000 psf is found at 13.5 ft below ground surface. The existence of the caliche layer dominated the lateral response of the drilled shafts.

The shaft considered herein is a 2-foot diameter drilled shaft. The 2-foot drilled shaft had an initial bending stiffnesses of 1.13×10^{11} lb-in². The properties of the shaft are presented in Table 5.2. A group of four such 2-foot diameter shafts was tested at site #1. The shafts of the group were spaced at 4-diamters on center. The isolated shaft and shaft group exhibit free head conditions under lateral load.

Table 5.1 Soil profile at site # 1

Depth (ft)	Soil type	Unit weight (pcf)	S _u (psf)	ε ₅₀
0.0 – 5.0	Stiff clay	120	1600	.007
5.0 – 9.0	Stiff clay	125	3000	0.005
9.0 – 13.5	Stiff clay	120	2000	0.0063
13.5 – 21.0	Caliche	140	690000	0.001
21.0 – 35.0	Stiff clay	125	3500	0.0048
35.0 – 38.8	Caliche	140	576000	0.001

Table 5.2 Pile properties

Shaft Diameter (ft)	Length (ft)	f_c (psi)	$EI \times 10^{11}$ (lb-in ²)
2	35	4600	1.13 (initial)

Comparison of Results of Load Test with Results Predicted by the SW Model

Zafir and Vanderpool (1998) assessed the lateral response of the shafts in question using COM624P (which is similar to LPILE) combined with the program STIFF. Using the computer program STIFF, the EI of the tested shaft was modified (for the whole length) based on the moment-curvature-bending stiffness ($M-\phi$ -EI) relationship at the section of maximum bending moment. This resulted in conservative EI values.

SW model linear and nonlinear analyses were employed to assess the lateral behavior of the drilled shaft. Figure 5.17 shows a comparison between the measured and predicted response for the loaded shaft using the SWM (linear and nonlinear analyses) and LPILE (cracked section EI). As judged from Fig. 5.17, the shaft experiences a large variation in bending stiffness due to cracking in the concrete. Nonlinear SW model analysis employs an EI that varies not only with position but with increasing load. The caliche layer at site # 1 is treated as rock and the pile is analyzed in this layer based on the rock model presented by Ashour et al. (2001).

Figure 5.18 provides a comparison between the observed and SW predicted data for the shaft group. The field data collected beyond ground deflection of 0.2 in was not accurate (Zafir and Vanderpool 1998). Therefore, the lateral response for the shaft group was very limited.

5.3.4 SOUTHERN CALIFORNIA FULL-SCALE LOAD TEST ON SHAFT IN STIFF CLAY

As documented by Bhushan et al (1987), lateral load tests were performed on drilled shafts for a transmission line at two sites located in Southern California. The lateral load test on shaft 8 is presented in this study.

Pile Configuration and Foundation Material Properties

Shaft 8 was a 2-foot diameter reinforced concrete drilled shaft. It is straight sided, reinforced with 3 percent steel over a 16-foot length. Average values of shaft stiffness and plastic moment were 6.45×10^7 kips-in² and 503 ft-kips, respectively.

The soils at the site are silty and sandy clays of low to medium plasticity. The liquid limit falls between 30 and 58 and the plasticity index was between 15 and 20. The natural water contents are located at or below their plasticity limit, indicating that the soil is heavily overconsolidated. The values of the undrained shear strength and ϵ_{50} were obtained from the undrained triaxial tests of intact samples. The reported average values of the undrained shear strength and ϵ_{50} are 4750 psf and 0.0072, respectively. In addition, the average value of total unit weight is 130 pcf.

The drilled shaft was only subjected to static loading. The lateral loads were applied incrementally, and each increment was held constant for at least 40 minutes. In addition, the incremental loads were applied at 1.0 ft above the ground surface.

Comparison of Results of Load Test with Results Predicted by the SW Model

Figure 5.19 shows the experimental results of the laterally loaded shaft compared to the shaft response predicted by the SW model and COM624 (Reese 1983). The measured response of the tested shaft exhibits a response stiffer than that computed by COM624, but in very good agreement with the linear SW model analysis. The results provided by the nonlinear SW model analysis are conservative at the higher levels of deflections. This conservative response could be related to the value of initial bending stiffness, EI_i , employed that is directly related to the concrete strength (5000 psi), and the longitudinal and transverse steel ratio (3% and 0.5%), respectively.

5.3.5 ISLAMORADA FULL-SCALE LOAD TEST ON A PILE DRIVEN IN ROCK

As reported by Reese (1997), a test was performed under sponsorship of the Florida Department of Transportation and was carried out in the Florida Keys (Nyman 1980). a 1.22-m diameter pile was bored to 13.3 m into a layer of limestone and tested under lateral load.

Pile Configuration and Foundation Material Properties

The profile of the test site consisted of a brittle, vuggy limestone. Two specimens were obtained for unconfined compressive tests. The compressive strengths were found to be 3.34 and 2.6 MPa. The axial deformations were measured and the average value of the initial modulus of rock was found to be 7,240 MPa. The rock site was further investigated using in situ grout-plug tests in which the ultimate resistance of the rock varied from 1.013 to 2.54 MPa.

The bored 1.22-m diameter shaft was 15.2 m long and laterally loaded at 3.51 m above the rock surface. The pile had an initial bending stiffness (EI_i) of 3.73×10^6 kN-m². Reese (1997) developed a p-y model for a pile in rock which he used to assess the lateral response of the shaft tested at the Islamorada site. A compressive strength of 3.45 MPa was selected by Reese for use with LPILE to represent the rock strength near the surface where the deflection of the shaft was most significant. Based on the data from the field investigations, a lower compressive strength of 1.75 MPa was selected to represent the rock strength near ground surface in the SW model analysis.

Comparison of Results of Load Test with Results Predicted by the SW Model

The SW model approach has been extended by Ashour et al. (2001) to incorporate the analysis of a laterally loaded pile in rock. This rock model is employed in the current version of the SWM computer code. There is close agreement between the results from LPILE and the linear SW model linear analysis as seen in Fig. 5.20. The use of a compressive strength of 1.75 or 3.45 MPa for rock in the linear SW model analysis has not significantly affected the pile response to 6 mm pile head deflection. A compressive strength of 1.75 MPa in the nonlinear SW model yields results in good agreement with the field behavior (Fig. 5.20). It should be noted that predicted pile response using the nonlinear SW model analysis has some scattered points and the pile response plotted in Fig. 5.20 represents an average curve fitting. The ratio of longitudinal and transverse reinforcement, and the steel and concrete strength have a significant influence on the predicted pile behavior.

5.3.6 UNIVERSITY OF CALIFORNIA AT LOS ANGELES FULL-SCALE LOAD TEST ON A PILE DRIVEN IN STIFF CLAY

As reported by Janoyan et al. (2001), UCLA tested a 6-foot-cast-in-drilled-hole (CIDH) shaft column to check the response of such large diameter member to bridge loads applied high above ground surface. The shaft was designed according to the standard Caltrans Bridge Design Specifications.

Pile Configuration and Foundation Material Properties

The shaft tested was 40 ft above ground and extended 48 feet below ground surface. The longitudinal and transverse reinforcement of the shaft consisted of 36-#14 bars and 6-inch spacing # 8 hoops. Based on the given shaft dimensions and longitudinal reinforcement, the shaft exhibited an initial bending stiffness (EI_i) of 3.75 kips-ft².

Three borings were made at the test site. The soil conditions generally consist of deep alluvial sediments. There is a surface layer of asphalt and concrete debris that extends to a depth of 2 to 5 ft. This layer is underlain by a silty clay layer that extends to a depth of 24 ft below ground surface. A second silty clay layer extends from 24 ft to 48 ft below ground surface. Figure 5.21 is the log of boring # 1. A seismic cone penetration (SCPT) test was performed at the shaft location prior to installation. Figure 5.22 shows the measured shear wave velocities at 0.5 m intervals at the location of boring # 1. As seen in Fig. 5.22, the average shear wave velocity is approximately 1000 ft/s. More detail on soil and shaft properties, the instrumentation, and testing procedure are presented by Janoyan et al. (2001).

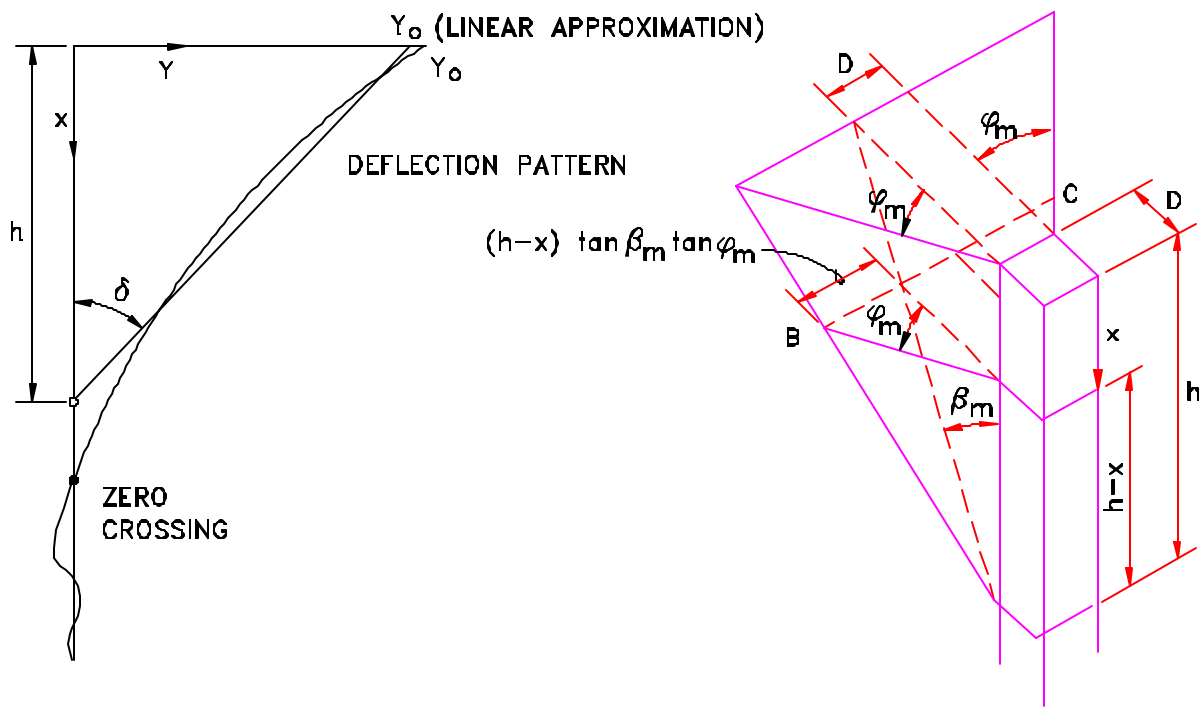
Comparison of Results of Load Test with Results Predicted by the SW Model

As seen in Fig. 5.23, linear and nonlinear SW model analyses yield good results at lower levels of shaft head deflection (up to 2 in). As the level of lateral deflection increases, the shaft response assessed using the nonlinear SW model continues to provide excellent match with measured data up to 8 in. Thereafter, the nonlinear SW model analysis predicts that the shaft experiences a dramatic drop in its bending stiffness (and, therefore, lateral resistance). Figure 5.23 indicates that the measured shaft response deteriorated beyond 8 in. of deflection, but not to the level indicated by the SW model. The difference between the measured and predicted shaft

response in this range may be due to the existence of the asphalt and concrete debris in the top 5 feet layer which was not characterized. It should be noted that the pile initial bending stiffness employed in the SW model analysis is based on the properties provided by Janoyan et al. (2001) (concrete strength used is 5000 psi).

5.4 SUMMARY

The nonlinear SW model shows tremendous promise for evaluating the realistic response of piles and shafts as the material experiences elastic behavior over a growing depth of the shaft/pile.



Pile deflection

SW model characterization

Fig. 5.1 Characterization of Soil and Pile Stresses in the SW Model

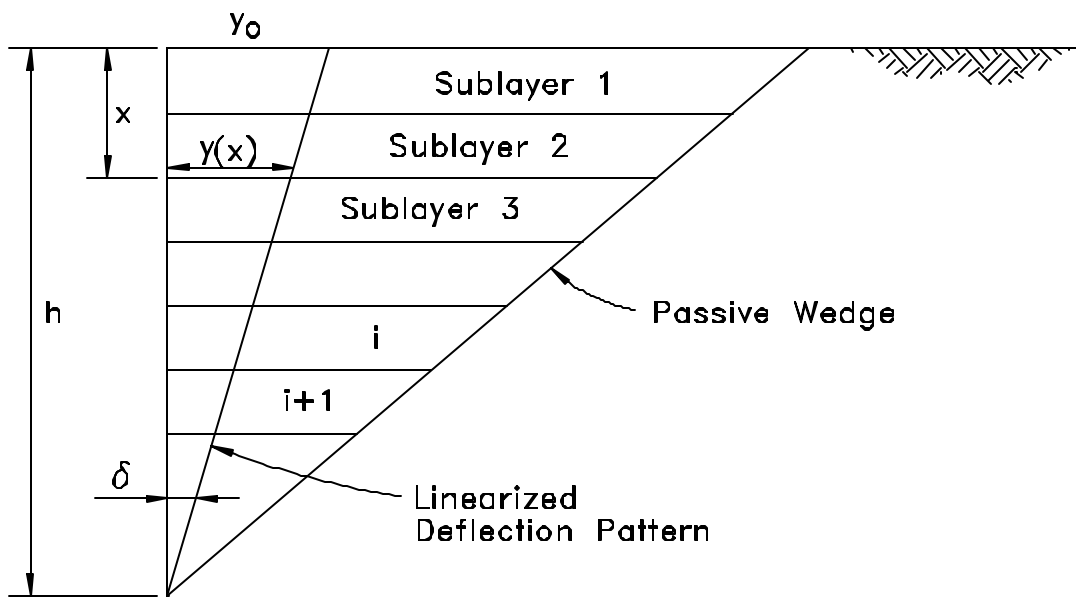


Fig. 5.2 Soil Passive Wedge Divided into Thin Soil Sublayers

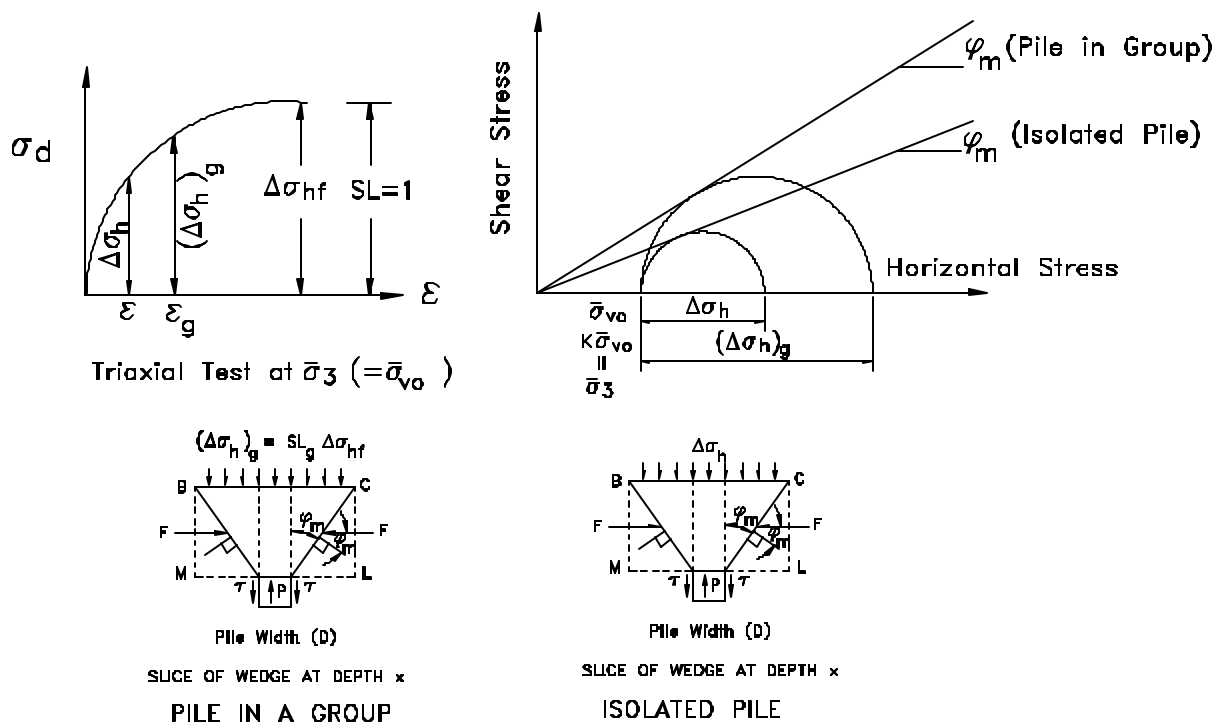


Fig. 5.3 Stress Changes in the SW Model for an Isolated Pile and an Individual Pile in a Pile Group

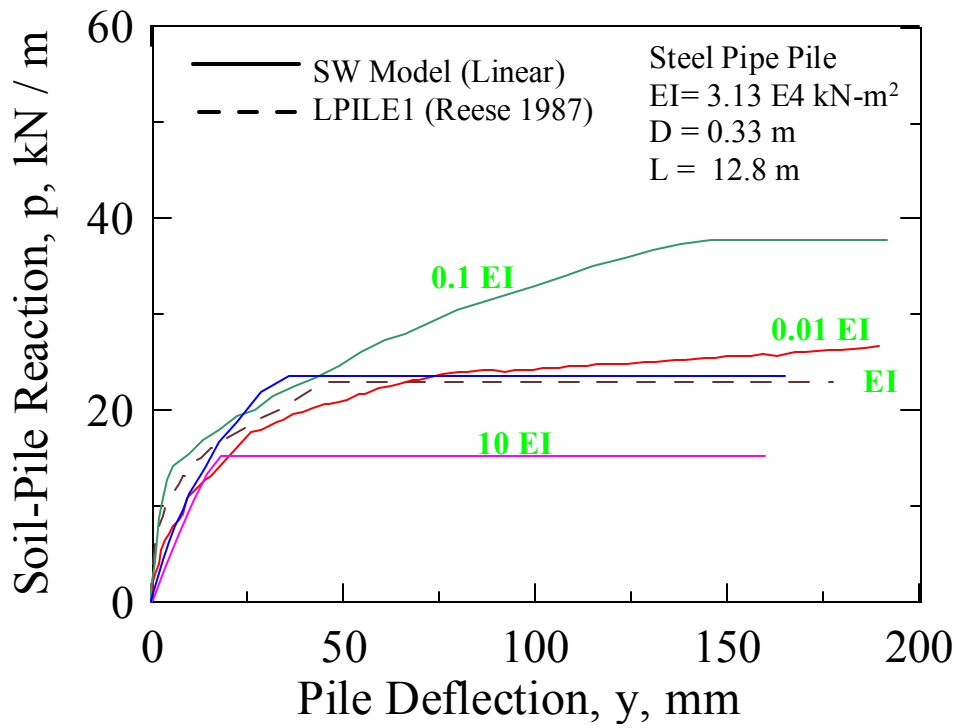


Fig. 5.4 Effect of Pile Bending Stiffness on the p-y Curve at 0.915-m Depth at Sabine River Test Site (Matlock 1970)

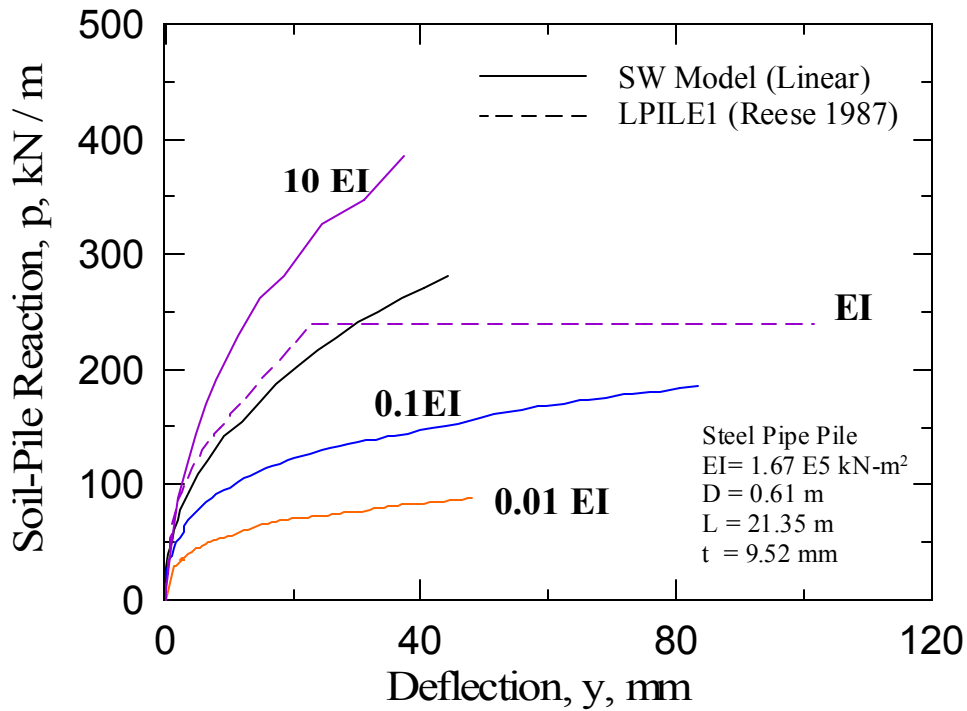


Fig. 5.5 Effect of Pile Bending Stiffness on the p-y Curve at 1.83-m Depth at the Mustang Island Test Site (Cox et al. 1974)

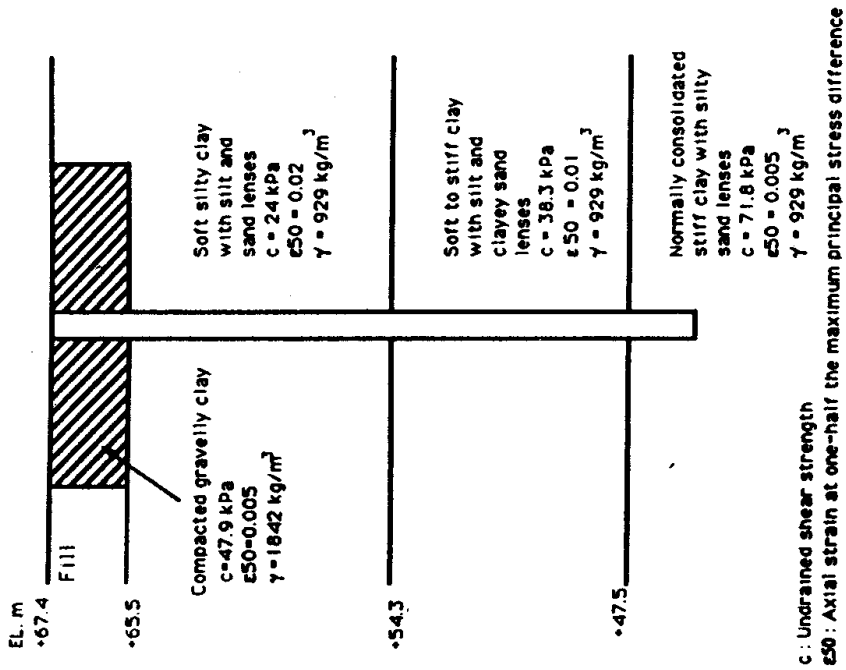


Fig. 5.6 Improved Soil Profile at the Pyramid Building Site (Reuss et al. 1992)

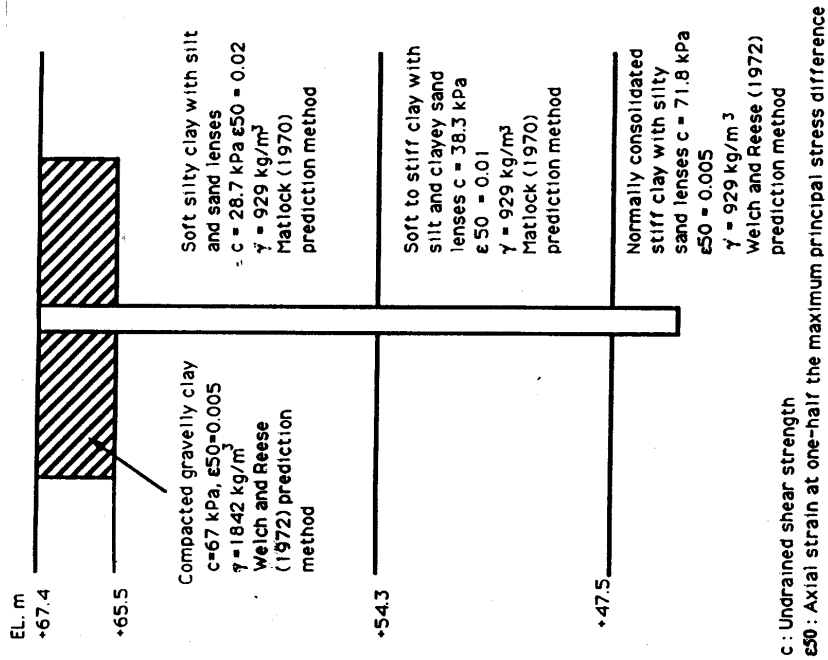


Fig. 5.7 Modified Soil Properties for the Improved Soil Profile Employed with LPILE to Obtain Good Agreement with the Observed Data

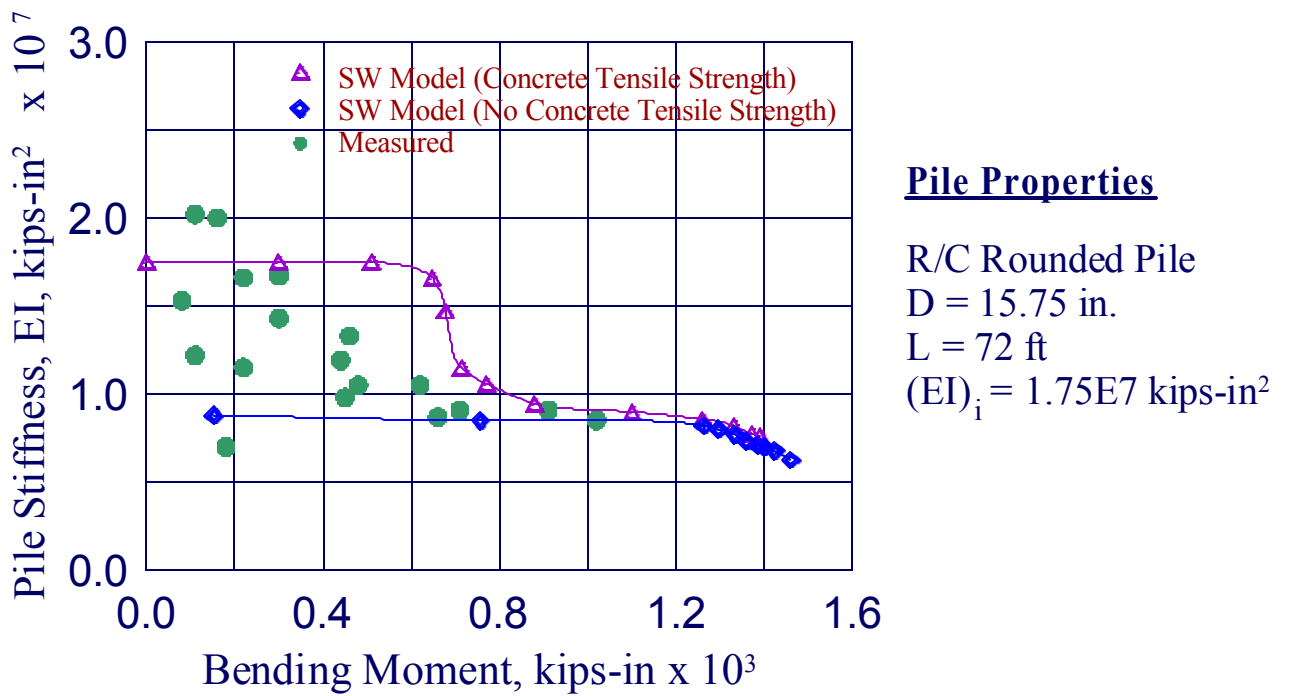


Fig. 5.8 Measured and Predicted Bending Stiffness of vs. Bending Moment

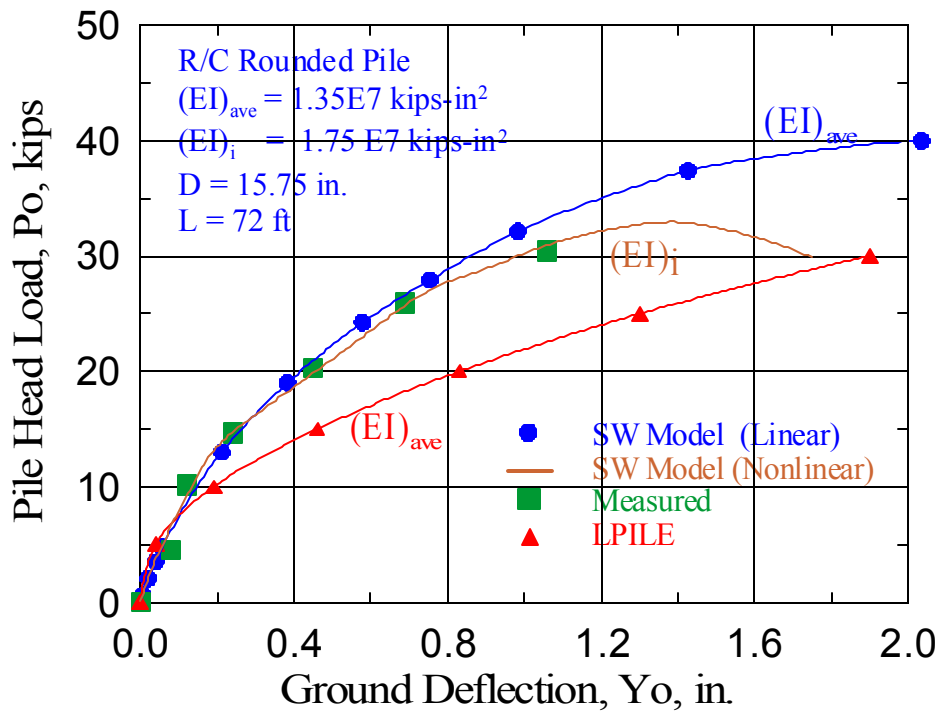


Fig. 5.9 Measured and Predicted Pile Head Response of the Pyramid Building Test

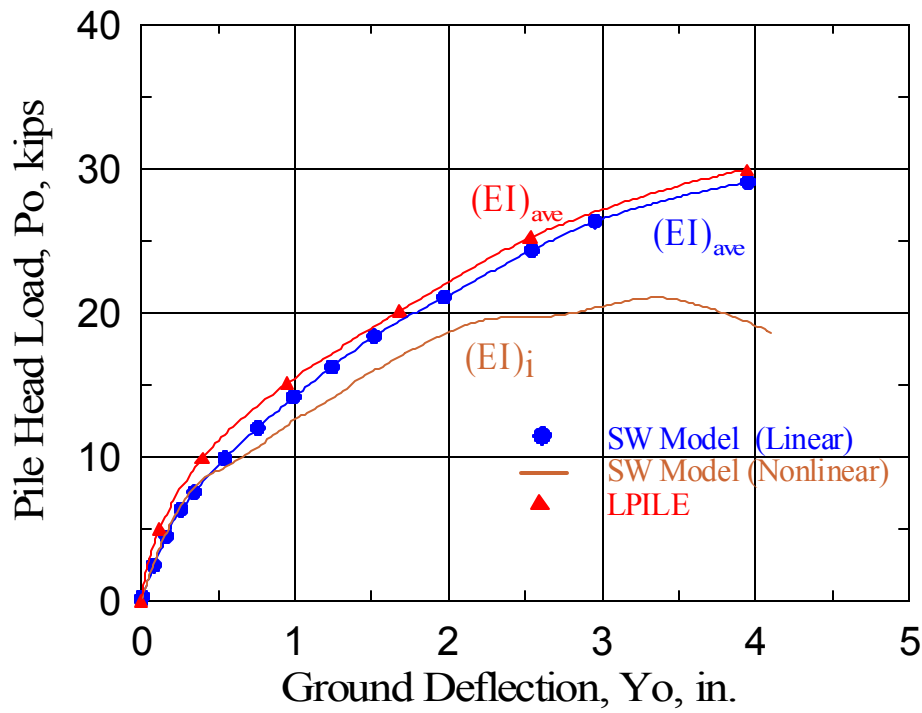


Fig. 5.10 Pile head Response Using SW Model and LPILE in the Original Soil Profile (no Improvement)

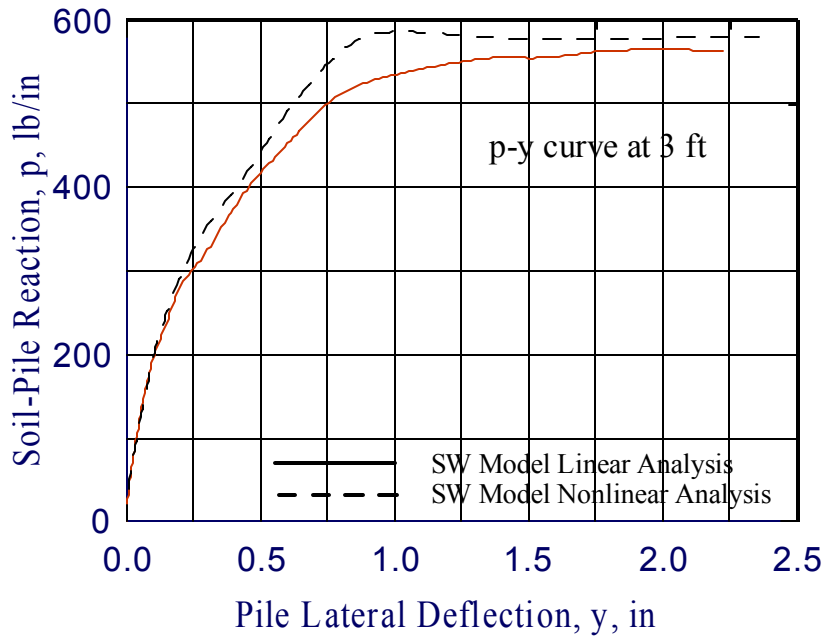


Fig. 5.11 p-y Curve at 3 ft Below Ground Surface for the Original Soil Profile

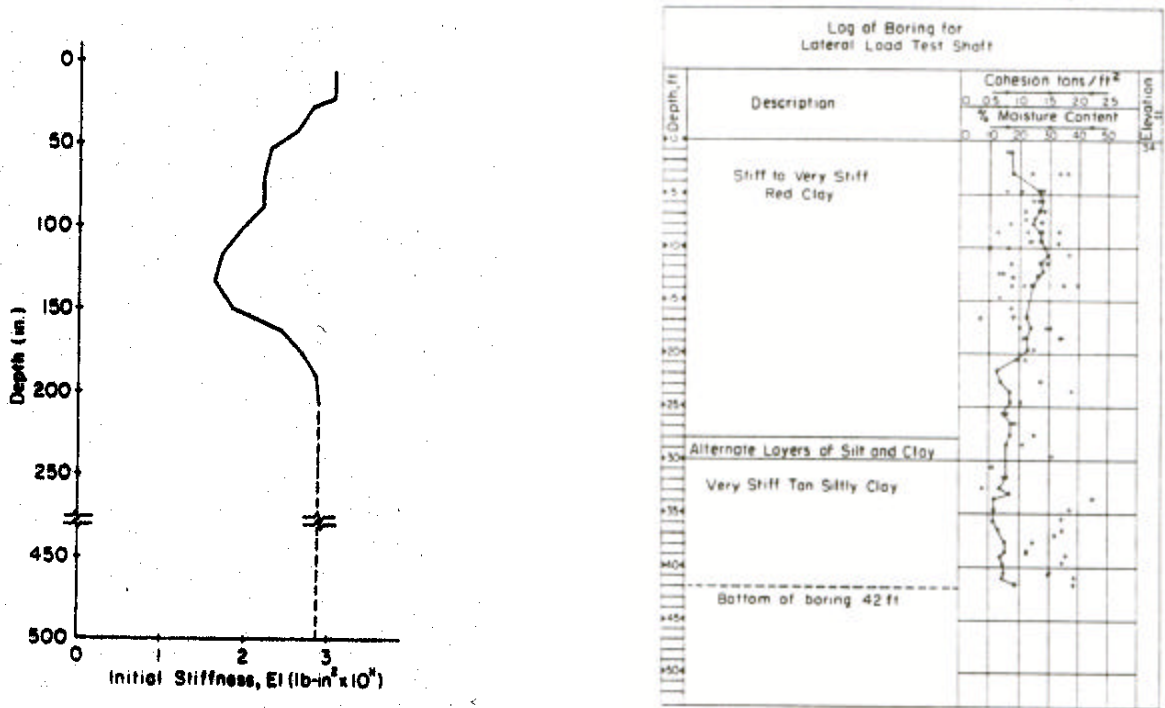


Fig. 5.12 Variation of Shaft Stiffness and Soil Strength with Depth (Reese and Welch 1975).

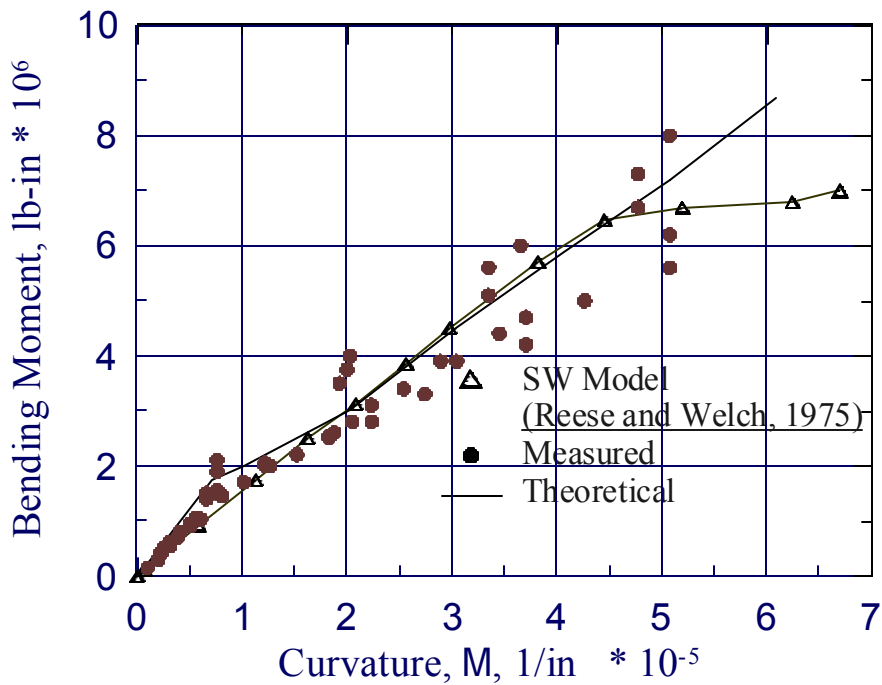


Fig. 5.13 Theoretical and Measured Moment-Curvature Relationship

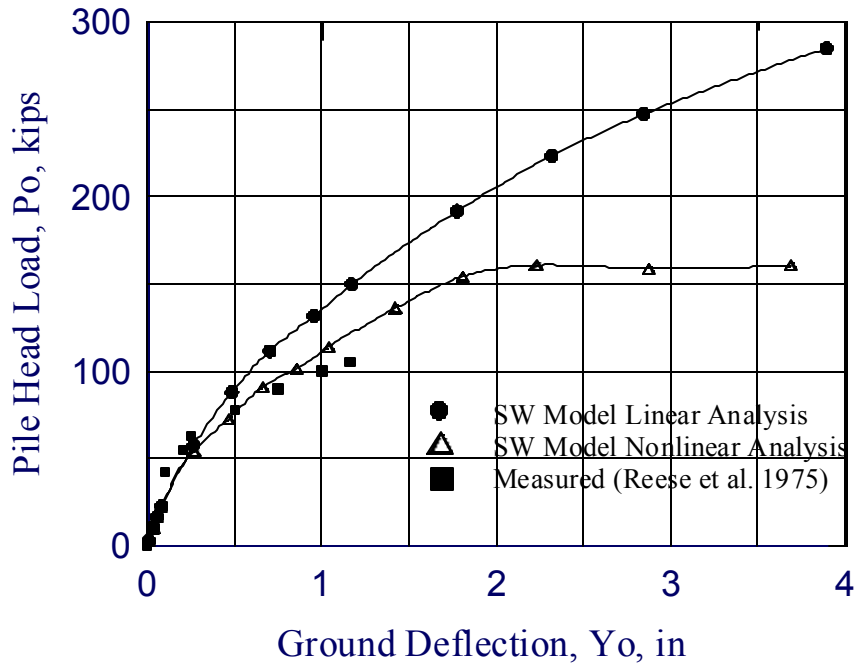


Fig. 5.14 A Comparison of Measured and the Calculated Pile-Head Deflections for Houston Test

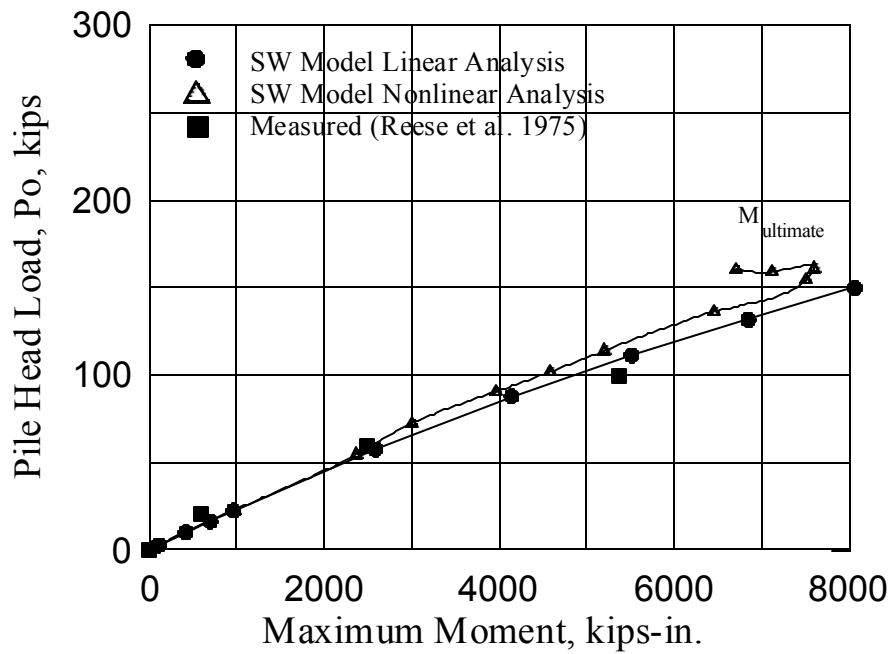


Fig. 5.15 A Comparison of Measured and the Calculated Maximum Moment of a Pile in Stiff Clay at Houston, Texas

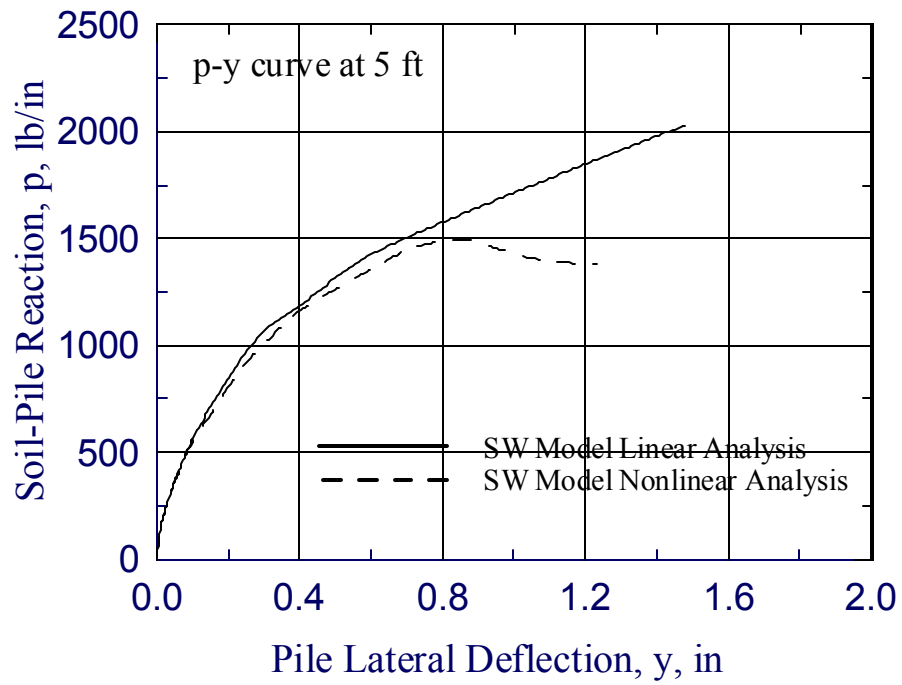


Fig. 5.16 Effect of Nonlinear Behavior of Drilled Shaft Material (R/C) on the Nature of the p-y Curve

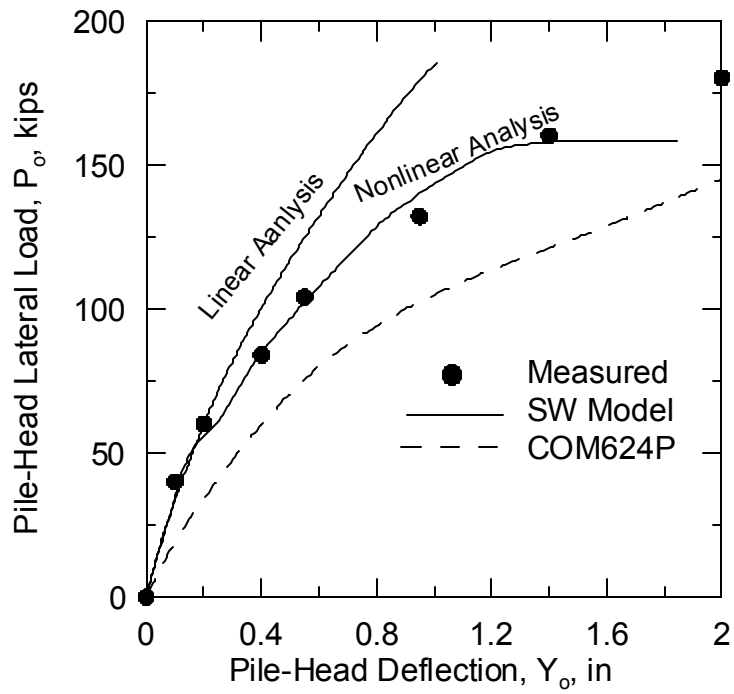


Fig. 5.17 Measured and Predicted Data for a 2-Foot Diameter Shaft at Las-Vegas Test (Zafir and Vanderpool 1998)

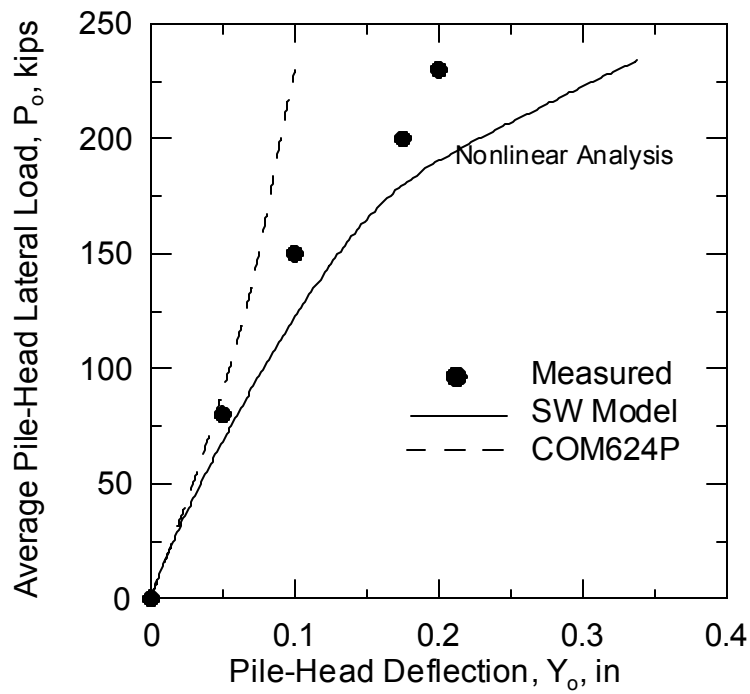


Fig. 5.18 Measured and Predicted Data for a 4-Shaft Group at Las Vegas Test (Zafir and Vanderpool 1998)

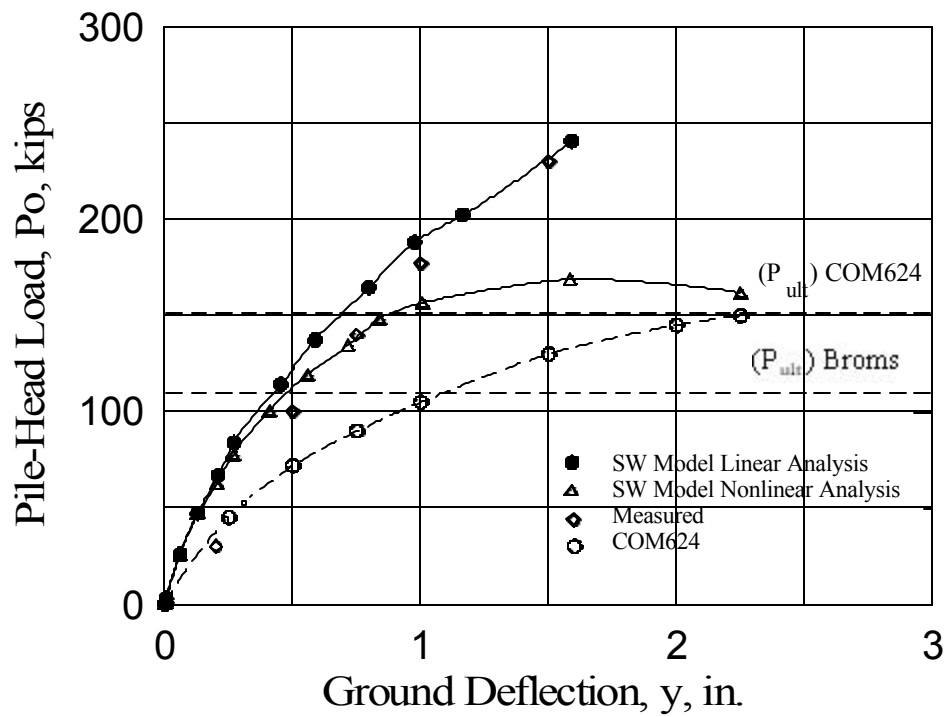


Fig. 5.19 A Comparison of Measured and the Predicted Deflections of Shaft 8 in Clay for the Southern California Test (Bhushan et al., 1978).

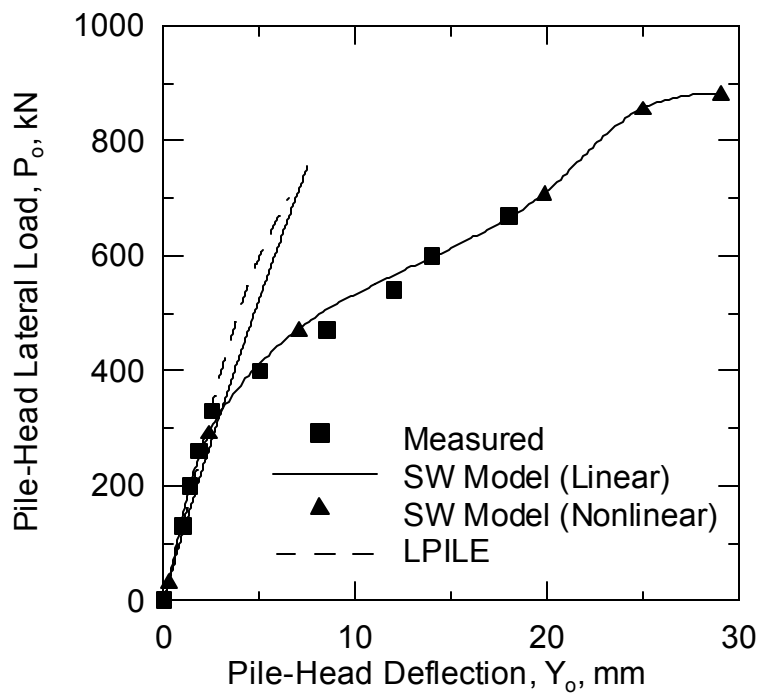


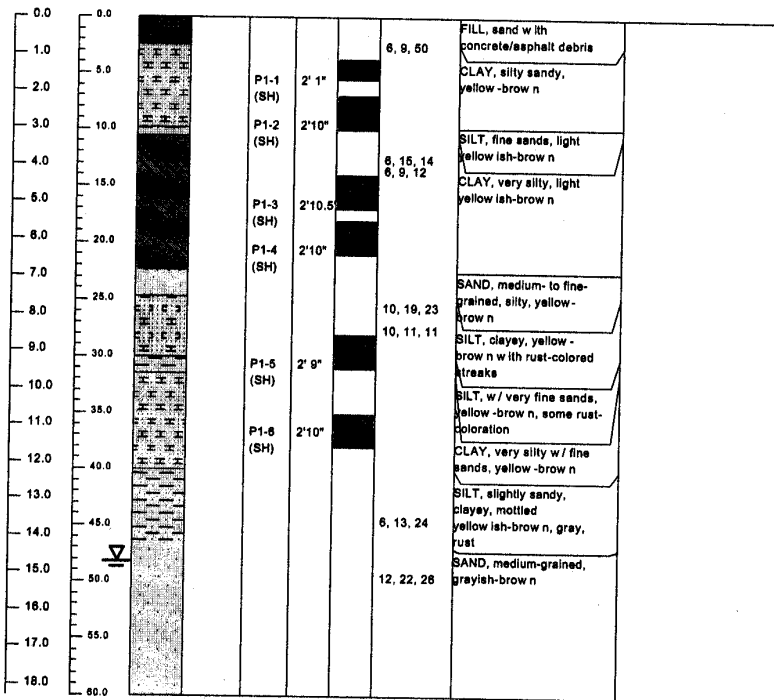
Fig. 5.20 A Comparison of Measured and the Predicted Deflections of 1.22-m Shaft at the Islamorada Test (Reese 1997)

UCLA DRILLED SHAFT PROJECT

Boring Log

PROJECT: UCLA Drilled Shaft Project	DRILLING CONTRACTOR: Regg In Situ	DATUM:
SITE LOCATION: Hawthorne, CA	DATES DRILLED:	LATITUDE: 33.82917
DIST./COUNTY/RTE/PMLA	DRILLING METHOD: Mud Rotary	LONGITUDE: 118.36389
EA: Unknown	SOLE DIAMETER (in): Unknown	ELEVATION:
BRIDGE NO: Unknown	TOTAL DEPTH (ft): 80	LOGGED BY:
STA/OFFSET: Unknown	DRILL RIG MODEL/NO: Unknown	ORGANIZATION: UCLA
BORING NO: B-1	SPT HAMMER: Unknown	ENTERED BY: D. Glass
		DATE: 02/03/01
		CHECKED BY:

DEPTH (m)	DEPTH (ft)	LITHOLOGY	USCS	SAMPLE TYPE AND NO.	RECOVERY/LENGTH (ft)	SAMPLE INTERVAL	SPT BLOWS PER 0.5'	DESCRIPTION	REMARKS
-----------	------------	-----------	------	---------------------	----------------------	-----------------	--------------------	-------------	---------



Sample Codes
 B = bag
 SH = Shelby tube
 SOT = split spoon
 T = wireline tube
 P = Pitcher tube
 USCS: caps = lab result, lower case = field interpretation

Fig. 5.21 Log of Boring # 1 (Janoyan et al. 2001)

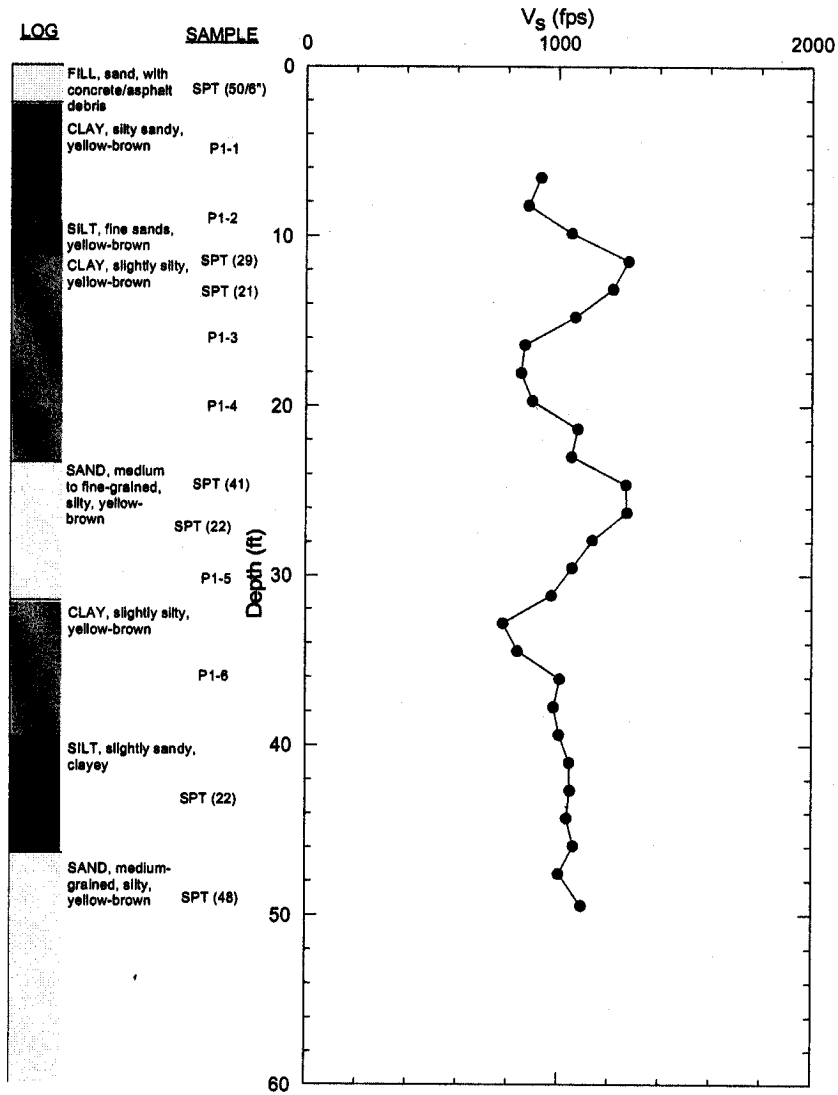


Fig. 5.22 Shear Wave Velocity Profile Measured at the Location of Boring # 1 (Janoyan et al. 2001)

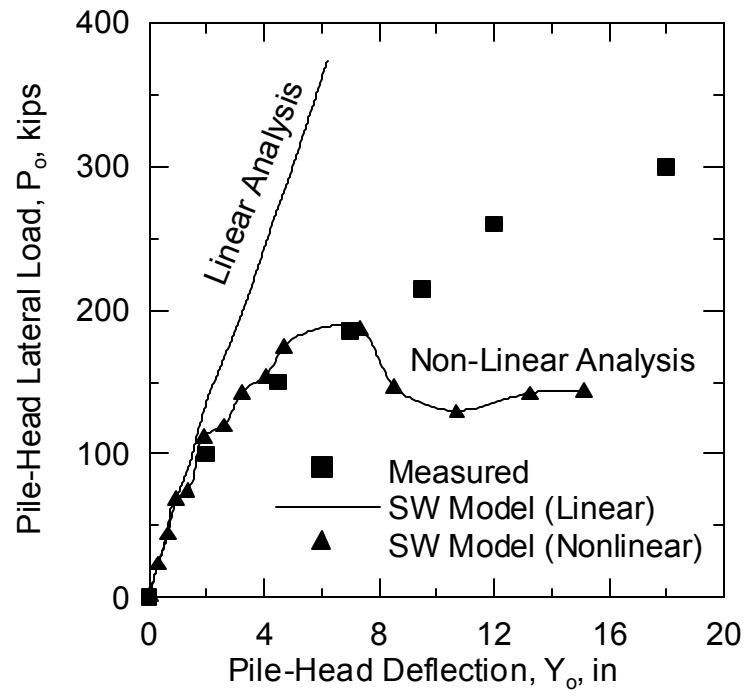


Fig. 5.23 Measured and Predicted Data for UC Los Angeles Test (Janoyan et al. 2001)

REFERENCES

Ashour, M., Norris, G. M., Bowman, S., Beeston, H, Billing, P. and Shamsabadi, A. (2001). “Modeling Pile Lateral Response in Weathered Rock..” Proceeding 36st Engineering Geology and Geotechnical Engineering Symposium, Las Vegas, Nevada, March 26-29.

Ashour, M. and Norris, G. (2000). “Modeling Lateral Soil-Pile Response Based on Soil-Pile Interaction.” Journal of Geotechnical and Geoenvironmental Engineering, ASCE, Vol. 126, No. 5, pp. 420-428.

Ashour, M., Norris, G., and Pilling, P. (1998). “Lateral Loading of a Pile in Layered Soil Using the Strain Wedge Model.” Journal of Geotechnical and Geoenvironmental Engineering, ASCE, Vol. 124, No. 4, pp. 303-315.

Ashour, M., Pilling, P., and Norris, G. M. (1998). “Updated Documentation of the Strain Wedge Model Program for Analyzing Laterally Loaded Piles and Pile Groups.” 33rd Engineering Geology and Geotechnical Engineering Symposium, March 25-27, Reno, Nevada, pp. 177-178.

Ashour, M., Pilling, P., and Norris, G. M. (1997). “Documentation of the Strain Wedge Model Program for Analyzing Laterally Loaded Piles and Pile Groups.” 32nd Engineering Geology and Geotechnical Engineering Symposium, March 26-28, Boise, Idaho, pp. 344-359.

Ashour, M., Pilling, P., Norris, G., and Perez, H.. (1996). “Development of Strain Wedge Model Program for Pile Group Interference and Pile Cap Contribution Effects.” CCEER, Report No. 96-4, Civil Engrg Dept., University of Nevada, Reno.

Briaud, J. L., Smith, T., and Mayer, B. (1984). "Laterally Loaded Piles and the Pressuremeter: Comparison of Existing Methods." *Laterally Loaded Deep Foundations*, ASTM, STP 835, pp. 97-111.

Brown, D. A. and Reese, L. C. (1985). "Behavior of a Large-Scale Pile Group Subjected to Cyclic Lateral Loading." U. S. Department of Interior, Reston, Virginia; Dept. of Research, Federal Highway Administration, Washington, D. C.; U. S. Army Engineer, Waterways Experiment Station, Vicksburg, Mississippi..

Brown, D. A., Morrison, C., and Reese, L. C. (1988). "Lateral Load Behavior of Pile Group in Sand." *Journal of Geotechnical Engineering*, ASCE, Vol. 114, No. 11, pp. 1261-1276.

Bhushan, K., Haley, S. C., and Fong, P. T. (1979). "Lateral Load Tests on Drilled Piers in Stiff Clays." *Journal of Geotechnical Engineering*, ASCE, Vol. 105, No. GT8, pp. 969-985.

Cox, W. R., Reese, L. C., and Grubbs, B. R. (1974). "Field Testing of Laterally Loaded Piles in Sand." *The Sixth Annual Offshore Technology Conference*, Houston, Texas, OTC 2079, pp. 459-472.

Coyle, H. M. and Reese, L. C. (1966). "Load Transfer for Axially Loaded Piles in Clay." *Journal of Soil Mechanics and Foundations Division*, ASCE, Vol. 92, NO. SM2.

Davisson, M. T. (1970). "Lateral Load Capacity of Piles." *Highway Research Record*, No. 333, pp. 104-112.

Douglas, B.M. and J.A. Richardson. (1984). "Maximum Amplitude Dynamic Tests of a Highway Bridge." *Proc.. Eighth World Conference on earthquake Engineering*, Vol. II, pp. 889-896.

Evans, Jr. L. T., and Duncan, G. M. (1982). "Simplified Analysis of Laterally Loaded Piles." UC Berkeley, Rept. No. UCB/GT/82-04, 245 pp.

Gowda, P. (1991). "Laterally Loaded Pile Analysis for Layered Soil Based on the Strain Wedge Model." M. S. Thesis, University of Nevada, Reno.

Janoyan, K., Stewart, J. P. and Wallace, J. W. (2001). "Preliminary Test Results for Full Scale Drilled Shaft Under Cyclic Lateral Loading." Report to Caltrans No. 59A0183, Civil Eng. Dept., UC Los Angeles.

Mander, J. B., Bristley, M. J. N., and Park, R. (1988). "Theoretical Stress-Strain Model for Confined Concrete." Journal of Structural Engineering, ASCE, Vol. 114, No. 8, pp. 1804-1826.

Matlock, H. (1970). "Correlations for Design of Laterally Loaded Piles in Soft Clay." The 2nd Annual Offshore Technology Conference, Houston, Texas, OTC 1204, pp. 577-607.

Matlock, H. and Reese, L. C. (1961). "Generalized Solution for Laterally Loaded Piles." Journal of Soil Mechanics and Foundations Division, ASCE, Vol. 86, No. SM5, pp. 673-694.

McVay, M., Casper, R., and Shang, Te-I. (1995). "Lateral Response of Three-Row Groups in Loose and Dense Sands at 3D and 5D Pile Spacing." Journal of Geotechnical Engineering, ASCE, Vol. 121, No. 5, pp. 436-441.

Morrison, C. and Reese, L. C. (1986). "Lateral-Load Test of a Full-Scale Pile Group in Sand." US Department of Interior, Reston, Virginia; Department of Research, Federal Highway Administration, Washington, D. C.; U. S. Army Engineer, Waterways Experiment Station, Vicksburg, Mississippi.

Norris, G. M. (1977). "The Drained Shear Strength of Uniform Quartz Sand as Related to Particle Size and Natural Variation in Particle Shape and Surface Roughness." Ph.D. Thesis, University of California , Berkeley, 523 pp.

Norris, G. M. (1986). "Theoretically Based BEF Laterally Loaded Pile Analysis." Third International Conference on Numerical Methods in Offshore Piling, Nantes, France, pp. 361-386.

Norris, G. M. (1994). "Seismic Bridge Pile Foundation Behavior." S-O-A paper, Proceedings International Conference on Design and Construction of Deep Foundations, FHWA, Vol. 1, pp. 27-136.

NAVFAC (1982). "Foundations and Earth Retaining Structures Design manual." Dept. of navy, DM 7.2, Alexandria, Va.

Paulay, T., and Priestley, M. J. N. (1992). "Seismic Design of Reinforced Concrete and Masonry." John Wiley and Sons, New York, N.Y., pp. 95-157.

Reese, L. C. (1987). "Documentation of The Computer Program LPILE1." Ensoft Inc., Post Office Box 180348, Texas 78718.

Reese, L. C. (1958). "Discussion of Soil Modulus for Laterally Loaded Piles." by Bramlette McClelland and John A. Focht, Jr., Transactions, ASCE, Vol. 123, pp. 1071.

Reese, L. C. (1977). "Laterally Loaded Piles: Program Documentation." Journal of Geotechnical Engineering, ASCE, Vol. 103, No. GT4, pp. 287-305.

Reese, L. C. (1983). "Behavior of Piles and Pile Groups Under Lateral Load." Report to the U.S. Department of Transportation, Federal Highway Administration, Office of Research, Development, and Technology, Washington, D.C.

Reese, L. C. (1984). "Handbook on Design of Piles and Drilled Shafts under Lateral Load." Geotechnical Engineering Center, Bureau of Engineering Research, University of Texas at Austin., Report No. FHWA-IP-84-11

Reese, L. C. and Sullivan, W. R. (1980). Documentation of Computer Program COM624, Parts I and II, Analysis of Stresses and Deflections for Laterally Loaded Piles Including Generation of p-y Curves. Geotechnical Engineering Software GS80-1, Geotechnical Engineering Center, Bureau of Engineering Research, University of Texas at Austin, August, 1980.

Reese, L. C. and Wang S. T. (1994). "Analysis of piles under lateral loading with nonlinear flexural rigidity." U.S. FHWA Int. Conf. On Design and Construction of Deep Foundation, FHWA, Washington, D.C.

Reese, L. C., Cox, W. R., and Koop, F. D. (1974). "Analysis of Laterally Loaded Piles in Sand." The Six Annual Offshore Technology Conference, Houston, Texas, OTC 2080, pp. 473-483.

Reese, L.C., and Welch, R. C. (1975). "Lateral Loading of Deep Foundations in Stiff Clay." Journal of Geotechnical Engineering Division, ASCE, Vol. 101, GT. 7, July, 1975.

Reuss, R., Wang, S. T., Reese, L. C. (1992). "Tests of Piles Under Lateral Loading at the Pyramid Building, Memphis, Tennessee." Geotechnical News, Vol. 10, No. 4, December, pp. 44-49.

Rollins, K. M., Peterson, K. T., and Weaver, T. J. (1998). "Lateral Load Behavior of Full Scale Pile Group in Clay." Journal of Geotechnical and Geoenvironmental Engineering, ASCE, Vol. 124, No. 6, pp. 468-478.

Skempton, A. W. (1954). "The Pore Pressure Coefficients A and B." *Geotechnique*, 4, pp. 148.

Terzaghi, K. (1955). "Evaluation of Coefficients of Subgrade Reaction." *Geotechnique*, Vol. 5, No. 4, pp. 297-326.

Tomlinson, M. J. (1957). "The Adhesion of Piles Driven in Clay Soils." *Proceedings of Fourth International Conf. on Soil mechanics and Foundation Engrg*, Vol. II, London, pp. 66-71.

US Army Corps of Engineers. (1996). "Design of Sheet Pile Walls." *Technical Engineering and Design Guides As Adapted from the*, No. 15, ASCE Press.

Vesic, A. (1961). "Bending of Beams Resting on Isotropic Elastic Solid." *Journal, ASCE, Engineering Mechanics Div.*, Vol. 87, SM 2, pp. 35-53.

Wu, T. H. (1966). *Soil Mechanics*, Boston, Allyn and Bacon Inc., pp. 169.

Zafir, Z. and Vanderpool, W. (1998). "Lateral Response of Large Diameter Drilled Shafts: I-15/US 95 Load Test Program." *33rd Engineering Geology and Geotechnical Engineering Symposium*, March 25-27, Reno, Nevada, pp. 161-176.